(2)

Magnetic Properties of Fe/Rare Earth Multilayers

Ko Mibu*

Doctoral Thesis

Faculty of Science, Kyoto University

*Institute for Chemical Research, Kyoto University
Uji, Kyoto-fu 611, Japan
Tel : 0774-32-3111 (Ext. 2212)
Fax : 0774-33-1247
E-mail : mibu@icrccc.kuicr.kyoto-u.ac.jp

Contents

§1. Introduction

Metallic multilayers with artificial superstructures have been attracting much attention both from scientific and technological viewpoints this decade.[1,2] Materials of this kind do not exist in nature and can only be made artificially with film growth techniques such as vacuum vapor deposition and sputtering. Many kinds of metallic multilayers have been prepared and studied as specimens for fundamental studies and as new materials for practical application in the field of magnetism, transport properties, crystallography, elastic properties, and so on.

In the field of magnetism, multilayers composed of magnetic and nonmagnetic layers were utilized for investigations of interface magnetism, magnetic size effects, and two-dimensional magnetic behaviors.[1] Magnetic coupling between magnetic layers through an intervening nonmagnetic layer was also reported.[3-7] From a technological point of view, multilayers with magnetic elements have been studied actively as potential materials for magneto-optical recording media,[8,9] magnetoresistance devices,[6,10,11] and soft magnetic materials.

Multilayers containing rare earth (RE) layers are expected to show novel magnetic properties reflecting characteristic RE magnetism such as helical magnetic structures and large magnetic anisotropy. Magnetic properties of RE/Y epitaxial multilayers were investigated by Salamon *et al.* and Majkrzak *et al.* and magnetic coupling between RE layers through an Y layer was studied.[3,4] Magnetic properties of multilayers composed of 3*d*

magnetic metal and RE metal are also of great interest because they have different characteristic magnetic properties. New magnetic properties which both metals do not have in the bulk are expected to appear in multilayers with an artificial period of several atomic layers.

In this dissertation, magnetic properties of Fe/RE multilayers, mainly those of Fe/Nd multilayers, are reported. A bulk bcc Fe metal is a 3*d* ferromagnet with a magnetic moment of $2.22\mu_{Y_B}$ and the Curie temperature is 1042K. On the other hand, RE metals have 4*f* localized magnetic moments and show various magnetic structures (Fig. 1). For example, Nd has a magnetic moment of $3.27\mu_B$ as the *gJ* value of the trivalent free ion. The magnetic moments of bulk Nd metal align antiferromagnetically below 19.9K, but several complex magnetic structures are observed below the Néel temperature.[12] Intermetallic compounds such as Fe_2RE and $Fe_{17}RE_2$ are known in the Fe-RE binary system but little solid solution exists in the equilibrium states. In most of the intermetallic compounds, the Curie temperature is higher than room temperature and it generally increases when the Fe concentration decreases. Amorphous Fe-RE thin films can be fabricated over a wide composition range, and show characteristic magnetic properties such as sperimagnetism[13] and perpendicular magnetic anisotropy.[14,15] Especially, amorphous Fe-heavy RE alloys have been investigated as erasable magneto-optical recording media.[14] Magnetic properties of Fe/RE multilayers have also been studied recently,[16-63] and magnetic interaction between Fe and RE layers, interface magnetism, perpendicular magnetic anisotropy, and random magnetic anisotropy have been discussed for

Fe/Y,[18,39,42,48,53] Fe/La,[41,53] Fe/Nd,[22,26,30,31,33,38,39,47,57,58,62] Fe/Sm,[20] Fe/Gd,[16-18,21,36,44,52,61] Fe/Tb,[19,21,24,29,35,43,45,46,49-51,53,55,56,59,60,63] Fe/Dy,[21,23,25-28,32,34,37,39,45,53,54] and Fe/Tm[30,38,40] systems. In the present work, Fe/RE multilayers were prepared by alternate deposition, and the magnetic properties were investigated mainly by ^{57}Fe Mössbauer spectroscopy, magnetization measurements, and neutron diffraction measurements.

§2. Experimental

2.1 Sample preparation

Iron/rare earth multilayers were prepared by alternate deposition with a plural electron gun system in ultrahigh vacuum (10^{-9}Torr range). The detail of the deposition system is shown in Fig. 2. To get a vacuum of 10^{-9}Torr range, the chamber is evacuated initially with a turbo-molecular pump and a backing rotary pump, baked for a few days, connected with a cryopump, and cooled with liquid nitrogen filled in vessels in the chamber. Deposited layer thickness is measured with a quartz thickness monitor and controlled by mechanical shutters connected with the monitor. Bulk densities of metals were used to estimate the layer thickness from the deposited mass, which affects frequency of the quartz. Individual Fe and RE layer thicknesses were varied from 2Å to 60Å. The deposition rate was controlled to be about 0.3Å/sec. An ultrahigh vacuum is a necessary condition to prevent RE layers from oxidization in such a low deposition rate.[17,20,64] The deposition was started with an Fe layer and ended with an Fe layer, so that the RE layers are not contaminated by the substrates or the open air. Total film thickness was usually about 2000Å, which is a sufficient thickness to reduce enough the thickness dependence of magnetic properties.[19] Iron and RE metals have different crystal structures and the ratio of the atomic radii is about 0.7, so that epitaxial growth was not aimed at in this work. Non-crystalline substrates, i.e. glasses for X-ray and neutron diffraction measurements, and polyimide films for

Mössbauer and magnetization measurements, were used for the convenience of the experiments. The substrate temperature was maintained to be about -50°C during deposition to prevent intermixture at the interfaces. The geometrical positions of the substrates, the crucibles, and the thickness monitor are shown in Fig. 3. The substrate holder has no rotatory system, and there is a distribution in the deposited film thickness. The tooling factor, which adjusts the difference in the deposited layer thicknesses between the substrate and the thickness monitor, is set up so that the designed layer thickness is obtained at the center of the polyimide substrate. Calculated distribution of thickness is shown in Table I. Here, the evaporation is assumed to be from a point source or from a planar source, whereas it is difficult to know the evaporation mode for electron gun heating. The distribution is calculated to be from -9% to +5%. The layer thicknesses estimated by ICP (radio frequency inductively-coupled plasma atomic emission spectrometer) and by magnetization of deposited pure Fe films are also shown in Table I. From now on, deposited layer thickness is expressed by the designed value, termed "nominal thickness".

2.2 *X-ray diffraction measurement*

X-ray diffraction measurement is a powerful method to get structural information of multilayers. A double-axis

diffractometer with a Cu target was used to get X-ray patterns. Copper Kα radiation (λ=1.5418Å) was picked out with an analyzer installed between the sample holder and the detector. Usually, the sample and the detector were rotated in the θ-2θ scanning mode with the scattering vector normal to the film plane.

Artificial periodicity is confirmed from low angle X-ray patterns. The artificial period Λ is estimated from the peak position 2θ with the Bragg's equation:

$$\Lambda=\lambda/2\sin\theta. \qquad (1)$$

Since the period is usually of the order of tens of Å, the peaks are in the low angle region. In this region, the peak position shifts to a higher angle because of the refraction effect, and the period derived from eq. (1) is smaller than the real period.[65] Generally, Fe/RE multilayers do not give Bragg peaks in a higher angle range where the refraction effect is negligible. In this work the Bragg's equation was corrected using the following equation:

$$\Lambda=\lambda/\{2\sin\theta[1-(1-n^2)/\sin^2\theta]^{1/2}\}$$
$$\cong\lambda/\{2\sin\theta[1-(1-n)/\sin^2\theta]\}. \qquad (2)$$

Here, n is the refractive index averaged over a period with a weight of each layer thickness. When eq. (2) was applied to an Fe/RE multilayer which shows several low angle peaks, the derived periods were almost constant for the peaks at higher 2θ than about 2°, but were overestimated for those at lower 2θ than about

2°. Therefore, only peaks at higher 2θ than 2° were used to estimate the artificial periods of multilayers.

Crystal structure, preferred orientation, and grain size in each layer were studied from X-ray patterns in the high angle region, i.e. from 25° to 90°. The grain size S was roughly estimated from the Scherrer's equation:

$$S=53.8\lambda/(W\times\cos\theta), \qquad (3)$$

where, W (deg.) is the full width at half maximum of a peak in the high angle region. For Fe/RE multilayers, the line width is usually wide enough to neglect the instrumental width.

2.3 *Mössbauer spectroscopy*

Hyperfine interactions between a nucleus and electrons provide us with microscopic information on the electronic structure of the relevant atom. Mössbauer spectroscopy has been developed as a method to study hyperfine interactions and applied in various scientific fields including solid state physics. The Mössbauer effect can occur in more than 100 nuclear transitions of more than 40 elements. In technical respect, the 14.4keV transition of ^{57}Fe nuclei is one of the most suitable transitions for applying the Mössbauer effect to material researches.

In this work, ^{57}Fe Mössbauer measurements were performed by

a conventional absorption method. A radioactive isotope ^{57}Co was used as the parent nucleus to get γ-rays of 14.4keV. In order to change the energy of the γ-rays by the Doppler effect, the source was vibrated with a frequency of several Hz. Gamma-rays which passed through a sample were detected by a proportional counter connected with a multichannel analyzer (MCA). The channel of the MCA was swept synchronously with the source vibration so that each channel corresponds to a certain Doppler velocity. The energy shift of the incident γ-ray is proportional to the velocity (mm/sec), which is usually used as the abscissa of Mössbauer spectra. The relation between the channel and the velocity was calibrated by referring to a spectrum of α-Fe at room temperature.

The energy schemes of ^{57}Fe nuclei and the corresponding Mössbauer absorption spectra in typical cases are shown in Fig. 4. Many pieces of information on electronic properties are obtained from the spectra through isomer shifts, quadrupole interaction, and magnetic hyperfine interaction. If an electric field gradient (EFG) and a magnetic hyperfine field do not exist, the ^{57}Fe nucleus has a single energy level in both the ground and the 1st exited states (Fig. 4 (a)). The energy levels are dependent on the size of the nucleus and the electron density at the nuclear site on account of an electric interaction between the nucleus and the electrons. As a result, the position of the center of the spectrum shifts from zero velocity. This shift is called isomer shift, and it is usually expressed relative to the center of the spectrum for pure α-Fe at room temperature instead of to zero velocity. The isomer shift is proportional to the

difference in the electron densities at the nuclear sites between the sample and the source (or α-Fe), and is useful to identify the valence state of Fe in the sample. In the case of Fe/RE multilayers, the isomer shifts are from -0.1 to 0.0mm/sec at room temperature; they are typical values for metallic absorbers. In addition, the second order Doppler effect due to lattice vibration gives temperature dependent shifts in the position of the spectra.

When a nucleus with the spin quantum number I larger than 1 experiences an EFG, the energy level splits into sublevels through an interaction between the nuclear quadrupole moment and the EFG. In the case of ^{57}Fe nuclei, the 1st exited state (I=3/2) splits into two sublevels, but the ground state (I=1/2) does not split. Consequently, the spectrum shows two split lines (Fig. 4 (b)). The EFG originates either from electrons directly associated with the ^{57}Fe atom or from those belonging to the surrounding atoms. The quadrupole splitting reflects the degree of deviation of the surrounding electron distribution and is useful to identify the crystallographic site. When the EFG is uniaxial, the intensity ratio of the two split lines is $(2+3\sin^2\theta):(3+3\cos^2\theta)$, where θ is the angle between the principal axis of the EFG and the incident γ-ray direction. When there is no preferred orientation in the EFG axis, the spectrum usually shows a symmetric doublet.

When a nucleus experiences a magnetic hyperfine field and no EFG, the nuclear level with I splits into $2I$+1 sublevels. In the case of ^{57}Fe nuclei, the ground state splits into two sublevels and the 1st excited state into four (Fig. 4 (c)). Six

transitions out of possible eight transitions are allowed and a six-line pattern appears in the spectrum. Spacing of the six-lines is proportional to the magnetic hyperfine field at the nuclear site. Magnetic hyperfine fields provide very useful pieces of information for microscopic studies of magnetism. The relation between the local magnetic moment and the magnetic hyperfine field is rather complicated and in general quantitative analysis is difficult. In many Fe alloys, however, the magnetic hyperfine field is found to be roughly proportional (and in the opposite direction) to the local magnetic moment. Although that is not applied to some special cases such as interface magnetism,[66] it is safely thought that the temperature dependence of the hyperfine field is proportional to that of the local magnetization. The direction of a magnetic hyperfine field (i.e. magnetization) is examined from the intensity ratio of six-lines in magnetically split Mössbauer spectra. When a sample has sufficiently thin effective thickness, the intensity ratio of the six-lines is expressed as $3:X:1:1:X:3$ with $X=4\sin^2\theta/(1+\cos^2\theta)$, where θ is the angle between the incident γ-ray direction (or the film normal, in the experimental configuration used in this work) and the average direction of the Fe magnetic moments. For example, if the magnetic moments of the sample are completely in the film plane, the intensity ratio is 3:4:1:1:4:3, and if they are perpendicular to it, the ratio is 3:0:1:1:0:3.

When an EFG coexists with a magnetic hyperfine field, mixing of $|I,M\rangle$ states can happen. In that case, an eight-line pattern possibly appears in the spectrum, and the eigenequation for the hyperfine Hamiltonian must be solved to fit the spectrum.

2.4 *Magnetization measurement*

Magnetization measurements were performed to investigate macroscopic magnetic properties of the multilayers. Samples 0.60mm in diameter were cut from the center of $85\times85mm^2$ polyimide substrates, where the layer thicknesses were set up to be the nominal values (Table I). Magnetization curves (M-H curves) were measured with a vibrating sample magnetometer (VSM) in external magnetic fields up to 15kOe at room temperature, and with a SQUID magnetometer up to 50kOe at temperatures from 5K to 300K. Temperature dependence of magnetization was also measured with the SQUID magnetometer. The sample temperature was decreased from 300K to 5K after a certain magnetic field was applied, so that influence of magnetic domains was diminished.

The magnetization values were often expressed by magnetization per unit Fe volume (emu/Fe cm^3), instead of that per unit volume (emu/cm^3). The volume was estimated using the nominal layer thickness. The former unit is convenient when magnetization is compared among samples with the same Fe layer thickness and different RE layer thicknesses. As a reference value, the expected Fe layer magnetization M_{Fe} was calculated on the assumption that every Fe atom has a magnetic moment of $2.22\mu_B$. It should be noted that this value has an error due to deviation of the thickness from the nominal value (§3.1.1), and of the Fe magnetic moment from $2.22\mu_B$, for instance, at the interfaces (§3.2.3). The gJ values for the ground state of trivalent free RE ions (or divalent for Eu and Yb) were tentatively used for estimation of reference RE layer

magnetization M_{RE}.

Magnetic anisotropy can be estimated by fitting M-H curves with theoretical curves. An Fe/RE multilayer may have two or more magnetic components which have different magnetic anisotropy. If there is a magnetic interaction between the components, the fitting turns out to be difficult. In such a case, it is convenient to estimate magnetic anisotropy using the area W surrounded by the M-H curve, the M-axis, and the $M=M_s$ line:

$$W=\int_0^{M_s} H dM. \qquad (4)$$

The uniaxial magnetic anisotropy constant K_u was evaluated with $W_\perp$ (W for the perpendicular M-H curve) subtracting from $W_\parallel$ (W for the in-plane M-H curve):

$$K_u=W_\parallel-W_\perp. \qquad (5)$$

When an M-H curve showed a hysteresis loop, two H values which gave the same M were averaged so that the curve was expressed as a single-valued function.

Magnetic anisotropy was also studied with a torque magnetometer at 300K and 77K. An Fe/RE multilayer usually has plural magnetic components, besides the highest applied field 20kOe was sometimes not sufficient to keep the magnetization in the field direction. Accordingly it was not easy to analyze the torque curves. For a rough estimation of the anisotropy constants, the curves were fitted with a single component with

the uniaxial anisotropy energy of the following form:

$$E=K_1\sin^2\theta+K_2\sin^4\theta+K_3\sin^6\theta. \qquad (6)$$

Here, K_1, K_2, and K_3 are the anisotropy constants. The uniaxial anisotropy constant K_U is sum of the three constants.

2.5 Neutron diffraction measurement

Neutron diffraction measurements were carried out with TOP (Time-of-Flight Spectrometer with Optical Polarizer, Fig. 5) installed at National Laboratory for High Energy Physics (KEK) in Tsukuba, Japan. Pulsed neutron beams are generated by irradiating an U target with pulsed proton beams. The neutrons are moderated to be cold neutrons with the wavelength from 3 to 9Å using solid methane at 20K. The cold neutrons are polarized with a total reflection polarizer. The beam polarization P_0 depends on the wavelength. The direction of the polarized neutron spins is set to be up (+) or down (-) with a spin flipper before the neutrons reach a sample. A magnetic field parallel to the polarization vector $\boldsymbol{P}_0$ is applied to the sample (in the z-direction). A film sample is mounted so that the magnetic field is in the film plane. Neutrons scattered with the scattering vector perpendicular to the z-axis are counted by a position sensitive detector (PSD). The intensity of the scattered

neutrons, for the incident neutron spins set to be up (I_+) and down (I_-), is recorded separately. A time spectrum at a certain position channel of the PSD corresponds to a diffraction pattern when the scattering vector $\boldsymbol{Q}$ is scanned in the film normal (the x-direction).

When the atomic configuration and magnetization of the film have a period of Λ along the x-axis, the intensity of the scattered neutrons with the scattering vector in the x-direction is calculated as follows:

$$I=\Phi L\{|B(Q)|^2+|\boldsymbol{P}(Q)|^2+P_0\cdot[B(Q)\boldsymbol{P}(Q)^*+B(Q)^*\boldsymbol{P}(Q)]\}d\Omega. \qquad (7)$$

Here, Φ is the incident neutron flux density and L is the Laue function. The Bragg peaks are observed when $Q=(2\pi/\Lambda)n$, or $2\Lambda\sin\theta=n\lambda$. The factors $B(Q)$ and $\boldsymbol{P}(Q)$ are the nuclear and magnetic structure factors for a single period. The intensity of the scattered neutrons depends on the terms Φ, L, and the solid angle and efficiency of the detector. To cancel them, polarization P is defined as follows:

$$P\equiv\frac{I_+-I_-}{I_++I_-}=\frac{B(Q)P_z(Q)^*+B(Q)^*P_z(Q)}{|B(Q)|^2+|\boldsymbol{P}(Q)|^2}P_0. \qquad (8)$$

For multilayers with two different layers A and B,

$$B(Q)=B_A(Q)+B_B(Q)\exp(iQd_A), \qquad (9)$$

$$\boldsymbol{P}(Q)=\boldsymbol{P}_A(Q)+\boldsymbol{P}_B(Q)\exp(iQd_A), \qquad (10)$$

where, $B_J(Q)$, $\boldsymbol{P}_J(Q)$, and d_J are the nuclear structure factor, the magnetic structure factor, and the thickness of J layer (J=A,B). In a small Q region, $B_J(Q)$ and $\boldsymbol{P}_J(Q)$ are expressed with atomic number density $\rho_J(x)$, the nuclear scattering amplitude $b_J(x)$, the magnetic scattering amplitude $p_J(x)$, the q-factor* $\boldsymbol{q}_J(x)$, and the irradiated area S:

$$B_J(Q)=S\int_0^{d_J} b_J(x)\rho_J(x)\exp(iQx)dx, \qquad (11)$$

$$\boldsymbol{P}_J(Q)=S\int_0^{d_J} p_J(x)\boldsymbol{q}_J(x)\rho_J(x)\exp(iQx)dx. \qquad (12)$$

In a multilayer with chemically uniform layers and sharp interfaces, $\rho_J(x)$ and $b_J(x)$ are set at the constants listed in the literature. On the other hand, the term $p_J(x)\boldsymbol{q}_J(x)$ depends on the magnitude and direction of the magnetic moments. When the magnetic moments lie in the plane made by the vectors $\boldsymbol{Q}$ and $\boldsymbol{H}$ (the xz-plane), the vector $p_J(x)\boldsymbol{q}_J(x)$ is in the z-direction and the magnitude is equal to the z component of the magnetic moment except a certain multiplied constant. The two functions $p_J(x)q_J(x)$ (J=A,B), when expressed with n parameters in total, are determined if the polarization up to the (n-1)th Bragg peak and the magnetization of the film are obtained experimentally. In the simplest case that the terms $p_J(x)q_J(x)$ (J=A,B) are independent of x,

---

*the orthographic projection of the unit magnetic moment to the plane perpendicular to the vector $\boldsymbol{Q}$

$$P=\frac{2(b_A\rho_A-b_B\rho_B)(p_Aq_A\rho_A-p_Bq_B\rho_B)}{|b_A\rho_A-b_B\rho_B|^2+|p_Aq_A\rho_A-p_Bq_B\rho_B|^2}P_0. \quad (13)$$

The constants p_Aq_A and p_Bq_B are evaluated from the 1st order polarization and the total magnetization. In the present work, the distribution of magnetization near the interfaces was taken into account with the following equation:

$$p_J(x)q_J(x)=A_J+B_J\{\exp[-x/C_J]+\exp[-(d_J-x)/C_J]\} \quad (J=A,B). \quad (14)$$

To determine the six parameters in this model analytically, polarization for five Bragg peaks must be obtained experimentally. For Fe/RE multilayers, however, only one or two Bragg peaks were observed. Hence, polarization and magnetization were calculated with numerous sets of parameters which are in a physically significant range. The distribution of the magnetization was discussed on the basis of the sets of parameters which reproduced the experimental values.

2.6 Heat treatment

Since multilayers are materials in non-equilibrium states, thermal stabitity and effects caused by heat treatment are important subjects to be studied. By heat treatment, intermixture may occur at the interfaces and new alloys may be generated

there. Crystal structures in each layer and at interface region also can be changed. In the present work, multilayers were annealed in air, a high vacuum (10^{-6}Torr range), and an ultrahigh vacuum (10^{-8}Torr range), at 200°C, for 24 hours. Ultrahigh vacuum is a necessary condition to prevent RE layers from oxidization. The annealing effects on the crystal structures and magnetic properties were investigated by X-ray diffraction measurements, Auger electron spectroscopy, and Mössbauer spectroscopy.

§3. Results and Discussion

3.1 Structural characterization

3.1.1 Artificial periodicity

Since multilayers are designed to have periods of the order of tens of Å, it is of the highest priority to confirm establishment of the artificial periodic structures by X-ray diffraction measurements. Low angle X-ray patterns for Fe/Nd multilayers are shown in Fig. 6. Iron and some RE metals are not favorable combination to get a high contrast for X-ray diffraction because they have relatively close electron densities in the bulk. Nevertheless, even when the nominal Nd layer thickness was 3Å (≅ one atomic layer), the 1st order Bragg peak was observed. Higher order Bragg peaks were usually weak, suggesting that the interfaces are rough to a certain degree. As shown in the map of Fig. 7, the artificial periodicity was confirmed for almost all prepared Fe/Nd multilayers except when both Fe and Nd layer thicknesses were a few Å. The same tendency was also seen for other Fe/RE systems. The relation between the nominal period $\Lambda_{nominal}$ and the period estimated from X-ray measurement $\Lambda_{X\text{-}ray}$ at the substrate position (2) is shown in Fig. 8. The refraction effect of X-rays was corrected by the method described in §2.2. According to the least squares method on an assumption that $\Lambda_{X\text{-}ray}$ is proportional to $\Lambda_{nominal}$, $\Lambda_{X\text{-}ray}$ is fitted to be 3.4% larger than $\Lambda_{nominal}$ with the standard deviation of 1.5Å. At the substrate position (2), the Fe and RE layer thicknesses

are expected to be 97% and 106% of the nominal values if the evaporation is from planer sources (See Table I). Even if $\Lambda_{nominal}$ is modified with these values, $\Lambda_{X\text{-}ray}$ is still larger than the modified period $\Lambda_{modified}$ by 2.5%. The discrepancy between $\Lambda_{X\text{-}ray}$ and $\Lambda_{modified}$ is thought to be caused by deviation of the tooling factors, of the evaporation mode from the planer evaporation mode, and/or of the densities from the bulk values, as well as errors in X-ray diffraction measurement. Notice that the nominal thickness is used in §3.2 when magnetization per unit volume is calculated.

3.1.2 Crystallographic structures of RE and Fe layers

In multilayers, the crystallographic structure of each layer depends on the combination of the metals, the substrates, the layer thicknesses, and the film growth conditions. The structures are sometimes different from those of bulk metals which are in the equilibrium states. The thickness dependence of the Nd layer structure in Fe/Nd multilayers was examined from X-ray diffraction patterns in the high angle region. Figure 9 shows the X-ray patterns when the Fe layer thickness is kept to be 39Å and the Nd thickness is varied from 10Å to 46Å. Peaks from the (110), (200), and (211) planes of bcc Fe appear at 2θ=45°, 65°, and 82°, respectively. No peak from the Nd layers is observed when the Nd layer thickness is smaller than 20Å. When the Nd layer is thicker

than 20Å, a broad peak is observed at around $2\theta=30^{\circ}$, where the peaks from bulk ABAC-type hexagonal Nd are expected to appear as indicated in the figure. The profile around $2\theta=30^{\circ}$ differs from the powder pattern of the hexagonal Nd: the maximum point does not coincide with the position of the (102) peak, which is the strongest peak in the powder pattern. For comparison, the X-ray diffraction patterns for thicker Nd layers are shown in Fig. 10. The Nd peak positions are consistent with the patterns in Fig. 9, and the profile is not the same as the powder pattern either. The peak at $2\theta=29.2^{\circ}$, which is expected from the ABAC-hexagonal structure but not from the ABAB stacking, is very weak. Existence of preferred orientation or stacking faults must be considered. Thus, the structure of the Nd layer is amorphous-like when the layer is thinner than about 20Å and polycrystalline when thicker than about 20Å. According to eq. (3), crystal grains of 20Å in size give an X-ray peak with the width of 4.3° at around $2\theta=30^{\circ}$. The X-ray resolution is too poor to discuss further about the crystallographic structure and orientation of the Nd layers.

Electron diffraction (ED) measurement gives better resolution than X-ray diffraction measurement. Cherifi *et al.* studied structures of Tb layers in Fe/Tb multilayers with electron microscopy and reported that the Tb layers consisted of two fcc phases which do not exist in the equilibrium states, while the nature of the two phases was uncertain.[67] Electron diffraction patterns for Fe/Nd multilayers are shown in Fig. 11. The plane spacing of the diffraction rings from the Nd layers is listed in Table II. The patterns are dependent on the Nd layer thickness. The multilayers with the Nd layers thinner than 20Å,

i.e. those giving amorphous-like Nd patterns in X-ray diffraction, show ring patterns from the Nd layers with very small grains. Although the ring pattern is similar to that of an fcc structure, it is not indexed with an fcc phase without allowing large displacement of the ring positions. When the Nd layers are thicker than 20Å, the pattern is similar to that of the ABAC-hexagonal structure. There is, however, a ring with the plane spacing 2.55Å, which is not expected from the ABAC-hexagonal structure. Possible origin of the diffraction ring is the (200) plane of an fcc structure. Mixture of the ABAC-hexagonal and fcc phases or existence of a stacking fault must be considered. The peak from the plane spacing 2.55Å was not observed in the X-ray patterns. Notice that the samples can be transformed by chemical effects during the sample preparation for electron microscopy or by annealing effects during the measurement. Identification of structures of RE layers is not easy even when the RE layers are much thicker.[64] The structures, including the degree of contamination, are thought to be dependent on the sorts of RE. The RE structures are not examined further in this work, while they possibly affect the magnetic properties of the Fe/RE multilayers.

The thickness dependence of the structures of the Fe layers is examined from the X-ray patterns in Fig. 12. Here, the Nd thickness is kept to be 7Å and the Fe layer thickness is varied. No peak from Fe is observed when the Fe layer thickness is smaller than about 20Å. That suggests that the structure of the Fe layers is amorphous-like. On the other hand, when the Fe layers are thicker than about 20Å, peaks from the (110), (200),

and (211) planes of bcc Fe are observed. For multilayers composed of bcc Fe layers and amorphous-like Nd layers, the (110) plane of bcc Fe is preferentially oriented in the film plane. For multilayers with bcc Fe and polycrystalline Nd layers, the orientation of the Fe crystal planes is almost random. In the latter multilayers, the Fe grain size estimated from the width of the Fe (110) peak is almost the same as the single Fe layer thickness. The structures of the Fe and Nd layers determined from X-ray diffraction, either polycrystalline or amorphous-like, are noted in Fig. 7.

The crystallographic structures of the Fe layers were also studied with ^{57}Fe Mössbauer spectroscopy. The spectra at 300K and 4.2K for Fe/Nd multilayers with the Fe layer thickness of 39Å are shown in Fig. 13. The major component of each spectrum is a sharp six-line pattern with the hyperfine field of 326±2kOe at 300K and 342±2kOe at 4.2K. This component is attributed to α-Fe which exists at the inner part of the Fe layer. Each spectrum is, however, not perfectly fitted with six Lorentzians but a minor component with smaller hyperfine fields exists beside the major component. The minor component is due to the Fe atoms in the vicinity of the interfaces (See §3.1.3 for the detail). Thus, the Fe layers of 39Å consist of α-Fe except at the interface region. For Fe/Nd multilayers with the Fe layer thickness of 13Å, the major component of each spectrum at 300K is a paramagnetic doublet (Fig. 14). The magnetic transition temperatures of the Fe layers are lower than or around room temperature, depending on the Nd layer thickness. The quadrupole splitting is estimated to be 0.45±0.03mm/sec. At 4.2K, the spectra are composed of six

broad lines, indicating a wide distribution of the hyperfine fields (Fig. 14). The broad line profile is a characteristic of amorphous ferromagnetic Fe alloys. The Mössbauer and X-ray results consistently suggest that the Fe layers with the thickness of 13Å have an amorphous structure. The hyperfine fields are appreciably larger than those in amorphous Fe-Nd alloys which are prepared by alternate deposition of monatomic Fe and Nd layers (Fig. 15) or coevaporation from two e-beam sources.[13] This fact suggests that the Fe layers are considered to be composed of chemically pure amorphous Fe. When the Fe layer thickness is 26Å, a paramagnetic component sometimes coexists with ferromagnetic components in the spectrum at 300K (Fig. 16). The ratio of the paramagnetic component is not perfectly reproducible, which means that the paramagnetic phase is somewhat unstable. At 4.2K, the paramagnetic component vanishes and the ratio of the ferromagnetic component with small hyperfine fields increases beside the major ferromagnetic six-lines (Fig. 16). The paramagnetic component disappears also after annealing (§3.1.5). These facts suggest that the paramagnetic component is due to an amorphous phase formed among bcc grains. The Fe thickness of 26Å seems to be near the critical thickness for crystallographic transformation from amorphous to bcc. The critical thickness probably depends on the preparation conditions, such as substrate temperatures, deposition energy, and residual gas. To explain the above-mentioned thickness dependence, amorphous-to-bcc transformation of Fe structures in the middle of the layer growth must be taken into consideration as discussed in §3.1.4.

The thickness dependence of Fe structures is qualitatively

the same for other Fe/RE systems although the critical thickness depends on the RE metals. Mössbauer spectra for [Fe(40Å)/RE(30Å)] and [Fe(40Å)/RE(10Å)] are shown later in Figs. 27-32. Each spectrum is fitted with two or three components, i.e. a major ferromagnetic, a minor ferromagnetic and an additional paramagnetic component. The paramagnetic component can be attributed to an amorphous phase which is in circumstances different from those of the interface component. The ratio of the component depends on the RE metals, and the quadrupole splitting is not exactly the same for all Fe/RE systems. Besides, in some multilayers, the component still exists at 4.2K with a very small hyperfine splitting. For Fe/Nd multilayers, the paramagnetic component is probably due to chemically pure amorphous Fe formed among α-Fe grains. For other Fe/RE multilayers, at the present stage, there is no sufficient evidence that the paramagnetic phase is chemically pure. There is a possibility that an amorphous alloy with the magnetic transition temperature lower than room temperature is formed at the interfaces in some Fe/RE systems.

3.1.3 Interface structures

Information on local crystallographic structures of Fe at the interface region is derived from Mössbauer spectra. Mössbauer spectra for Fe/Nd multilayers with the Nd layer thickness of 28Å

are shown in Fig. 17. As mentioned in the preceding section, when the Fe layer thickness is greater than 20Å, the spectrum consists of the major ferromagnetic component from α-Fe formed at the inner part of the Fe layers and the minor ferromagnetic component due to the Fe atoms in the vicinity of the interfaces. On the other hand, the spectra for multilayers with the Fe layers thinner than 20Å show a feature of amorphous Fe. The relative ratio of the interface component for the former multilayers was estimated on the basis of the fitted lines in Fig. 17, and the result is shown in Fig. 18. The Fe thickness corresponding to the interface component is about 8Å per single layer (per two interfaces) for the three multilayers, almost independent of the Fe layer thickness. This value is roughly the same as that for Fe/Dy multilayers.[27] The spectrum from the interface region is derived by subtracting the spectrum of α-Fe from the measured spectrum (Fig. 19). The S/N ratio is, however, not sufficient to discuss further about the interface structure.

In order to study microscopic crystal structures at the interfaces in detail, two [Fe(39Å)/Nd(28Å)] multilayers were prepared with ^{57}Fe (50%) enriched interfaces deposited at one side of each Fe layer. The samples were made with the sequence of ^{56}Fe(33Å)/^{57}Fe(6Å)/Nd(28Å) (Sample A) and Nd(28Å)/^{57}Fe(6Å)/^{56}Fe(33Å) (Sample B), as shown in Fig. 20. Mössbauer spectra at 300K for Samples A and B are shown in Fig. 21 (a). For both samples, the hyperfine field is distributed continuously with a maximum at 320kOe (Fig. 21 (b)). The component with the peak hyperfine field is attributed to the ^{57}Fe atoms adjacent to the ^{56}Fe layer, and the continuously distributed component with

smaller hyperfine fields is from those near to the Nd layer. In an ideal case, the enriched layer of 6Å consists of three Fe atomic layers. In the present case, the situation is not ideal and the spectrum cannot be fitted with a few sites. Possible origin of the reduction of the hyperfine field is formation of an amorphous Fe-Nd alloy due to intermixture and/or formation of chemically pure amorphous-like Fe at the interfaces, as well as intrinsic interface effects. The intermixture at the interfaces takes place only in two or less atomic layers, if it does. The spectra for Samples A and B are relatively similar if compared with the case of Fe/Sb[68] or Fe/Mn[69] interfaces. (Notice that the enriched layer is a little thicker in the present work.) However, Sample B has larger ratio of the component with the smaller hyperfine fields than Sample A has, which means that the Fe interface deposited on a Nd layer is chemically or crystallographically disarranged rather than the other interface. Interface magnetism is also discussed with the Mössbauer spectra of the ^{57}Fe enriched samples in §3.2.2.

3.1.4 Amorphous-to-bcc transformation in Fe layers

According to the Mössbauer spectra in Fig. 17, the Fe layers in [Fe(19Å)/Nd(28Å)] is amorphous and those in [Fe(26Å)/Nd(28Å)] have a bcc structure except at the interface region. To explain the thickness dependence of the Fe structures, amorphous-to-bcc

transformation in Fe layers in the middle of the layer growth must be taken into consideration. When an Fe layer is deposited on a Nd layer, it has an amorphous structure until the thickness reaches 19Å. If the Fe layer is covered with another Nd layer, the amorphous Fe layer is stabilized. If the layer is kept growing, the structure except at the interface region changes to bcc before the thickness reaches 26Å. According to the estimation in Fig. 18, the interface region of 9Å in [Fe(26Å)/Nd(28Å)] may have a structure other than bcc. Here, the contribution from the Fe interface deposited on a Nd layer is 7Å or less, since the contribution from the other interface is thought to be at least 2Å. Thus, at least 12Å (six atomic layers) of Fe must be transformed from amorphous to bcc in the middle of the layer growth, as illustrated in Fig. 22. The thickness of 26Å is near the critical thickness for the transformation, and the amorphous phase sometimes remains among crystallized α-Fe grains as observed in the Mössbauer spectra in Fig. 16. The transformation to α-Fe does not occur if the Fe layer is composed of amorphous Fe-Nd alloy unless negative diffusion takes place. Thus, the Fe layer of 19Å is mainly made up of chemically pure amorphous Fe. The transformation in Fe layers is also reported for Fe/Gd multilayers[70] and other nonepitaxial multilayers such as Fe/Mg and Fe/C.[71]

3.1.5 Annealing effects

Since multilayers are materials in non-equilibrium states, the structures are expected to change by heat treatment. Several Fe/Nd multilayers were annealed in 10^{-6}Torr at 200°C for 24 hours. The surface of the multilayers loses the luster when annealed in this condition. The periodicity is not destroyed in this annealing condition; the X-ray peaks due to an artificial period are clearly observed in the low angle region after the annealing. The peaks shift a little to lower angles, indicating an increase in the period by the annealing (Fig. 23). Since the low angle X-ray peaks are still sharp after the annealing, each bilayer must have increased its thickness by the same degree independently of the depth. The intensity of the 1st Bragg peak usually increases after the annealing. (Although peak intensity in the low angle region is sensitive to the measurement conditions.)

High angle X-ray patterns for some multilayers also change after the annealing. New peaks appear at 2θ=28° and 58° in the X-ray pattern for [Fe(39Å)/Nd(28Å)] (Fig. 24). The peaks are probably from the (222) and (444) planes of cubic Nd_2O_3, whereas the resolution is not sufficient to conclude it. On the other hand, no change is observed in the X-ray patterns for [Fe(26Å)/Nd(15Å)], which has amorphous-like Nd layers before annealed. In this multilayer, the Nd layers are amorphous or microcrystalline and the grain size is not sufficient to give X-ray peaks even if the Nd layers are oxidized. The peaks from Fe layers do not change much in both multilayers. As mentioned later, Mössbauer measurements show that the Fe layers are not oxidized after the annealing. Thus, the Nd layers are thought to

be selectively oxidized when the multilayers are annealed in this condition.

The depth profile of the multilayers was measured with Auger electron spectroscopy (AES) by sputtering the samples with Ar^+ ions. The intensity of the oxygen Auger peaks is stronger in the annealed samples. Before the sample is annealed, the oxygen peaks are marked only near the surface. This result indicates that oxidization of the prepared sample is not significant before it is annealed. (Note that the measurement was not performed *in situ*.) Further experiments are necessary to estimate the degree of the oxidization quantitatively. In a multilayer with the Fe and Nd layers thicker than the depth resolution of the Auger measurement, the intensity of the Fe and Nd peaks oscillates alternately as the sample is etched deeply. The intensity of the oxygen perks changes in phase with that of the Nd peaks. The Nd layers seem to be selectively oxidized throughout the sample. The Nd layers may be oxidized from the side of columnar grains, not sequentially from the layer near the surface. It has also been reported that selective oxidization of RE takes place in amorphous Fe-RE alloy films.[72)]

When Fe/Nd multilayers are annealed in an ultrahigh vacuum of 10^{-8}Torr range, they do not lose the luster and the X-ray peak at $2\theta=28^\circ$ appears very weakly (Fig. 24 (c)). Oxidization of the Nd layers is negligible in this annealing condition. An ultrahigh vacuum of 10^{-8}Torr is a necessary condition to avoid oxidization of the Nd layers while annealing. When Fe/Nd multilayers are annealed in air, the artificial periodicity is maintained as well. The X-ray peaks at $2\theta=28^\circ$ and 58° are also observed after

the annealing and the peaks from the Fe layers do not change. According to Mössbauer measurements, the Fe layers are not oxidized except for a multilayer with thick Fe layers, [Fe(200Å)/Nd(200Å)], where 14% of Fe is oxidized.

If Nd is oxidized to be cubic Nd_2O_3, the volume is expected to expand by 24%. In Fig. 23, the increment of the artificial periods is plotted versus the deposited Nd layer thickness. The increments are independent of the Nd layer thicknesses. In the multilayer annealed in an ultrahigh vacuum, there is only a little increase of the artificial period. The relation between the increase of the period and the oxidization is not clear enough at the present stage. The period may change in consequence of structural transformation at the interface region. The increase of the intensity of the 1st Bragg peak also can be explained with oxidization: the difference in electron density of the Fe and Nd layers increases when the Nd layers are oxidized.

Microscopic information about annealing effects on the Fe structures is given by Mössbauer spectra. Mössbauer spectra for [Fe(26Å)/Nd(10Å)] before and after annealing in a high vacuum are shown in Fig. 25. No component from iron oxides is observed in the spectra after the annealing. Multilayers with the Fe layer thickness of 26Å, such as [Fe(26Å)/Nd(10Å)], have three Mössbauer components at 300K before annealed. Changes of the three components with annealing give information on the nature of the components. The paramagnetic component, which is thought due to chemically pure amorphous-Fe formed among bcc Fe grains, disappears after the annealing. Instead, the relative intensity of

the ferromagnetic component from α-Fe increases. Thus, the amorphous phase is crystallized by the annealing. The crystallization occurs at 200°C or below. If the amorphous phase is composed of an Fe-Nd alloy, negative diffusion must take place during the annealing in order that the amorphous phase is transformed into pure α-Fe. The annealing result, therefore, supports the view that the amorphous phase is chemically pure. The minor ferromagnetic component from the interface region also decreases after the annealing. The spectra in Fig. 25, however, do not have sufficient resolution to discuss further about this component. To investigate the interface component in detail, the sample with ^{57}Fe enriched interfaces (Sample B) was annealed in an ultrahigh vacuum. The Mössbauer spectra at 300K before and after the annealing are shown in Fig. 26. After the annealing, the component with smaller hyperfine fields decreases. Since negative diffusion of Fe atoms from an Fe-Nd amorphous alloy is not likely to occur, the decreased component is thought to be due to chemically pure amorphous Fe formed at the interface region. Magnetic anisotropy also changes with annealing as observed in the Mössbauer spectra in Figs. 25 and 26, which is discussed in §3.2.5.

3.2 *Magnetic properties*

3.2.1 *Fe layer magnetization*

Iron layer magnetization was studied through magnetic hyperfine fields derived from Mössbauer spectra, since the hyperfine field is roughly proportional to the local magnetization. As discussed in §3.1.2, Fe layers in Fe/Nd multilayers are mainly composed of α-Fe when the layer thickness is larger than about 20Å. Each Mössbauer spectrum for these multilayers can be separated into two ferromagnetic components. The major component with the hyperfine field of 326±2kOe at 300K and 342±2kOe at 4.2K is attributed to α-Fe which exists at the inner part of the Fe layers. The minor component with smaller hyperfine fields is due to the Fe atoms at the interface region. (The interface magnetism is discussed in §3.2.3.) The Curie temperature for both components is much higher than room temperature. The temperature dependence of the magnitude of the hyperfine fields shows the same tendency for both components. The hyperfine field at 300K is smaller by 5% than that at 4.2K for the major component. The size effect of thin layers makes the decrease of the hyperfine fields larger than that in bulk α-Fe.

The magnitude of the hyperfine fields in Fe(40Å) layers is almost the same for all Fe/RE systems. Mössbauer spectra for [Fe(40Å)/RE(30Å)] and [Fe(40Å)/RE(10Å)] are shown in Figs. 27-32. Each spectrum is fitted with two or three components, i.e. a major ferromagnetic, a minor ferromagnetic, and an additional paramagnetic component. Both ferromagnetic components have the

Curie temperature much higher than room temperature; the temperature dependence of the magnitude of the hyperfine fields shows the same tendency for both components as observed in Fe/Nd multilayers. The paramagnetic component is attributed to an amorphous phase which is in different circumstances from those of the interface ferromagnetic component. The relative ratio of the paramagnetic component decreases at 4.2K, while it still exists with a very small hyperfine splitting in some multilayers. In Fe/Nd multilayers, the paramagnetic component is thought to be due to chemically pure amorphous Fe formed among α-Fe grains (See §3.1.5). In other Fe/RE multilayers, there is no sufficient evidence at the present stage that the paramagnetic phase is chemically pure.

For Fe/Nd multilayers with the Fe layer thickness smaller than 20Å, the Mössbauer spectra are mainly composed of a paramagnetic component at 300K, and of a ferromagnetic component with a wide distribution of hyperfine fields at 4.2K (Fig. 14). The broad line profile at 4.2K is a characteristic of amorphous ferromagnetic Fe alloys. The hyperfine fields are larger than those in amorphous Fe-Nd alloys; this is thought to be a feature of chemically pure amorphous Fe. The magnetic transition temperature (the Curie temperature for a paramagnet or the blocking temperature for a superparamagnet) of the Fe layers is lower than or around room temperature. The transition temperature depends on the Nd layer thickness even if the Fe layer thickness is the same (e.g. 13Å for the multilayers in Fig. 14). The temperature dependence of the average hyperfine field for [Fe(13Å)/Nd(15Å)] is shown in Fig. 33. The transition temperature

is about 310K. For Fe/Dy multilayers, the transition temperature of amorphous Fe layers is estimated to be 270K.[27)]

The transition temperatures are also dependent on the substrate temperatures. Three [Fe(13Å)/Nd(14Å)] multilayers were prepared at the substrate temperatures -50°C, 30°C, and 150°C. According to X-ray diffraction measurements, all the samples have well established artificial periodicity and amorphous-like Fe layers. The Mössbauer spectra at 300K indicate that the transition temperatures are different for the three samples (Fig. 34). The transition temperatures are thought to be dependent on the degree of intermixture at the interfaces, since the sample prepared at 150°C has the highest transition temperature and the smallest average hyperfine fields at 4.2K among the three samples (Fig. 34).

3.2.2 RE layer magnetization

Since Fe and RE (except Y, La, and Lu) are both magnetic elements, magnetization of Fe/RE multilayers is superposition of Fe and RE contributions. The RE layer magnetization is obtained if the Fe contribution is subtracted from the total magnetization. Temperature dependence of magnetization for [Fe(39Å)/Nd(10Å)] and [Fe(39Å)/Nd(46Å)] is shown in Fig. 35. An external field of 24kOe was applied parallel to the film plane, then the sample was cooled from 300K to 5.0K. The magnetization

is almost saturated in the applied field of 24kOe, while it still increases slightly in higher fields particularly at low temperatures. The magnetization values are expressed by magnetization per unit Fe volume (emu/Fe cm^3). (Note that the values have some errors mainly because of deviation of the Fe layer thickness from the nominal value (§3.1.1).) The broken line represents the magnetization expected in the Fe layers. The magnetization is assumed to be proportional to the average hyperfine field derived from Mössbauer measurements. Whereas the relation between the local magnetization and the hyperfine field at interfaces is not understood clearly, the temperature dependence of the hyperfine field is considered proportional to that of the local magnetization. Thus, the difference between the measured magnetization and the broken line is attributed to the contribution from Nd atoms. The Nd contribution is not zero even at 300K, although the Néel temperature of bulk Nd metal (20K) is much lower than 300K. The Nd magnetization is almost the same for the two samples above 100K, in spite of the 4.6 times difference in the Nd layer thicknesses. This result indicates that the Nd magnetization above 100K is caused mostly by the interface Nd atoms, and that it contributes parallel to the Fe layer magnetization. Below 100K, there is a significant difference in the magnetization between the two samples. The magnetization in [Fe(39Å)/Nd(46Å)] increases markedly with a decrease in temperature. This increase is attributed to the magnetization of the inner Nd atoms. The above-mentioned temperature dependence of the Nd layer magnetization is illustrated in Fig. 36. In [Fe(39Å)/Nd(10Å)], the contribution from the interface Nd atoms

gradually increases when the temperature decreases from 300K. The magnetization reaches the full value ($M_{Fe}+M_{Nd}$) at about 100K, and no more increase in magnetization is observed below 100K. In [Fe(39Å)/Nd(46Å)], the Nd atoms in the vicinity of the interfaces alone contribute to the Nd magnetization above 100K; the inner Nd atoms, which are paramagnetic above 100K, contribute additionally below 100K.

Possible origins of the ferromagnetic contribution from the interface Nd atoms are formation of ferromagnetic Fe-Nd alloy at the interfaces and intrinsic interface effects. As discussed in the next section, chemically pure Nd must contribute, more or less, to the interface Nd magnetization through interface effects. The transition temperature of the inner Nd is about 100K, which is higher than the Néel temperature of bulk Nd metal. It may be a feature of Nd metal which has another structure than the ABAC-hexagonal structure. The magnetization of the inner Nd atoms is not saturated to the full value. Bulk Nd metal, which is antiferromagnetic below 20K, has strong magnetocrystalline anisotropy.[73] The Nd layers in [Fe(39Å)/Nd(46Å)] are polycrystalline and each grain has its own magnetic easy direction through the magnetocrystalline anisotropy. Thus, it is difficult to align all the Nd magnetic moments at the inner part of the Nd layers to the same direction.

In order to study RE layer magnetization in all sorts of Fe/RE multilayers, temperature dependence of magnetization is measured for [Fe(40Å)/RE(30Å)] and [Fe(40Å)/RE(10Å)] in external fields of 12, 24, and 50kOe (Figs. 37-51). The experimental results on each system are discussed in the following:

(i) Fe/Y, Fe/La, and Fe/Lu multilayers

The magnetization of these multilayers increases monotonously with a decrease in temperature (Figs. 37, 38, and 51). Yttrium, La, and Lu are paramagnetic, and the contributions to the total magnetization are thought to be negligibly small. The magnetization of the six samples, however, does not coincide with each other. The result indicates a difference in the Fe layer magnetization. According to the Mössbauer spectra in Figs. 27-32, the Fe layers in these samples consist of a major ferromagnetic, a minor ferromagnetic, and an additional paramagnetic component (§3.2.1). The ratio of the three components differs among the three systems: for the Fe/La multilayers the third component is negligible, and for the Fe/Y and Fe/Lu multilayers the third component accounts for a larger ratio in [Fe(40Å)/RE(30Å)] than in [Fe(40Å)/RE(10Å)]. As a result the Fe layer magnetization estimated with the assumption that the average hyperfine field is proportional to the Fe layer magnetization differs among the six samples, as shown in the figures. The disagreement between the measured magnetization and the estimated Fe layer magnetization may be due to errors in estimation of the Fe layer magnetization. The M-T curves for the Fe/Y and Fe/Lu multilayers have an inflection point at about 250K, suggesting a magnetic transition of the third component.

(ii) Fe/Ce multilayers

In the Fe/Ce multilayers, it appears that Ce does not contribute to the magnetization within the experimental errors (Fig. 39). However, [Fe(40Å)/Ce(30Å)] shows a slight increase in

the magnetization below 20K, which suggests a possible magnetic order of the inner Ce atoms. The calculated full magnetization, which is expected when magnetic moments of trivalent Ce ions couple ferromagnetically with Fe magnetic moments, is shown in the figure.

(iii) Fe/Pr multilayers

Temperature dependence in magnetization for Fe/Pr multilayers is similar to that for Fe/Nd multilayers (Figs. 40 and 41). Bulk Pr metal has an ABAC-type hexagonal structure and is probably antiferromagnetic below 25K. The experimental results are explained likewise the case of Fe/Nd multilayers: the contribution from the interface Pr magnetic moments gradually increases with a decrease in temperature, and the inner Pr moments in [Fe(40Å)/Pr(30Å)] contribute additionally below 100K.

(iv) Fe/Sm multilayers

In the Fe/Sm multilayers, the Sm magnetization for the lowest *J* multiplet of the trivalent state is calculated to be small, as shown in Fig. 42. It cannot be concluded that the Sm layers contribute to the total magnetization because of the experimental errors. Unlike Fe/Nd and Fe/Pr systems, an increase of the magnetization due to a contribution from the inner Sm atoms is not observed in [Fe(40Å)/Sm(30Å)].

(v) Fe/Eu multilayers

Europium is in a divalent state in bulk metal. The divalent Eu has the same 4*f* electron configuration as Gd^{3+} and the

magnetic moments are expected to couple antiferromagnetically with Fe magnetic moments. The measured magnetization is smaller than the estimated Fe layer magnetization, and decreases with the temperature in a certain temperature range (Fig.43). These results indicate an antiferromagnetic contribution of the Eu magnetic moments on the total magnetization. The magnetization in 50kOe for [Fe(40Å)/Eu(30Å)] increases below the Néel temperature of bulk Eu metal (90K). The increase is thought to be a contribution from the inner Eu atoms. The M-T curves for [Fe(40Å)/Eu(30Å)] and [Fe(40Å)/Eu(10Å)] have different gradients above the Néel temperature. The reason is not clear at the present stage. The magnetization in 12, 24, and 50kOe for [Fe(40Å)/Eu(30Å)] is considerably different below the Néel temperature. The same feature is also observed in Fe/heavy RE systems as shown next.

(vi) Fe/Gd, Fe/Tb, Fe/Dy, Fe/Ho, Fe/Er, and Fe/Tm multilayers

Magnetization vs. temperature curves for these Fe/heavy RE systems show the same tendency (Figs. 44-49). For [Fe(40Å)/RE(10Å)], the measured magnetization is smaller than the estimated Fe layer magnetization; even at 300K for Fe/Gd and Fe/Tb systems. The magnetization decreases in a certain temperature range as the temperature is lowered. Above the magnetic transition temperature of bulk RE metal, the magnetization (per unit Fe volume) is almost the same for [Fe(40Å)/RE(10Å)] and for [Fe(40Å)/RE(30Å)]. These results indicate that the RE magnetic moments at the interfaces contribute to the magnetization antiparallel to the applied

field, and that the interface RE magnetization gradually increases with a decrease in temperature. The antiparallel alignment of the Fe and RE magnetization at the interfaces is confirmed for Fe/Dy multilayers by neutron diffraction measurements.[32] Magnetization for [Fe(40Å)/RE(30Å)] in 50kOe increases gradually below the magnetic transition temperature of bulk RE metal, suggesting that the RE magnetic moments at the inner part of the RE layers contribute to the total magnetization parallel to the applied field. In this temperature range, the magnetization in 12kOe is considerably smaller than that in 50kOe. Magnetic order of the inner RE moments makes the Fe layer magnetization difficult to be saturated in the direction of the applied field. The magnetic configuration is not simple below the Curie temperature of bulk RE metal, since the RE layers are expected to be ferromagnetic and the Fe and RE magnetic moments couple antiferromagnetically at the interfaces: the "aligned-Fe", "twisted", and "aligned-RE" structures[74] are expected to appear dependently on temperatures and magnetic fields, as reported for Fe/Gd multilayers.[36,44,52,61] In addition, large magnetocrystalline anisotropy in the RE layers must be taken into account for other Fe/heavy RE systems than Fe/Gd.

(vii) Fe/Yb multilayers

Ytterbium is nonmagnetic if it is divalent as in bulk metal. If it is in a trivalent state, magnetic contribution antiparallel to the Fe magnetization is expected to be observed. It cannot be concluded that the Yb magnetic moments in Fe/Yb multilayers contribute to the total magnetization because of the errors in

the magnetization measurements (Fig. 50). According to the Mössbauer measurements, the direction of the Fe magnetic moment in [Fe(40Å)/Yb(30Å)] shows the temperature dependent change (§3.2.5). Ytterbium may have a magnetic moment at the interfaces, since the interface Yb atoms are thought to be responsible for the magnetic anisotropy of the Fe layers.

In summery, the interface RE atoms in some Fe/RE systems contribute to the total magnetization even at temperatures higher than the magnetic transition temperature of bulk RE metal. The interface RE magnetization is parallel to the Fe layer magnetization in Fe/Pr and Fe/Nd multilayers, and antiparallel in Fe/Eu, Fe/Gd, Fe/Tb, Fe/Dy, Fe/Ho, Fe/Er and Fe/Tm multilayers. The coupling is explained with an exchange coupling between Fe and RE spins, which results in a ferromagnetic coupling between Fe and light RE magnetic moments and an antiferromagnetic coupling between Fe and heavy RE magnetic moments. For the above-mentioned nine Fe/RE systems, the total magnetization of [Fe(40Å)/RE(30Å)] increases gradually below a certain temperature, because of contribution from the RE magnetic moments at the inner part of the RE layers. In this temperature range, the magnetization of these [Fe(40Å)/RE(30Å)] multilayers gets difficult to be saturated. These tendencies are not observed in [Fe(40Å)/RE(10Å)]. The transition temperature of the inner RE moments is around the magnetic transition temperature of bulk RE metal for the Fe/Eu, Fe/Gd, Fe/Tb, Fe/Dy, Fe/Ho, Fe/Er and Fe/Tm systems. The transition temperature for the Fe/Pr and Fe/Nd systems is raised possibly because of a change of the RE crystal

structure from the bulk structure.

For Fe/heavy RE multilayers, it is not easy to obtain Fe and RE layer magnetization separately from M-T curves because of an antiferromagnetic coupling at the interfaces. Only when the magnetic structure is "aligned-Fe", the RE contribution is derived by subtraction of the Fe contribution from the measured magnetization. In order to separate Fe and RE layer magnetization when the Fe layer magnetization is not saturated, neutron diffraction measurements are performed for Fe/Dy multilayers with the method described in §2.5. A magnetic structure expressed with eq. (14) is assumed to analyze the data. Figure 52 shows the temperature dependence of average magnetization of the Fe and Dy layers for [Fe(40Å)/Dy(60Å)] in a field of 9.8kOe. As the temperature is lowered from 300K to 50K, the Fe layer magnetization decreases monotonously. The average Dy layer magnetization, on the other hand, increases gradually and changes its sign at about 110K. These features indicate an appearance of the "twisted structure" at low temperatures. The detail is discussed in ref. 32.

Magnetization for Fe/Dy multilayers in Fig. 46 is not saturated even in 50kOe, especially at lower temperatures. Magnetization curves (M-H curves) for [Fe(40Å)/Dy(40Å)] and [Fe(44Å)/Dy(12Å)] are measured in pulsed high magnetic fields up to 300kOe at 4.2K (Fig. 53). The magnetization is not saturated even in the high magnetic fields. That is due to strong local magnetic anisotropy in the Dy layers as well as an antiferromagnetic coupling between Fe and Dy magnetic moments at the interfaces.

From the magnetization and neutron diffraction measurements, the Dy magnetic moments at the inner part of the layers appear to be magnetically ordered below about 180K. According to ^{161}Dy Mössbauer measurements, however, the major part of the Dy moment in [Fe(15Å)/Dy(30Å)], which has amorphous Fe layers, is not magnetically ordered at 77K (Fig. 54).[37] The discrepancy suggests a superparamagnetic feature of the Dy magnetic moments in this sample.

3.2.3 *Interface magnetism*

Since interfaces have lower symmetry than the inside of the bulk, novel magnetic properties are expected to appear at the interfaces. The interface magnetism plays an important role in magnetic properties of multilayers. In this section, interface magnetism is discussed for Fe/RE multilayers with bcc Fe layers. Local magnetic properties at the interface Fe sites were studied by ^{57}Fe Mössbauer spectroscopy. As discussed in §3.1.3, Mössbauer spectra for Fe/Nd multilayers with the Fe layers greater than 20Å have a minor ferromagnetic component due to the interface Fe atoms besides a major ferromagnetic component from the inner Fe atoms. It is not easy to separate the two components, since the hyperfine fields are distributed continuously. With a rough estimation, the Fe thickness corresponding to the interface component is about 8Å per single Fe layer (per two interfaces),

and the average hyperfine field for the interface component is about 90% of that for the major component. The temperature dependence of the magnitude of the hyperfine fields shows the same tendency for both components; the Curie temperature of the interface component is much higher than room temperature. The magnitude of the hyperfine fields of the interface component is almost the same for all the Fe/RE multilayers in Figs. 27-32, where the Fe layer thickness is 40Å. The relative ratio of the interface component is a little dependent on the sort of RE: the smallest in the Fe/Eu system and the largest in the Fe/Tb system.

Mössbauer spectra for two [Fe(39Å)/Nd(28Å)] multilayers with ^{57}Fe enriched interfaces, Samples A and B in Fig. 20, furnish detailed information on interface magnetism (cf. §3.1.3). For both samples, the hyperfine field is distributed continuously with a maximum at 320kOe (Fig. 21). The component with the peak hyperfine field is attributed to the ^{57}Fe atoms adjacent to the ^{56}Fe layer, and the continuously distributed component with smaller hyperfine fields is from those near to the Nd layer. The enriched layer of 6Å consists of three Fe atomic layers in an ideal case. If the distribution of the hyperfine field is divided into three parts tentatively, the average hyperfine field for each portion is estimated to be 205kOe, 298kOe, and 319kOe for Sample A, and 121kOe, 251kOe, and 313kOe for Sample B. Possible origin of the reduction of the hyperfine field is formation of an amorphous Fe-Nd alloy due to intermixture and/or formation of chemically pure amorphous-like Fe at the interfaces, as well as intrinsic interface effects. When Sample B is annealed, the ratio of the component with smaller hyperfine fields decreases and the

distribution of the hyperfine fields becomes similar to that for non-annealed Sample A (Figs. 21 and 26). The annealing result indicates that chemically pure amorphous Fe, which is formed at the Fe interfaces on Nd layers and makes the ratio of the component with smaller hyperfine fields larger in Sample B than in Sample A, is crystallized by annealing (§3.1.5). Thus, the distribution of hyperfine fields in the spectrum for annealed Sample B is thought to be closer to that for an ideal Fe-Nd interface, although intermixture at the interface may take place in two or less atomic layers. The spin configuration at the interface region is discussed in §3.2.5 with Mössbauer spectra for Sample B.

Interface magnetism at the RE sites is summarized as follows (See §3.2.2). According to magnetization measurements, the interface RE atoms in some Fe/RE multilayers contribute to the total magnetization even at temperatures higher than the magnetic transition temperature of bulk RE metal. The interface RE magnetization is parallel to the Fe layer magnetization in Fe/Pr and Fe/Nd multilayers, and antiparallel in Fe/Eu, Fe/Gd, Fe/Tb, Fe/Dy, Fe/Ho, Fe/Er and Fe/Tm multilayers. Distribution of magnetization at the interface region was also studied with neutron diffraction measurements. The second term in eq. (14) represents interface magnetism. For [Fe(40Å)/Dy(60Å)], the neutron result indicates that the interface Dy atoms have magnetization antiparallel to the Fe layer magnetization.[32)]

For Fe/Nd multilayers with the Fe layer thickness of 39Å, the temperature dependent change in the average hyperfine field at the interface Fe sites (Fig. 13) is considerably smaller than

the change in the interface Nd magnetization (Fig. 35). The interface Fe and Nd atoms seem to be in different magnets. The interface RE magnetization is also observed in Fe/Eu multilayers, where Fe and Eu are immiscible. These results indicate that a ferro(ferri)magnetic amorphous Fe-RE alloy is not the principal origin of the interface RE magnetization. Intrinsic interface effects are, thus, thought to be the origin of the interface RE contribution. The exchange fields which originate from ferromagnetic Fe act at the interface RE sites and make the RE magnetic moments aligned. The crystal fields at the interface RE sites, which cause characteristic level splittings in the *J* multiplets of the RE atoms, may favor occurrence of magnetic order.[75] Interface magnetic anisotropy, which is one of the most attracting magnetic properties at the interfaces, is discussed in §3.2.5.

3.2.4 Magnetic coupling between Fe layers

Magnetic coupling between magnetic layers through an intervening nonmagnetic layer is an attractive subject in relation to giant magnetoresistance observed in multilayers.[5,6,10] In Fe/RE multilayers, the Fe layers can be coupled through a magnetically ordered RE layer. The magnetization and neutron measurements in §3.2.2 indicate that individual Fe layers in a Fe/RE multilayer cannot act independently at low temperatures for

some Fe/RE systems. If the intervening RE layer is composed of a well oriented single crystal, the direction of the Fe magnetic moments may be influenced by the RE layer thickness reflecting a long range magnetic structure of the RE metal. In the present study, the RE layers are generally polycrystalline with no preferred orientation, so that there is no guiding principle on the direction of the Fe magnetic moments. Magnetic coupling between the Fe layers in a temperature range where the inner RE is paramagnetic is also a subject to be investigated. When two magnetic layers are coupled antiferromagnetically through a nonmagnetic layer, the M-H curve shows little residual magnetization.[6,10] So far, no certain evidence for an antiferromagnetic coupling between Fe layers through a nonmagnetic RE layer is observed in M-H curves for Fe/RE multilayers. Note that residual magnetization may be reduced on account of magnetic anisotropy in some Fe/RE systems.

A multilayer composed of two kinds of magnetic layers with different coercive fields is useful to check existence of a magnetic (including ferromagnetic) coupling between the magnetic layers: if there is no coupling, the M-H curve shows a magnetization process with two magnetic components as observed in NiFe/Cu/Co/Cu multilayers.[11] One of the simplest methods to control the coercive fields of magnetic layers is changing the thicknesses of the magnetic layers, as is attempted for Co/Au/Co/Au multilayers.[76] In Fe/RE multilayers, an Fe layer thinner than about 20Å is paramagnetic at room temperature and it is not easy to make desirable Fe layers with different coercive fields. The coercive fields are also dependent on the

sorts of RE metal, for example 440 Oe for [Fe(40Å)/Tb(30Å)] and 30 Oe for [Fe(40Å)/Tm(30Å)] at 300K with in-plane magnetic fields. Thus, two kinds of Fe layers in a Tb/Fe/Tb/Tm/Fe/Tm multilayer, where the Fe layers are sandwiched between Tb layers or between Tm layers (Fig. 55), are expected to have different coercive fields. Three samples were prepared to study magnetic coupling between Fe layers through Tm and Tb layers:

Sample C, [Tb(15Å)/Fe(40Å)/Tb(15Å)/Tm(15Å)/Fe(40Å)/Tm(15Å)],

Sample D, [Tb(30Å)/Fe(40Å)/Tb(30Å)/Tm(30Å)/Fe(40Å)/Tm(30Å)],

Sample E, [Tb(30Å)/Fe(50Å)/Tb(30Å)/Tm(30Å)/Fe(50Å)/Tm(30Å)].

Magnetization process at 300K shows existence of two magnetic components for Samples D and E, and nearly a single component for Sample C (Fig. 56). The Fe layers are coupled strongly through Tb(15Å)/Tm(15Å) but not through Tb(30Å)/Tm(30Å) at 300K. The magnetization process for Sample D or E is simply illustrated in Fig. 57. Two magnetic components exist in the M-H curves for Sample E down to 100K, whereas the Fe layers seem to get less independent at low temperatures (Fig. 58). According to the discussion in §3.2.2, the Tb and Tm layers, except near interfaces, are magnetically ordered below about 230K and 60K respectively. Thus, the magnetic coupling between the Fe layers, which is weak above 60K, is expected to get stronger below 60K.

3.2.5 Magnetic anisotropy and spin reorientation

Multilayers often show characteristic magnetic anisotropy which is originated from interface effects, strain effects, and so forth. Some multilayers with perpendicular magnetic anisotropy are studied as promising candidates for magneto-optical recording media.[8,9] Magnetic anisotropy in Fe/RE multilayers has also been studied by several groups (most papers in refs. 16-63), while the origin of the magnetic anisotropy is still open for discussion. In this section, magnetic anisotropy in Fe/RE multilayers is examined from experimental results and possible origins of the magnetic anisotropy are discussed.

3.2.5(a) Iron spin directions from Mössbauer measurements

When a multilayer contains Fe atoms, ^{57}Fe Mössbauer spectroscopy is useful to study the magnetic anisotropy: the intensity ratio of magnetically split six-lines reflects the direction of the Fe magnetic moments. In Mössbauer spectra for Fe/Nd multilayers with the Fe layer thickness of 39Å, the intensity ratio of the six lines changes with the Nd layer thickness, while the distribution of the hyperfine fields is almost independent of the Nd thickness (Fig. 13). When the Nd thickness is greater than 20Å, the intensity ratio at 300K is 3:4:1:1:4:3, which means the direction of the Fe magnetic moment is parallel to the film plane. When the Nd thickness is smaller than 20Å, the ratio at 300K is approximately 3:1:1:1:1:3, suggesting that the average direction of the Fe magnetic moments is about 40° relative to the film normal. In this way, the direction of the Fe magnetic moment depends on the Nd layer thickness.

Mössbauer spectra at 4.2K for the same samples are also shown in Fig. 13. There is a notable difference in the intensity ratio of the six lines between the spectra at 300K and 4.2K. For the multilayers with the Nd layers thicker than 20Å, the intensity ratio is 3:4:1:1:4:3 at 300K and approximately 3:0.7:1:1:0.7:3 at 4.2K. The average direction of the Fe magnetic moments relative to the film normal changes from 90° to 30° when the temperature decreases from 300 to 4.2K. For the multilayers with the Nd layers thinner than 20Å, little temperature dependence is observed in the intensity ratio. The Fe magnetic moment is oriented to the perpendicular direction both at 300K and 4.2K. The temperature dependent change in the direction of magnetic moment is called "spin reorientation". Spin reorientation in multilayers is first reported for Fe/Dy multilayers,[27] and is also observed for other Fe/RE systems when the Fe and RE layer thicknesses are properly controlled (See the paragraph after next). Temperature dependence of the relative intensity of the Δm=0 (2nd and 5th) lines for [Fe(39Å)/Nd(28Å)] is shown in Fig 59. The direction of the Fe magnetic moment changes at about 200K. The spin reorientation temperature depends on both Fe and Nd layer thicknesses as shown in Fig. 60, where Fe/Nd multilayers are grouped into three according to the feature of the major component of the Mössbauer spectra.

Perpendicular Fe magnetic moment is also observed in Fe/Nd multilayers with the Fe layer thickness of 13Å, where the Fe layers consist of amorphous Fe. The spectra at 4.2K are composed of six broad lines with wide distribution of hyperfine fields (Fig. 14). For [Fe(13Å)/Nd(28Å)], a reasonable distribution of

hyperfine fields is obtained when the spectrum is fitted with an assumption that the direction of the Fe magnetic moment is 20° relative to the film normal (Fig. 17 (e)). The asymmetry in the measured spectrum is due to distribution of the isomer shift, which is neglected in the fitting for simplicity. The other samples in Fig. 14 also have similar distribution of hyperfine fields and the Fe magnetic moment is oriented to the perpendicular direction. The "magic angle" method is useful for more accurate determination of the distribution of the hyperfine fields and the direction of the Fe magnetic moments.[49)]

In order to study the role of RE on the magnetic anisotropy of Fe/RE multilayers, the direction of the Fe magnetic moment was examined for all the Fe/RE systems (Figs. 27-32). For [Fe(40Å)/RE(30Å)], where the Fe and RE layer thicknesses are chosen from the region where spin reorientation occurs in the Fe/Nd system, the Fe magnetic moment lies in the film plane at 300K independent of the sort of RE metal. In the Fe/Pr, Fe/Nd, Fe/Tb and Fe/Dy multilayers the Fe magnetic moment turns to the perpendicular direction when the temperature decreases; in the other multilayers, by contrast, the Fe magnetic moment remains in the film plane even at lower temperatures. For [Fe(40Å)/RE(10Å)], which has the same Fe layer thickness and thinner RE layers, the situation is more complicated. The Fe magnetic moment is oriented to the perpendicular direction even for the Fe/Eu multilayer as well as for the Fe/Pr, Fe/Nd, and Fe/Tb multilayers at both 300K and 4.2K. The Fe/Y, Fe/Gd, Fe/Ho, Fe/Er, Fe/Tm, and Fe/Lu multilayers show no indication of perpendicular magnetic anisotropy. For the Fe/La, Fe/Ce, and

Fe/Sm multilayers, the Fe magnetic moment is not perfectly in the film plane. The spin reorientation occurs in the Fe/Dy multilayer with the shift in the angle θ larger than that for [Fe(40Å)/Dy(30Å)]. In the Fe/Yb multilayer, the Fe magnetic moment turns in the opposite direction to that in the Fe/Dy multilayer. The average directions of the Fe magnetic moments estimated from Mössbauer spectra are summarized in Table III.

Thus, the direction of the Fe magnetic moment in Fe/RE multilayers is dependent on the sort of RE metal. This result indicates that the 4*f* electron orbital of RE is responsible for the magnetic anisotropy of the Fe layers. Besides, the direction is found to be dependent on the RE layer thickness. If the direction of the Fe magnetic moment is determined by competition between the volume anisotropy of the Fe layer and the magnetic anisotropy due to interface effects, the direction must be independent of the RE layer thickness. The result suggests existence of additional effects on the magnetic anisotropy. The thickness region where the spin reorientation occurs in Fe/Pr, Fe/Nd, Fe/Tb, and Fe/Dy multilayers is shown in Fig. 61.

The direction of Fe magnetic moment was also estimated for [Tb(30Å)/Fe(40Å)/Tb(30Å)/Tm(30Å)/Fe(40Å)/Tm(30Å)] and [Pr(30Å)/Fe(40Å)/Pr(30Å)/Tm(30Å)/Fe(40Å)/Tm(30Å)]. These multilayers have two kinds of Fe layers: one is sandwiched between Tb (or Pr) layers, and the other is sandwiched between Tm layers. If the direction of the Fe magnetic moment is determined simply by competition between the above-mentioned two anisotropies, the Fe magnetic moment sandwiched by Tb (or Pr) layers changes its direction at the temperature where the spin reorientation occurs

in [Fe(40Å)/Tb(30Å)] (or [Fe(40Å)/Pr(30Å)]). Thus, the magnetic structure illustrated in Fig. 62 is expected to appear in a certain temperature range. The average direction of the Fe magnetic moments was found to be 90° at 300K and 70° at 4.2K for the former multilayer, and 90° at 300K and 60° at 4.2K for the latter; the directions at 4.2K are significantly closer to the film plane than expected from the simple superposition of the directions in the Fe/Tb (or Fe/Pr) and Fe/Tm multilayers. Besides, the temperature where the spin reorientation occurs was lower than that for the Fe/Tb (or Fe/Pr) multilayer. Magnetic interaction between the Fe layers may have influence on the magnetic anisotropy, whereas the interaction through Tb(30Å)/Tm(30Å) does not appear to be strong down to 100K (See §3.2.4).

3.2.5(b) Magnetic anisotropy from magnetization measurements

Magnetic anisotropy of a multilayer as a whole was studied by magnetization measurements. Temperature dependence of magnetization for [Fe(39Å)/Nd(28Å)] in various magnetic fields parallel to the film plane is shown in Fig. 63. According to the Mössbauer measurements, the direction of the Fe magnetic moment in this multilayer changes at around 200K. The magnetization decreases below 150K when the in-plane applied field is sufficiently small. The decrease is ascribed to an increase of perpendicular anisotropy at low temperatures. Note that magnetization can decrease on account of an antiparallel configuration of the Fe and RE layer magnetization in the case of Fe/heavy RE multilayers (§3.2.2), even if there is no

perpendicular magnetic anisotropy.

Magnetic anisotropy constants were estimated for [Fe(39Å)/Nd(28Å)] from the M-H curves (Fig. 64) with the method described in §2.4. The estimated anisotropy constants are negative in all the temperature range, indicating that the multilayer has in-plane magnetic anisotropy (Fig. 65). Note that Mössbauer spectra measured in zero applied fields indicate that the Fe magnetic moment is oriented to the perpendicular direction below 200K. The absolute value of the anisotropy constant decreases with the temperature; the magnetic anisotropy grows to the perpendicular direction at lower temperatures. Torque curves for this sample also show that the easy axis is in the film plane at both 300K and 77K (Fig. 66). It is not easy to estimate the anisotropy constants from the torque curves, because the curves may be superposition of signals from different magnetic components, and the highest applied field of 20kOe is not sufficient to saturate the magnetization. For a rough estimation of the anisotropy constants, the curves were fitted with a single magnetic component with uniaxial anisotropy energy expressed by eq. (6). The estimated uniaxial anisotropy constant K_u is plotted in Fig. 65. Magnetic anisotropy constants were also estimated for [Fe(26Å)/Nd(28Å)], where the Fe layers are thinner so that perpendicular anisotropy is expected to be larger. The anisotropy constant K_u estimated from the M-H curves (Fig. 67) is turned positive at 140K (Fig. 68). In the torque curves, the phase at 77K is the opposite of that at 300K (Fig. 69). The curve at 77K indicates that the easy direction is about 20° relative to the film normal, and that the 4th and 6th order terms in eq. (6) are

not negligible in the uniaxial anisotropy energy. For comparison, anisotropy energy is estimated for [Fe(50Å)/Tm(15Å)], which shows no perpendicular anisotropy in Mössbauer spectra. Little temperature dependence is observed in the anisotropy constants, as shown in Fig. 70.

Directions of Fe and RE layer magnetization were separately obtained for Fe/Nd multilayers with combination of neutron diffraction and magnetization measurements,[62] or Mössbauer and magnetization measurements.[57] The results suggest that the direction of the Nd layer magnetization is closer to the film normal than that of the Fe layer magnetization, i.e. perpendicular magnetic anisotropy is stronger in the Nd layers than in the Fe layers. As discussed in §3.2.5(a), the magnetic anisotropy of the Fe layers is thought to be related to the 4*f* electron orbital of the RE. In the case of Fe/Nd multilayers, at around the temperature where the Fe spin reorientation occurs, the Nd magnetic moments at the inner part of the Nd layers are paramagnetic and those at the interfaces are magnetically ordered; the interface magnetization increases gradually with a decrease in temperature (§3.2.2). Thus, the 4*f* electron orbital of the interface RE atoms, not of the inner RE atoms, is thought to play an important role on the magnetic anisotropy of the Fe layers.

3.2.5(c) Iron spin directions at the interface region

Directions of the Fe magnetic moments at the interface region were studied with Mössbauer spectra for the ^{57}Fe enriched sample (Sample B). The temperature dependent change in the

Mössbauer spectra is shown in Fig. 71. The intensity ratio of the magnetically split six-lines shows that the Fe magnetic moments in this sample turn to the perpendicular direction at around 150K. In order to compare the directions of the Fe magnetic moments at different positions in the enriched layer, the intensity ratio of magnetically split six-lines was estimated for two different hyperfine fields: one is at the peak in the distribution and the other is 78% of the peak value. The former component is due to the ^{57}Fe atoms adjacent to the ^{56}Fe layer, and the latter is due to the ^{57}Fe atoms in the middle atomic layer of the enriched layer (See §3.2.3). The Fe magnetic moments for both components turn to the perpendicular direction at the same temperature. As mentioned in §3.2.5(c), the direction of the Fe layer magnetization forms a certain angle with that of the Nd layer magnetization. From the present result, the Fe-Fe ferromagnetic interaction at the interface region is strong enough to keep the Fe magnetic moments collinear. The direction of the Fe magnetic moments just adjacent to the Nd layer is difficult to determine, since the average hyperfine field is 38% of the peak value so that the six-line pattern overlaps with components with larger hyperfine fields.

Behavior of the interface Fe magnetic moments in applied fields was also studied with Mössbauer spectra for Sample B. The spectra at 5.0K in magnetic fields parallel to the film plane are shown in Fig. 72. When a large field is applied, all the Fe magnetic moments align parallel to the film plane ferromagnetically. An antiparallel component, which is observed in Fe/Tb multilayers,[59] dose not appear in this system. When the

field is reduced, the Fe magnetic moments turn gradually to the perpendicular direction. The Fe magnetic moments at the interface region are kept collinear even when an external field is applied.

3.2.5(d) Annealing effect on iron spin directions

As described so far, interface magnetic anisotropy is thought to contribute greatly to gross magnetic anisotropy of the Fe/RE multilayer. The interface anisotropy is expected to be dependent on the interface structure, which can be changed by annealing in appropriate conditions (§3.1.5). Directions of the Fe magnetic moments in Fe/Nd multilayers were estimated from Mössbauer spectra before and after annealing in 10^{-6}Torr at 200°C for 24 hours. For [Fe(39Å)/Nd(28Å)], the direction (relative to the film normal) at 300K is estimated to be 90° before the annealing and 40° after the annealing (Figs. 73 (a) and (b)). The annealing results for several Fe/Nd multilayers are shown in Fig. 74. Perpendicular magnetic anisotropy increases after the annealing in a certain thickness region.

The Nd layers are oxidized to some degree after annealed in this condition. The influence of the oxidization on the magnetic anisotropy was examined by annealing of [Fe(39Å)/Nd(28Å)] in air. The Nd layers are oxidized heavily after the annealing, and perpendicular magnetic anisotropy disappears coincidently (Fig. 73 (c)). Consequently, the oxidization itself is not the major origin of the increase in perpendicular anisotropy. According to the annealing result for the ^{57}Fe enriched sample (Sample B), the ratio of the interface component in the Mössbauer spectra decreases after annealing in 10^{-8}Torr, and perpendicular magnetic

anisotropy increases coincidently (Fig. 26). The result suggests that the change in the magnetic anisotropy is caused by reconstruction of the interface structure, such as crystallization of chemically pure amorphous Fe and negative diffusion of Fe atoms from an amorphous Fe-RE alloy (§3.1.5). Thus, perpendicular magnetic anisotropy in certain Fe/Nd multilayers increases when the interface structure is crystallographically or chemically improved by annealing.

3.2.5(e) Mechanism of the magnetic anisotropy

The origin of the perpendicular magnetic anisotropy observed in certain Fe/RE multilayers is discussed by several researchers. Sato suggested that the most important origin of the perpendicular magnetic anisotropy in Fe/Tb multilayers is Fe-Tb atomic pairs aligned at the interfaces.[21] Umemura *et al.* observed perpendicular magnetic anisotropy in Fe/Gd and Fe/Sm multilayers with oxidized RE layers, and suggested that the anisotropy is due to magnetoelastic effect in the Fe layers.[17,20] There is a proposition that the perpendicular magnetic anisotropy in Fe/RE multilayers originates from magnetic anisotropy in an amorphous Fe-RE alloy formed at the interfaces. In the present work, the 4*f* electron distribution of RE atoms is found to have influence on the magnetic anisotropy, so that the magnetic anisotropy cannot be explained with pure magnetic dipolar interaction associated with atomic pair ordering nor magnetoelastic anisotropy in the Fe layers. The results on annealing effects do not support the proposition that the magnetic anisotropy originates in an amorphous Fe-RE alloy. At the present stage,

microscopic structures of the Fe-RE interfaces is not clear enough to discuss the mechanism of the magnetic anisotropy in detail. There is, however, no doubt that interface magnetic anisotropy connected with the 4*f* electron distribution of RE atoms plays an important role on the perpendicular magnetic anisotropy.

For a phenomenological interpretation of the magnetic anisotropy and spin reorientation in an Fe/RE multilayer, a simple model is shown in Fig. 75. Here, the magnetic structure of an Fe/Nd multilayer at around the temperature where the spin reorientation occurs is taken into consideration (See Fig. 36). It is assumed that the Fe layer is a uniform ferromagnet with the magnetization M_{Fe}, and that the RE layer consists of interface ferromagnetic regions (xd_{RE} in thickness) with the magnetization M_{RE} and an inner paramagnetic region ($(1-x)d_{RE}$ in thickness). Note that the situation is more complicated when the inner RE is magnetically ordered, since the inner magnetic structure and anisotropy must be taken into account. The magnetic energy per unit volume is phenomenologically expressed with the following equation:

$$\begin{aligned} E=&-M_{Fe}H\sin\theta_{Fe}\times(d_{Fe}/\Lambda) \\ &-M_{RE}H\sin\theta_{RE}\times(xd_{RE}/\Lambda) \\ &-2\pi M_{Fe}{}^2\sin^2\theta_{Fe}\times(d_{Fe}/\Lambda) \\ &-2\pi M_{RE}{}^2\sin^2\theta_{RE}\times(xd_{RE}/\Lambda) \\ &+(K_1\sin^2\theta_{RE}+K_2\sin^4\theta_{RE}+K_3\sin^6\theta_{RE})\times(2/\Lambda) \\ &-2J'\cos(\theta_{Fe}-\theta_{RE})\times(2/\Lambda). \end{aligned} \qquad (15)$$

The 1st and 2nd terms represent the Zeeman energy of the Fe and RE layers. The 3rd and 4th terms are the volume anisotropy energy of the Fe and RE layers. For simplicity, the magnetocrystalline and magnetoelastic anisotropies are neglected, and the magnetostatic energy is expressed for an infinite layer with uniform magnetization. In real multilayers, the magnetostatic energy will be more complicated since magnetic domains may be formed in each layer and the shape of the layers may not be an ideal flat board. The 5th term is the interface anisotropy energy at the interface RE sites. The anisotropy is assumed to be uniaxial, since the RE layers are composed of polycrystalline RE grains and there is no special orientation of the crystal axes in the film plane. The constants K_1, K_2, and K_3 are dependent on temperature. The K_2, and K_3 terms must be taken into consideration to explain the canting angles of the Fe magnetic moment observed in the Mössbauer spectra and the shape of the torque curves. The 6th term is the exchange energy at the interface which couples the Fe and RE layer magnetization. In the absence of an external field, the direction of the Fe magnetization is determined by competition between the volume anisotropy of the Fe layer and the interface magnetic anisotropy, which originates in the interface RE sites and is connected with the Fe layer through the exchange coupling. If, for example, the term $K_1 \sin^2\theta_{RE}$ with positive K_1 is dominant in the interface anisotropy and the value of K_1 gets larger at lower temperatures, the Fe magnetic moment tends to be oriented to the perpendicular direction at low temperatures.

The most probable origin of the interface RE anisotropy is

single ionic anisotropy due to interaction between the crystal field and the 4*f* electrons, which is discussed for an ideal hexagonal (001) interface[38] and for an amorphous alloy-like interface.[46] At an ideal hexagonal interface site with C_{3v} symmetry, the crystal field Hamiltonian is expressed by the following equation:[77,78]

$$H_{CEF}=B_2^0O_2^0+B_4^0O_4^0+B_6^0O_6^0+B_6^6O_6^6+B_4^3O_4^3+B_6^3O_6^3. \quad (16)$$

Here, B_n^m are the crystal field parameters and O_n^m are the Steven's operators ($O_2^0=3J_z^2-J(J+1)$, etc.). The parameters B_n^m are connected with the crystal field at the site through parameters A_n^m and with the shape of the 4*f* electron orbital through $\langle r^n\rangle$ (the average of r^n over the radial part of the 4*f* wave function) and θ_n (the Steven's factors):[78]

$$B_n^m=A_n^m\langle r^n\rangle\theta_n. \quad (17)$$

The crystal field Hamiltonian expressed by eq. (17) leads to single ionic anisotropy of the following equation:[77]

$$E=K_1\sin^2\theta+K_2\sin^4\theta+K_3\sin^6\theta+K_4\sin^6\theta\cos6\phi$$
$$+K_5\cos\theta\sin^3\theta\cos3\phi+K_6\sin^3\theta(11\cos^3\theta-3\cos\theta)\cos3\phi. \quad (18)$$

The last two terms in eqs. (16) and (18) do not appear in a bulk hexagonal site with D_{3h} symmetry. Baczewski *et al.* pointed out that the B_2^0 term, which vanishes at the bulk site of an ideal hexagonal close-packed structure, is dominant at the interface

site.[38] If the other B_n^m are neglected, only the K_1 term is alive in eq. (18):

$$E=K_1\sin^2\theta$$
$$=-3J(J-1/2)B_2^0\sin^2\theta \quad (T=0K). \qquad (19)$$

Perpendicular magnetic anisotropy appears when the constant K_1 is positive. The sign of K_1 is determined by the sign of B_2^0, which is dependent on the sign of θ_2 if the crystal field is the same for all the Fe/RE interfaces. The Steven's factors θ_n for trivalent RE ions are shown in Table IV. According to the present study, perpendicular magnetic anisotropy is relatively strong in Fe/Pr, Fe/Nd, Fe/Tb, and Fe/Dy multilayers, in which the RE's have negative θ_2's. This result supports the proposition that the perpendicular magnetic anisotropy originates from the single ionic anisotropy. However, no perpendicular magnetic anisotropy is observed in Fe/Ho and Fe/Ce multilayers, although the RE's also have negative θ_2's. Furthermore, an Fe/Eu multilayer showed perpendicular magnetic anisotropy, although θ_2 is naught for both trivalent and divalent Eu. The problems in this proposition are as follows: (i) the interface structure in real multilayers is not with the ideal symmetry and probably depends on the Fe/RE systems, (ii) the valence may not be trivalent in certain RE's at the interface sites, (iii) the influence of the excited J multiplets must be considered in certain RE's, (iv) the effect of the conduction electrons on the crystal field is not clear enough in these metallic systems.

In conclusion, the interface magnetic anisotropy, which

reflects the 4f electron distribution of RE atoms, is considered as the principal origin of the perpendicular magnetic anisotropy observed in certain Fe/RE multilayers. However, this idea does not give an explanation for the magnetic anisotropy in Fe/Ce, Fe/Eu and Fe/Ho multilayers. Furthermore, the magnetic anisotropy in Fe/RE multilayers is dependent on the RE layer thickness even if the Fe layer thickness is the same. This result cannot be explained with the simple model in Fig. 75. An additional mechanism must be proposed to explain all the experimental results.

§4 Summary

Iron/rare earth multilayers were prepared by alternate deposition in ultrahigh vacuum. The artificial periodicity is well established even when the Fe or RE layer thickness corresponds to one atomic layer. When the Fe layer thickness is smaller than a certain critical thickness (about 20Å for the Fe/Nd system), the Fe layers are composed of amorphous Fe and the magnetic transition temperature is lower than room temperature. When the Fe layer thickness is greater than the critical thickness, the Fe layers are bcc polycrystalline and the Curie temperature is much higher than room temperature. The structure of the RE layers estimated from X-ray patterns also changes from amorphous-like to polycrystalline at a certain thickness (about 20Å for Nd layers). In some Fe/RE multilayers with bcc Fe layers, the interface RE atoms contribute to the total film magnetization at much higher temperatures than the transition temperature of bulk RE metal. The interface magnetization is parallel to the Fe layer magnetization in Fe/Pr and Fe/Nd multilayers, and antiparallel in Fe/Eu, Fe/Gd, Fe/Tb, Fe/Dy, Fe/Ho, Fe/Er, and Fe/Tm multilayers. For the above-mentioned nine Fe/RE systems, the RE magnetic moments at the inner part of the layers also contribute to the total film magnetization below a certain temperature. This temperature is around the magnetic transition temperature of bulk RE metal for the Fe/Eu, Fe/Gd, Fe/Tb, Fe/Dy, Fe/Ho, Fe/Er, and Fe/Tb systems, and higher than the bulk magnetic transition temperature for the Fe/Pr and Fe/Nd systems. For Fe/Pr, Fe/Nd, Fe/Eu, Fe/Dy and Fe/Tb multilayers, when the

Fe and RE layer thicknesses are properly controlled, the average direction of the Fe magnetic moments is oriented nearly perpendicular to the film plane. Temperature dependent change in the direction of the Fe magnetic moment (Fe spin reorientation) is distinctly observed in the Fe/Pr, Fe/Nd, Fe/Dy, and Fe/Tb systems. On the other hand, Fe/Y, Fe/Gd, Fe/Ho, Fe/Er, Fe/Tm and Fe/Lu multilayers show no indication of perpendicular magnetic anisotropy. Interface magnetic anisotropy, which reflects the 4*f* electron distribution of RE atoms, is considered as the principal origin of the perpendicular magnetic anisotropy in Fe/RE multilayers.

Acknowledgments

I would like to thank Prof. T. Shinjo for his direction and guidance during this study. Thanks are also due to Dr. N. Hosoito for his cooperation, and the researchers as follows:

Prof. Y. Endoh (Tohoku Univ.) for neutron measurement,

Dr. N. Nakayama (Kyoto Univ.)* for X-ray and ED,

Mr. H. Yamamoto (NEC Corp.) for torque measurement,

Mr. T. Okuyama (TOYOBO Corp.) for ICP and AES,

Mr. P. Kearney (Univ. of Arizona) for AES,

Mr. K. Yoden (Kyoto Univ.)** for Fe/DY multilayers,

Mr. S. Ogawa (Kyoto Univ.)** for Fe/Y and Fe/Tm multilayers,

Mr. N. Mima (Kyoto Univ.)** for electron diffraction.

*Present position: Yamaguchi Univ.

**graduated

In addition, I thank all the people in Prof. Shinjo's laboratory for their kind support to my work.

References

1) T. Shinjo and T. Takada: *Metallic Superlattices* (Elsevier, Amsterdam, 1987).

2) T. Shinjo: Surf. Sci. Rep. **12** (1991) 49.

3) M. B. Salamon, S. Sinha, J. J. Rhyne, J. E. Cunningham, R. W. Erwin, J. Borchers and C. P. Flynn: Phys. Rev. Lett. **56** (1986) 259.

4) C. F. Majkrzak, J. W. Cable, J. Kwo, M. Hong, D. B. McWhan, Y. Yafet, J. V. Waszczak and C. Vettier: Phys. Rev. Lett. **56** (1986) 2700.

5) P. Grünberg, R. Schreiber, Y. Pang, M. B. Brodsky and H. Sowers: Phys. Rev. Lett. **57** (1986) 2442.

6) S. S. P. Parkin, N. More and K. P. Roche: Phys. Rev. Lett. **64** (1990) 2304.
S. S. P. Parkin: Phys. Rev. Lett. **67** (1991) 3598.

7) H. Yamazaki, Y. Ajiro, N. Hosoito and T. Shinjo: J. Phys. Soc. Jpn. **60** (1991) 764.

8) P. F. Carcia, A. D. Meinhaldt and A. Suna: Appl. Phys. Lett. **47** (1985) 178.
P. F. Carcia: J. Appl. Phys. **63** (1988) 5066.

9) S. Hashimoto and Y. Ochiai: J. Magn. & Magn. Mater. **88** (1990) 211.

10) M. N. Baibich, J. M. Broto, A. Fert, F. Nguyen van Dau, F. Petroff, P. Etienne, G. Creuzet, A. Friederich and J. Chazelas: Phys. Rev. Lett. **61** (1988) 2472.

11) T. Shinjo and H. Yamamoto: J. Phys. Soc. Jpn. **59** (1990) 3061.

12) K. A. McEwen and S. W. Zochowski: J. Magn. & Magn. Mater. **90&91** (1990) 94.

13) R. C. Taylor, T. R. McGuire, J. M. D. Coey and A. Gangulee: J. Appl. Phys. **49** (1978) 2885.

14) P. Chaudhari, J. J. Cuomo and R. J. Gambino: Appl. Phys. Lett. **22** (1973) 337.

15) T. Suzuki: J. Magn. & Magn. Mater. **50** (1985) 265.

16) T. Morishita, Y. Togami and K. Tsushima: J. Phys. Soc. Jpn. **54** (1985) 37.

17) S. Umemura, H. Tajika, E. Kita and A. Tasaki: IEEE Trans. Magn. **MAG-21** (1985) 1942.

18) T. Morishita, Y. Togami and K. Tsushima: J. Magn. & Magn. Mater. **54-57** (1986) 789.

19) N. Sato: J. Appl. Phys. **59** (1986) 2514.

20) S. Umemura, H. Tajika, E. Kita and A. Tasaki: Adv. Ceramics **16** (1986) 621.

21) N. Sato and K. Habu: J. Appl. Phys. **61** (1987) 4287.

22) D. J. Sellmyer, Z. R. Zhao, Z. S. Shan and S. Nafis: J. Appl. Phys. **61** (1987) 4323.

23) N. Hosoito, K. Yoden and T. Shinjo: Hyp. Int. **41** (1988) 583.

24) H. Yamamoto, M. Tanaka and M. Naoe: J. Appl. Phys. **63** (1988) 3212.

25) T. E. Tiwald, J. A. Woollam and D. J. Sellmyer: J. Appl. Phys. **63** (1988) 3215.

26) Z. S. Shan, S. Nafis, K. D. Aylesworth and D. J. Sellmyer: J. Appl. Phys. **63** (1988) 3218.

27) K. Yoden, N. Hosoito, K. Kawaguchi, K. Mibu and T. Shinjo:

Jpn. J. Appl. Phys. **27** (1988) 1680.

28) Z. S. Shan and D. J. Sellmyer: J. Appl. Phys. **64** (1988) 5745.

29) K. Yamauchi, K. Habu and N. Sato: J. Appl. Phys. **64** (1988) 5748.

30) M. Piecuch, L. T. Baczewski, J. Durand, G. Marchal, P. Delcroix and H. Nabli: J. de Phys. **49** (1988) C8-1755.

31) N. Hosoito, K. Yoden, K. Mibu and T. Shinjo: J. de Phys. **49** (1988) C8-1777.

32) N. Hosoito, K. Yoden, K. Mibu, T. Shinjo and Y. Endoh: J. Phys. Soc. Jpn. **58** (1989) 1775.

33) K. Mibu, N. Hosoito and T. Shinjo: J. Phys. Soc. Jpn. **58** (1989) 2916.

K. Mibu, N. Hosoito and T. Shinjo: Hyp. Int. **54** (1990) 831.

34) S. Honda, S. Nishimura and T. Kusuda: IEEE Trans. Magn. **25** (1989) 4027.

35) G. Choe and R. M. Walser: IEEE Trans. Magn. **25** (1989) 4033.

G. Choe and R. M. Walser: J. Appl. Phys. **67** (1990) 5686.

36) Y. Kamiguchi, Y. Hayakawa, and H. Fijimori: Appl. Phys. Lett. **55** (1989) 1918.

37) T. Shinjo, K. Yoden, N. Hosoito, J.-P. Sanchez and J.-M. Friedt: J. Phys. Soc. Jpn. **58** (1989) 4255.

38) L. T. Baczewski, M. Piecuch, J. Durand, G. Marchal and P. Delcroix: Phys. Rev. **B40** (1989) 11237.

39) T. Shinjo, K. Mibu, S. Ogawa and N. Hosoito: Mat. Res. Soc. Symp. Proc. **151** (1989) 87.

40) L. T. Baczewski, M. Piecuch, J. Durand, G. Marchal and P. Delcroix: J. Magn. & Magn. Mater. **83** (1990) 67.

41) C. Ferrater, B. Martinez, F. Badia, R. Ribas, A. Lousa and J. Tejada: J. Magn. & Magn. Mater. **83** (1990) 69.

42) F. Badia, C. Ferrater, A. Lousa, B. Martinez, A. Labarta and J. Tejada: J. Appl. Phys. **67** (1990) 5652.
F. Badia, C. Ferrater, B. Martinez, A. Lousa and J. Tejada: J. Magn. & Magn. Mater. **93** (1991) 429.

43) Z. S. Shan and D. J. Sellmyer: J. Appl. Phys. **67** (1990) 5713.

44) H. Fujimori, Y. Kamiguchi and Y. Hayakawa: J. Appl. Phys. **67** (1990) 5716.

45) Z. S. Shan and D. J. Sellmyer: Phys. Rev. **B42** (1990) 10433.

46) Z. S. Shan, D. J. Sellmyer, S. S. Jaswal, Y. J. Wang and J. X. Shen: Phys. Rev. **B42** (1990) 10446.

47) F. Baudelet, E. Dartyge, G. Krill, J. P. Kappler, C. Brouder, M. Piecuch and A. Fontaine: J. Magn. & Magn. Mater. **93** (1991) 539.
F. Baudelet, E. Dartyge, A. Fontaine, C. Brouder, G. Krill, J. P. Kappler and M. Piecuch: Phys. Rev. **B43** (1991) 5857.

48) R. Żuberek, H. Szymczak, R. Krishnan and T. Morishita: J. Magn. & Magn. Mater. **93** (1991) 449.

49) B. Scholz, R. A. Brand, W. Keune, U. Kirschbaum, E. F. Wassermann, K. Mibu and T. Shinjo: J. Magn. & Magn. Mater. **93** (1991) 499.

50) K. Cherifi, C. Dufour, M. Piecuch, A. Bruson, Ph. Bauer, G. Marchal and Ph. Mangin: J. Magn. & Magn. Mater. **93** (1991) 609.

51) Y. J. Wang and W. Kleemann: Phys. Rev. **44** (1991) 5132.

52) K. Cherifi, C. Dufour, Ph. Bauer, G. Marchal and Ph.

Mangin: Phys. Rev. **B44** (1991) 7733.

K. Cherifi, C. Dufour, G. Marchal, Ph. Mangin and J. Hubsch: J. Magn. & Magn. Mater. **104-107** (1992) 1833.

53) J. Tejada, F. Badia, B. Martinez and J. M. Ruiz: J. Magn. & Magn. Mater. **101** (1991) 181.

54) R. D. Kirby, J. X. Shen, Z. S. Shan and D. J. Sellmyer: J. Appl. Phys. **70** (1991) 6200.

55) F. Badia, M. A. Badry, X. X. Zhang, J. Tejada, R. A. Brand, B. Scholz and W. Keune: J. Appl. Phys. **70** (1991) 6206.

56) H. Hoffmann and G. Endl: J. Appl. Phys. **70** (1991) 6230.

57) N. Hosoito, K. Mibu, T. Shinjo and W. Keune: Hyp. Int. **68** (1991) 337.

58) K. Mibu, N. Hosoito and T. Shinjo: Hyp. Int. **68** (1991) 341.

59) B. Scholz, R. A. Brand and W. Keune: Hyp. Int. **68** (1991) 409.

B. Scholz, R. A. Brand and W. Keune: J. Magn. & Magn. Mater. **104-107** (1992) 1889.

60) F. Pierre, P. Boher, Ph. Houdy, J. Ferré, G. Pénissard, V. Grolier, J. Teillet and A. Fnidiki: J. Magn. & Magn. Mater. **104-107** (1992) 1033.

61) M. Nawate, H. Kiriake, K. Doi, S. Honda and T. Kusuda: J. Magn. & Magn. Mater. **104-107** (1992) 1861.

62) N.Hosoito, K.Mibu, T.Shinjo and Y.Endoh: J. Phys. Soc. Jpn. **61** (1992) 2477.

63) C. Dufour, M. Vergnat, K. Cherifi, G. Marchal, Ph. Mangin and C. Vettier: Physica **B180&181** (1992) 489.

64) M. Gasgnier: Phys. Status Solidi **a 57** (1980) 11.

65) N. Nakayama, I. Moritani, T. Shinjo, Y. Fujii and S.

Sasaki: J. Phys. **F18** (1988) 429.

66) S. Ohnishi, A. J. Freeman and M. Weinert: Phys. Rev. **B28** (1983) 6741.

67) K. Cherifi, P. Donovan, C. Dufour, Ph. Mangin and G. Marchal: Phys. Status Solidi **a 122** (1990) 311.

68) T. Shinjo, N. Hosoito, K. Kawaguchi, T. Takada, Y. Endoh, Y. Ajiro and J. M. Friedt: J. Phys. Soc. Jpn. **52** (1983) 3154.

69) N. Nakayama, T. Katamoto and T. Shinjo: J. Phys. **F18** (1988) 935.

70) J. Landes, Ch. Sauer, B. Kabius and W. Zinn: Phys. Rev. **B44** (1991) 8342.

71) T. Shinjo: Struct. Chem. **2** (1991) 281.

72) R. B. van Dover, E. M. Gyorgy, R. P. Frankenthal, M. Hong and D. J. Siconolfi: J. Appl. Phys. **59** (1986) 1291.

73) B. Lebech and B. O. Rainford: J. de Phys. **32** (1971) C-1370.

74) R. E. Camley and D. R. Tilley: Phys. Rev. **B37** (1988) 3413. R. E. Camley: Phys. Rev. **B39** (1989) 12316.

75) P. Fulde: *Handbook on the Physics and Chemistry of Rare Earths* (edited by K. A. Gschneidner, Jr. and L. Eyring, North-Holland, Amsterdam, 1979), vol. 2, Chap. 17.

76) C. Dupas, P. Beauvillain, C. Chappert, J. P. Renard, F. Trigui, P. Veillet, E. Vélu and D. Renard: J. Appl. Phys. **67** (1990) 5680.

77) Š. Zajac: Physica **B86-88** (1977) 51.

78) M. T. Hutchings: Solid State Phys. **16** (1966) 227.

Table I. Distribution of Fe and RE layer thicknesses (relative to the designed layer thicknesses).

		Calculated value		Experimental value	
		Evaporation from a point source	Evaporation from a planer source	ICP (Fe/Nd multilayer)	Magnetization of pure Fe films
Substrate (1)	Fe layer	−8%	−9%	−	−7%
	RE layer	−3%	−5%	−	−
Substrate (2)	Fe layer	−5%	−3%	−	−
	RE layer	+5%	+6%	−	−
Substrate (3)	Fe layer	+1%	+5%	−	+8%
	RE layer	+2%	+2%	−	−
The center of the polyimide substrate	Fe layer	−2%	±0%	−2%	+6%
	RE layer	+1%	±0%	+2%	−

Table II. Plane spacing of the diffraction rings from the Nd layers.

[Fe(39Å)/Nd(7Å)]	[Fe(39Å)/Nd(10Å)]	[Fe(39Å)/Nd(28Å)]	[Fe(39Å)/Nd(46Å)]
		3.20Å strong	3.18Å strong
3.02Å strong	3.08Å strong		
		2.79Å	2.85Å
2.52Å strong	2.56Å strong	2.55Å	2.55Å
		1.95Å	1.91Å
1.61Å weak	1.60Å weak	1.66Å	1.65Å
1.48Å	1.49Å	1.46Å weak	1.58Å weak
		1.25Å weak	1.25Å weak
			1.11Å weak

Table III. The average directions of the Fe magnetic moments relative to the film normal for [Fe(40Å)/RE(30Å)] and [Fe(40Å)/RE(10Å)] at 300K and 4.2K.

	[Fe(40Å)/RE(30Å)]		[Fe(40Å)/RE(10Å)]	
	300K	4.2K	300K	4.2K
Fe/Y, Fe/Gd, Fe/Ho Fe/Er, Fe/Tm, Fe/Lu	90°	90°	90°	90°
Fe/La, Fe/Ce, Fe/Sm	90°	90°	60~70°	60~70°
Fe/Yb	90°	90°	50°	60°
Fe/Eu	90°	90°	40°	40°
Fe/Dy	90°	70°	80°	40°
Fe/Pr, Fe/Nd, Fe/Tb	90°	30~40°	40°	30~40°

Table IV. Steven's factors for trivalent RE ions. (After K. H. W. Stevens: Proc. Phys. Soc. (London) **A65** (1952) 209.)

	θ_2	θ_4	θ_6
	$\times 10^{-2}$	$\times 10^{-4}$	$\times 10^{-6}$
Ce^{3+}	-5.71	63.5	0.
Pr^{3+}	-2.10	-7.35	61.0
Nd^{3+}	-0.643	-2.91	-38.0
Pm^{3+}	0.771	4.08	60.8
Sm^{3+}	4.13	25.0	0.
Eu^{3+}	0.	0.	0.
Gd^{3+}	0.	0.	0.
Tb^{3+}	-1.01	1.22	-1.12
Dy^{3+}	-0.635	-0.592	1.03
Ho^{3+}	-0.222	-0.333	-1.30
Er^{3+}	0.254	0.444	2.07
Tm^{3+}	1.01	1.63	-5.60
Yb^{3+}	3.17	-17.3	148.

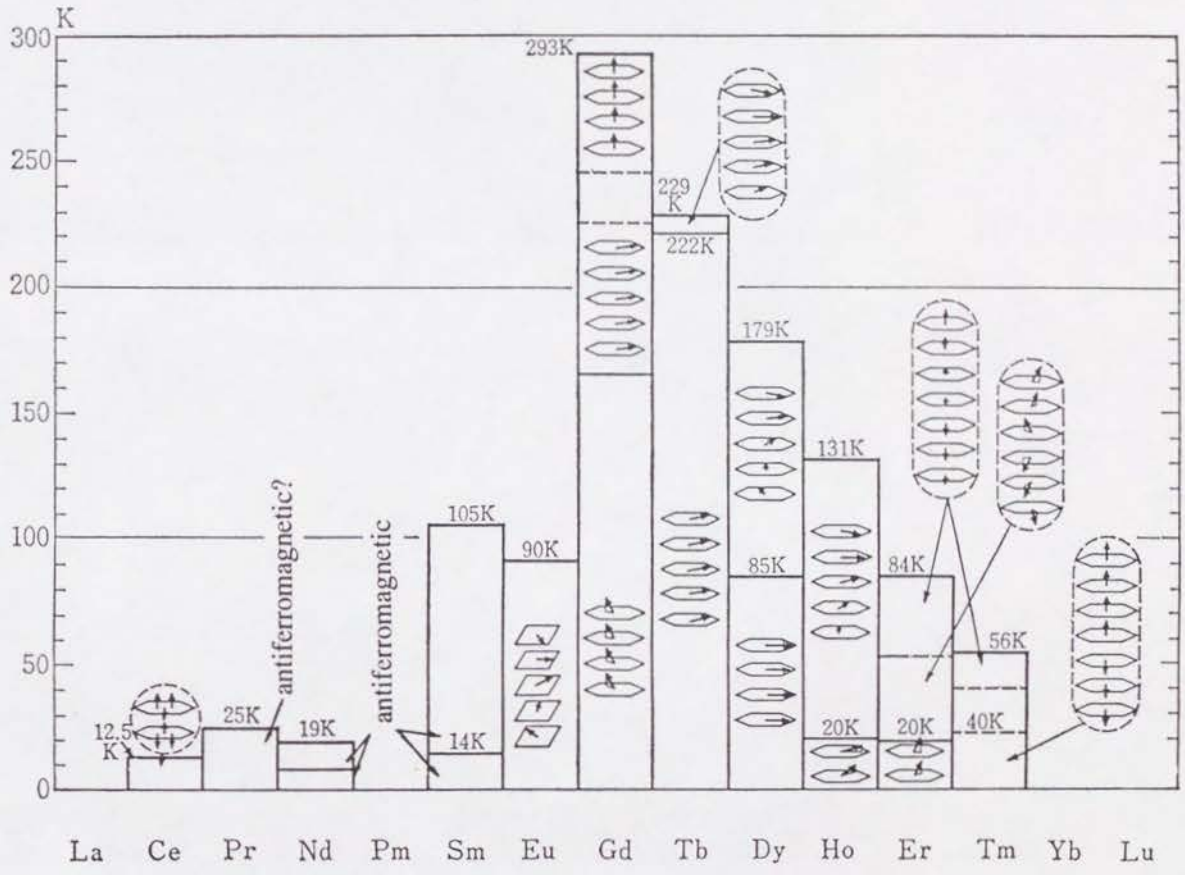

Fig. 1. Magnetic structures of bulk RE metals. (After R. M. Bozorth and C. D. Graham, Jr.: General Electric Report 66-C-225 (1966).)

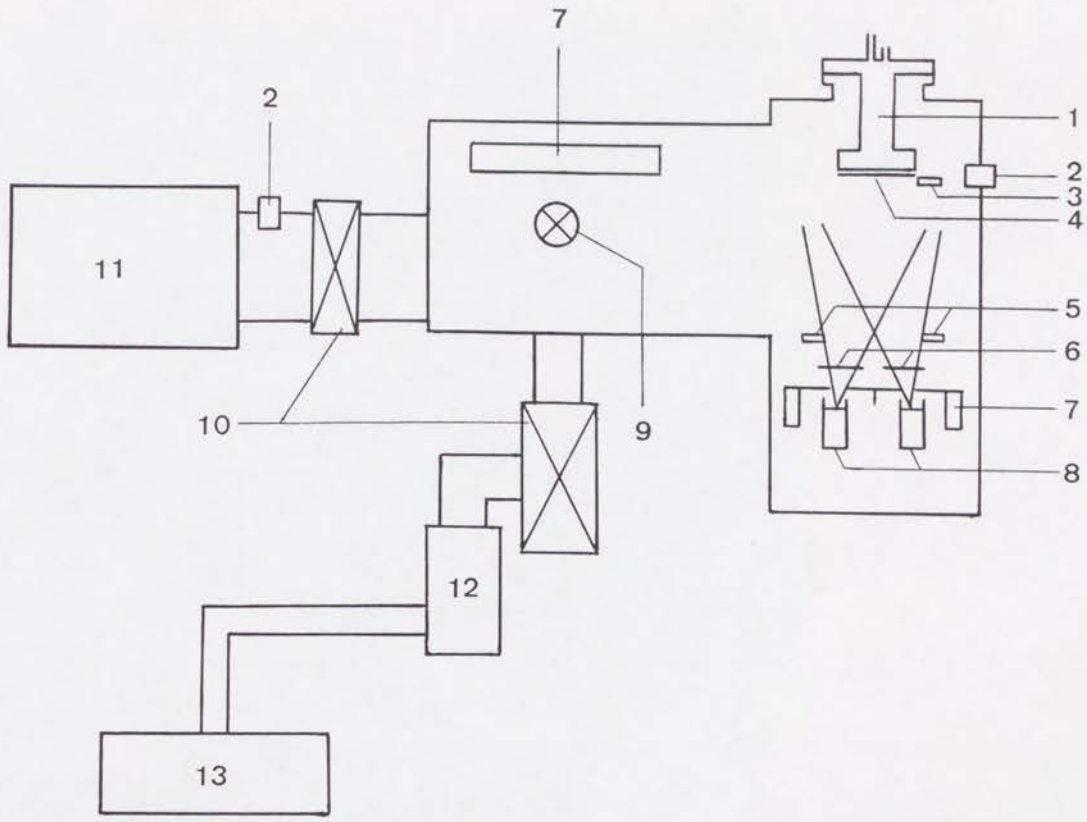

1. Substrate holder
2. Vacuum gauge
3. Controlling thickness monitor
4. Substrate
5. Thickness monitor
6. Shutter
7. Liquid N_2 vessel
8. Electron beam gun
9. Air inlet valve
10. Gate valve
11. Cryopump
12. Turbo-molecular pump
13. Rotary pump

Fig. 2. Schematic view of the deposition system.

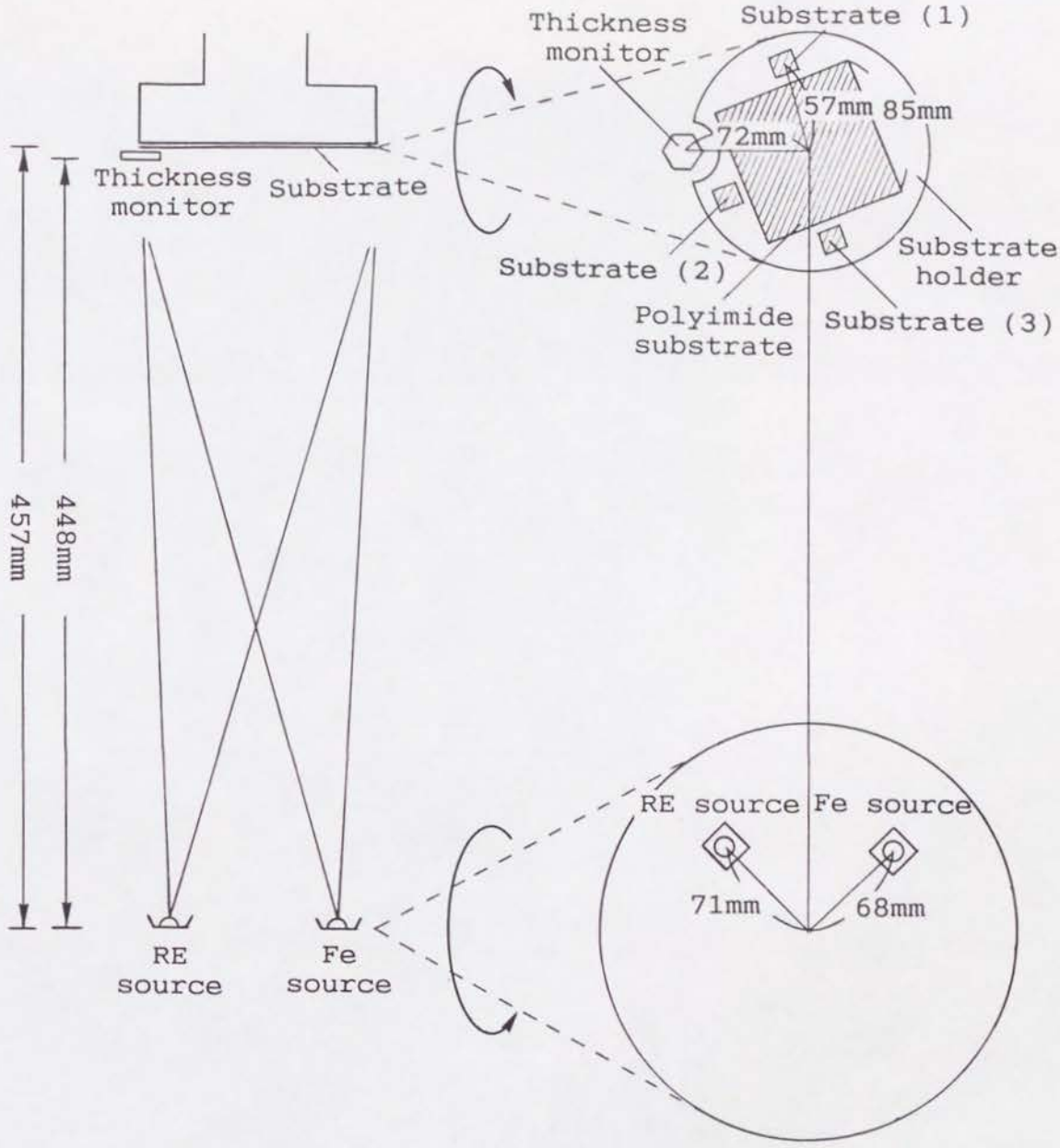

Fig. 3. Geometrical positions of the substrates, the crucibles, and the thickness monitor.

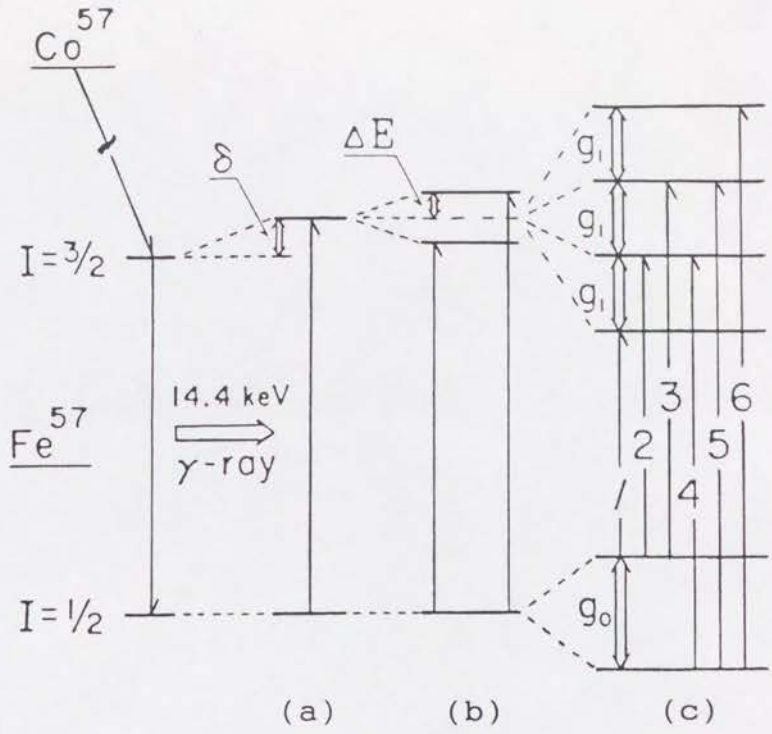

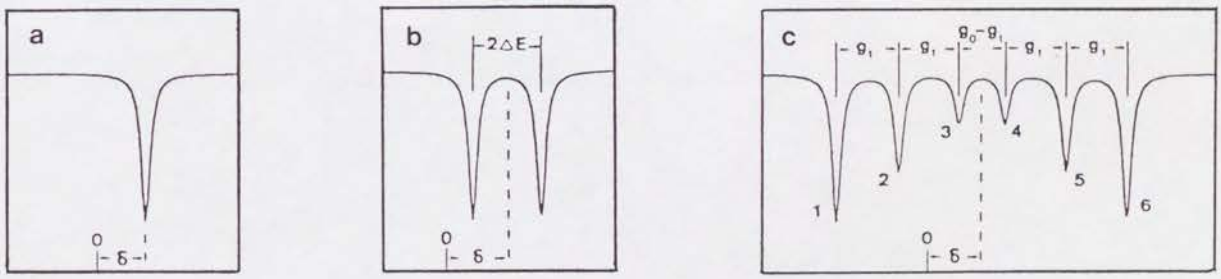

Velocity (mm/sec)

Fig. 4. Schematic diagram of the energy levels of ^{57}Fe nuclei and the corresponding Mössbauer spectra.

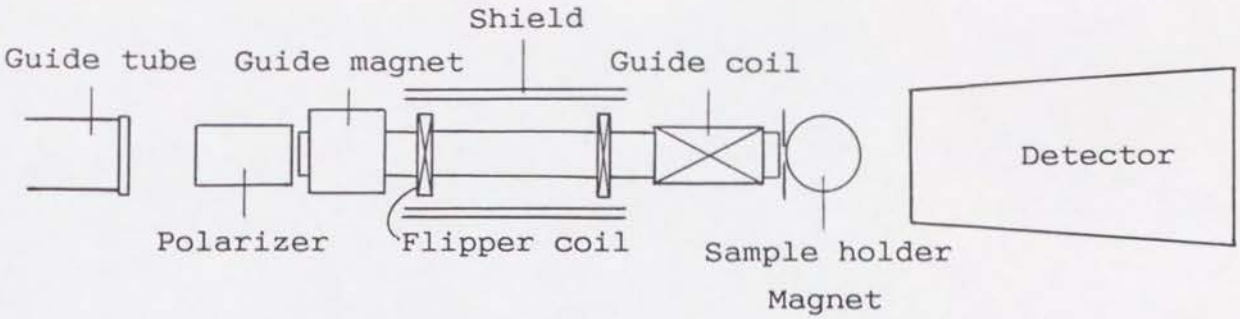

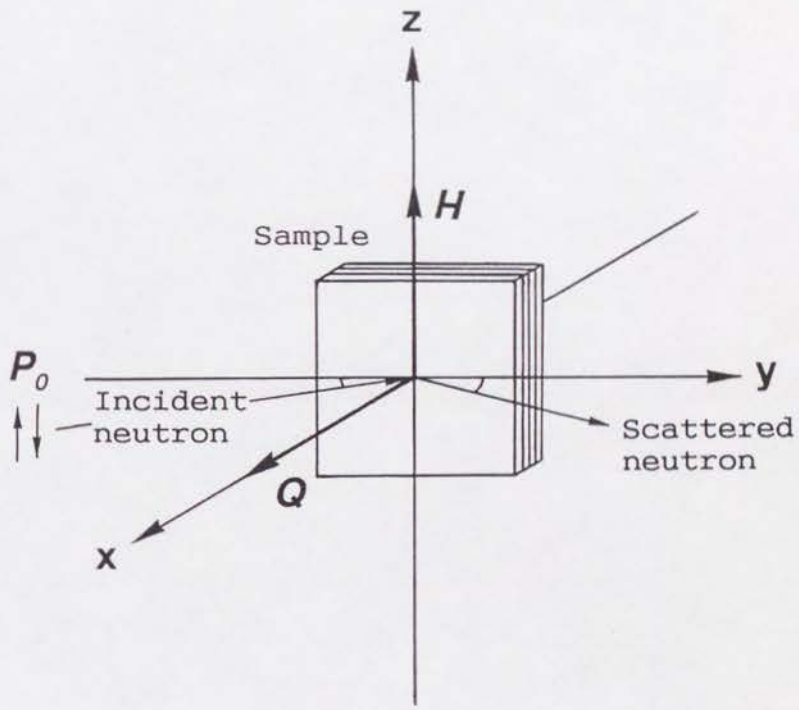

Fig. 5. Apparatus for neutron diffraction measurement (TOP), and the experimental geometry.

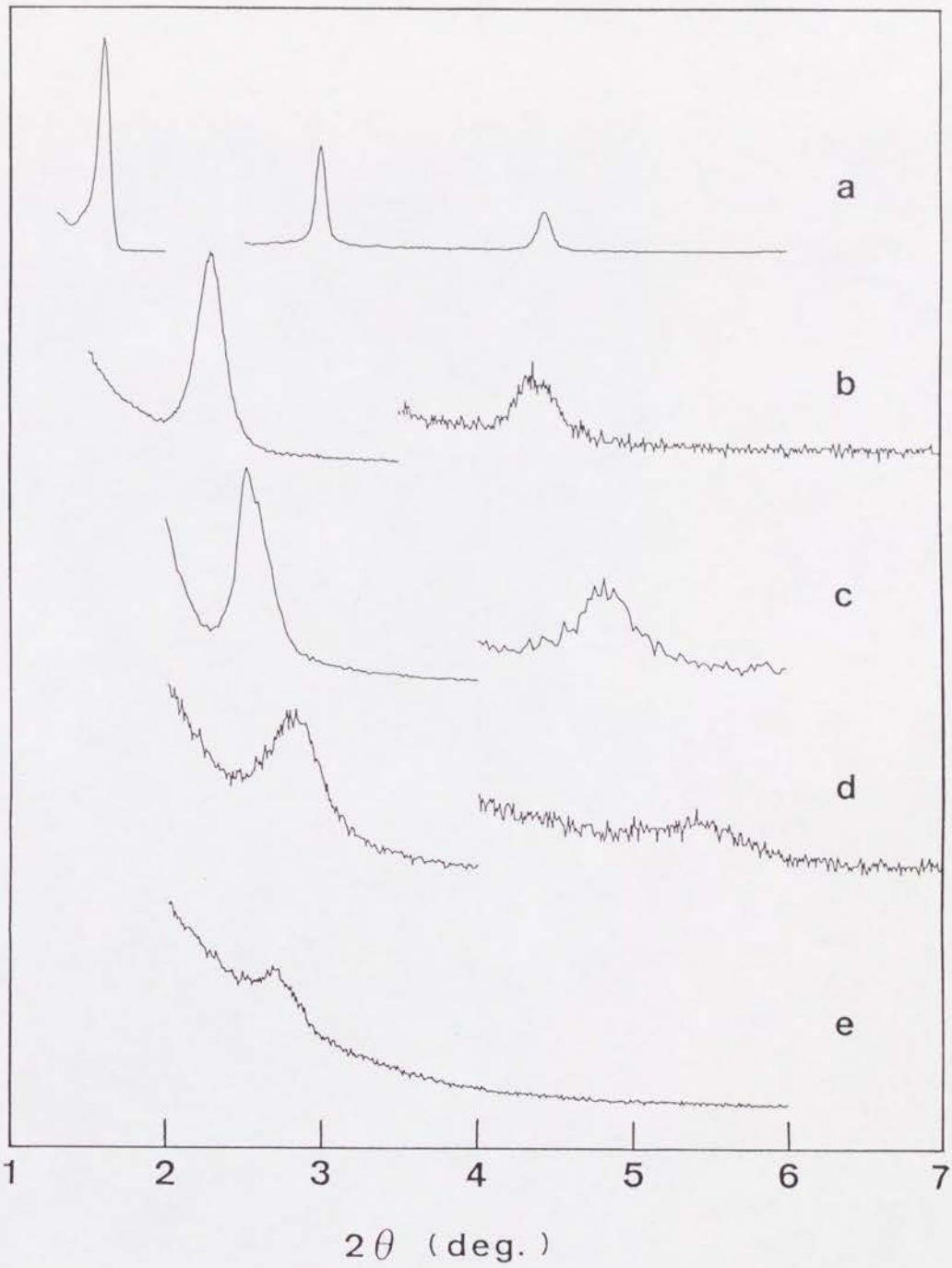

Fig. 6. Low angle X-ray patterns for Fe/Nd multilayers. (a) [Fe(26Å)/Nd(35Å)], (b) [Fe(26Å)/Nd(14Å)], (c) [Fe(26Å)/Nd(10Å)], (d) [Fe(26Å)/Nd(7Å)], and (e) [Fe(26Å)/Nd(3Å)].

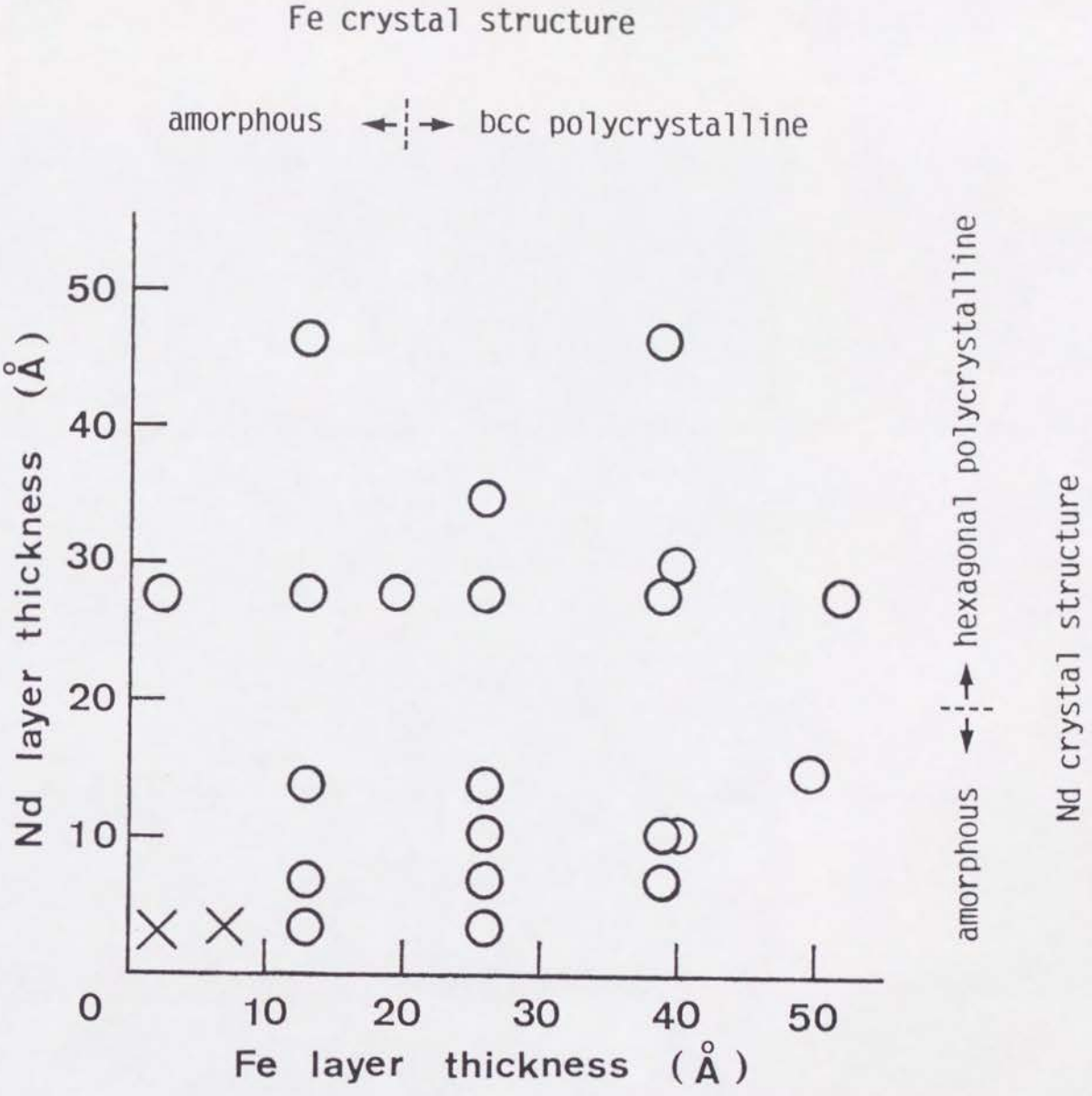

Fig. 7. Prepared Fe/Nd multilayers and the X-ray results. ○: The samples which show low angle X-ray peaks for the artificial periodicity. ×: The samples showing no X-ray peak in the low angle region. The structures of the Fe and Nd layers, whether they are polycrystalline or amorphous-like, are also shown in the figure.

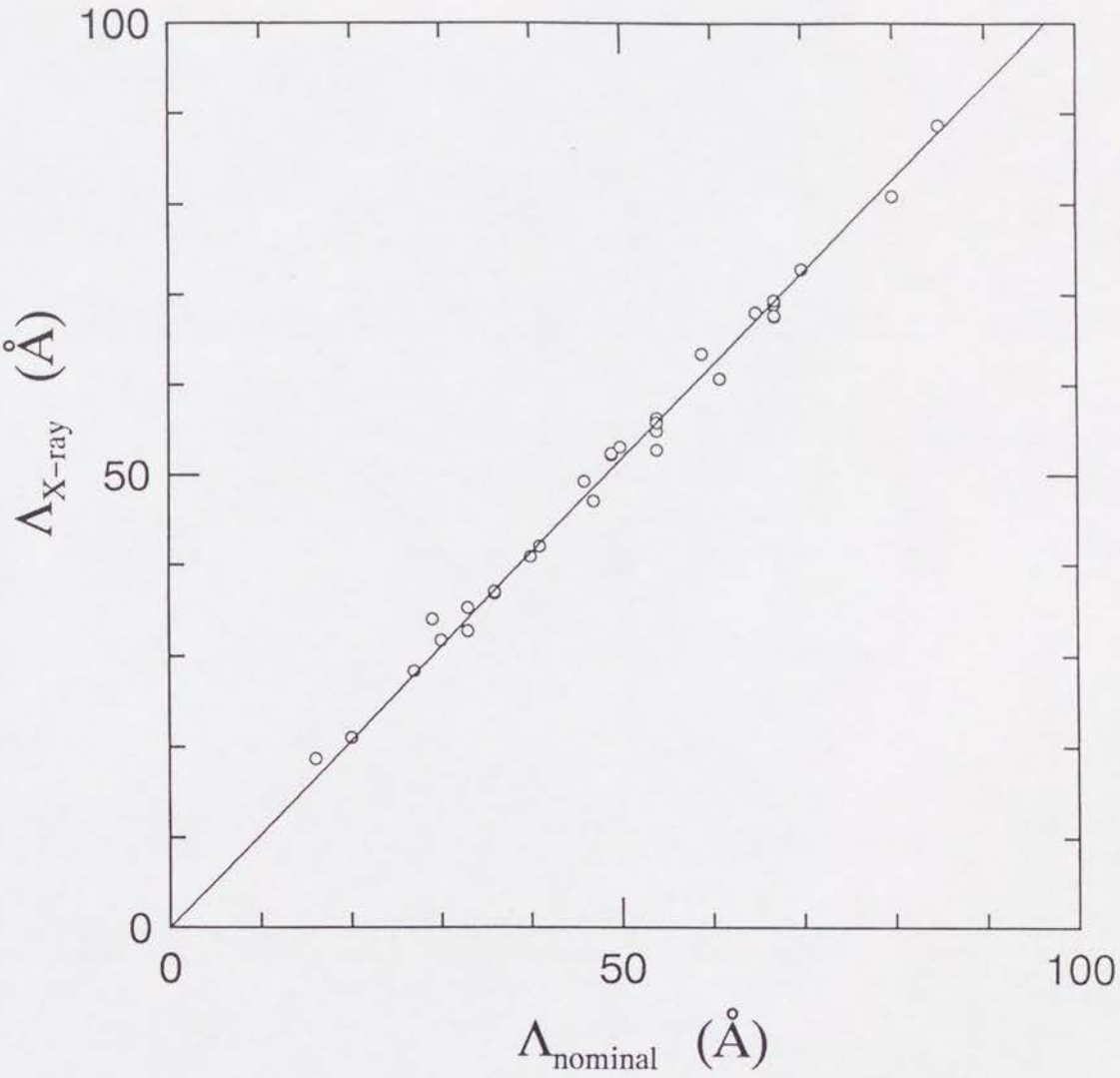

Fig. 8 Relation between the nominal period $\Lambda_{nominal}$ and the experimentally estimated period $\Lambda_{X\text{-}ray}$ at the substrate position (2) for Fe/Nd multilayers.

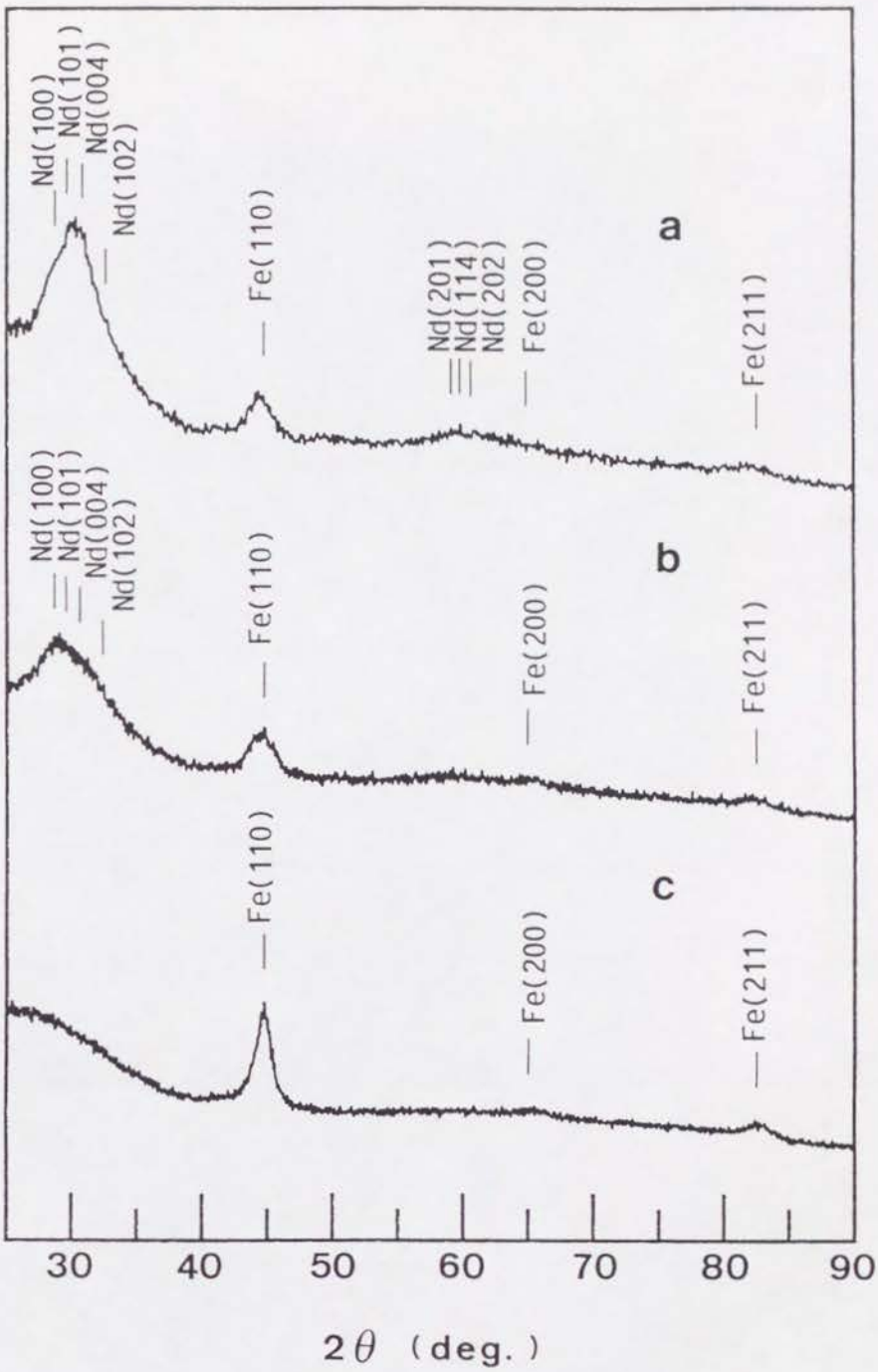

Fig. 9. High angle X-ray patterns for Fe/Nd multilayers with the Fe layer thickness of 39Å. (a) [Fe(39Å)/Nd(46Å)], (b) [Fe(39Å)/Nd(28Å)], and (c) [Fe(39Å)/Nd(10Å)]. The peak positions for bulk bcc Fe and bulk hexagonal Nd are shown for comparison.

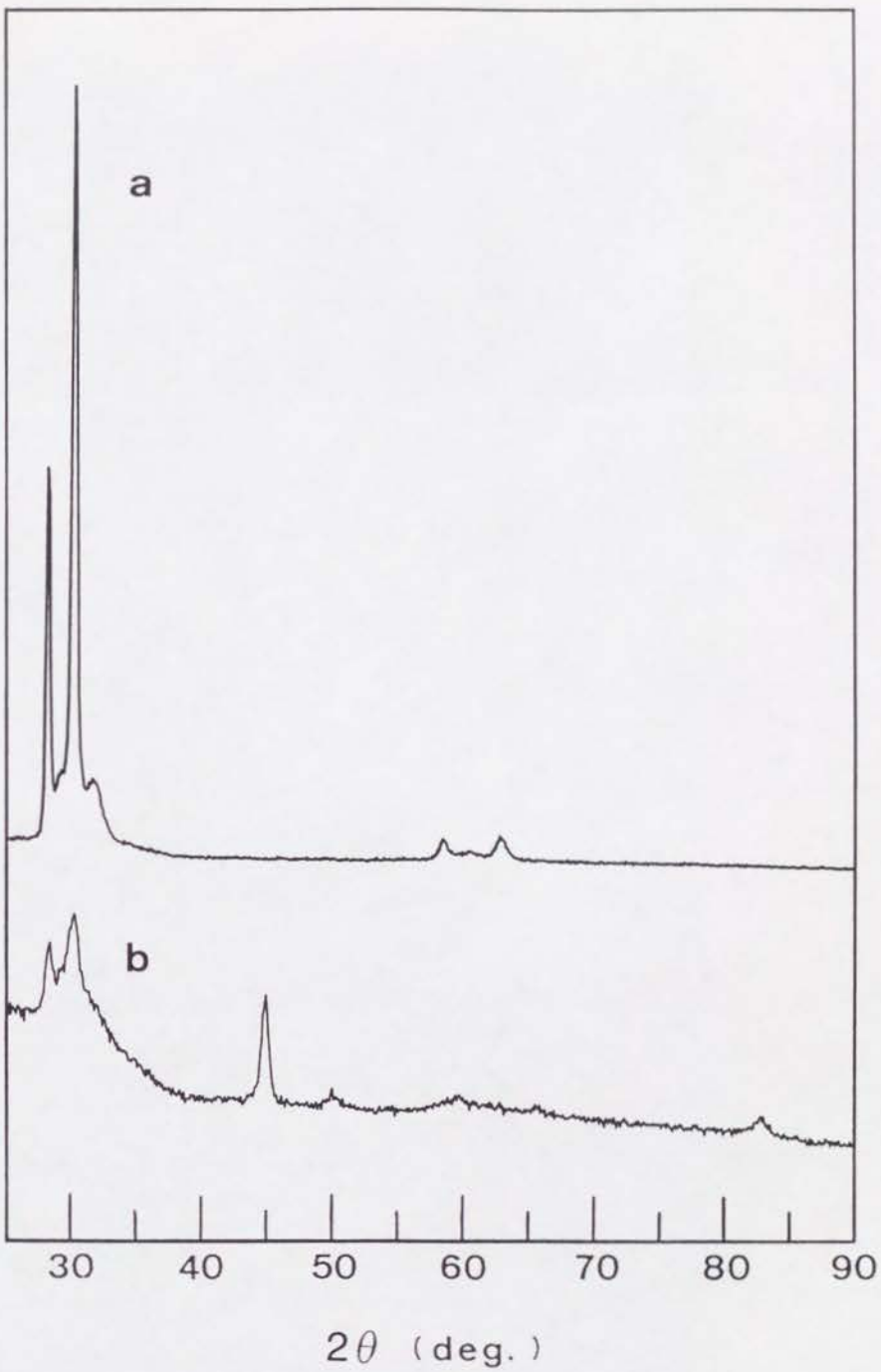

Fig. 10. High angle X-ray patterns for thick Nd layers. (a) Nd(2000Å) and (b) [Fe(200Å)/Nd(200Å)].

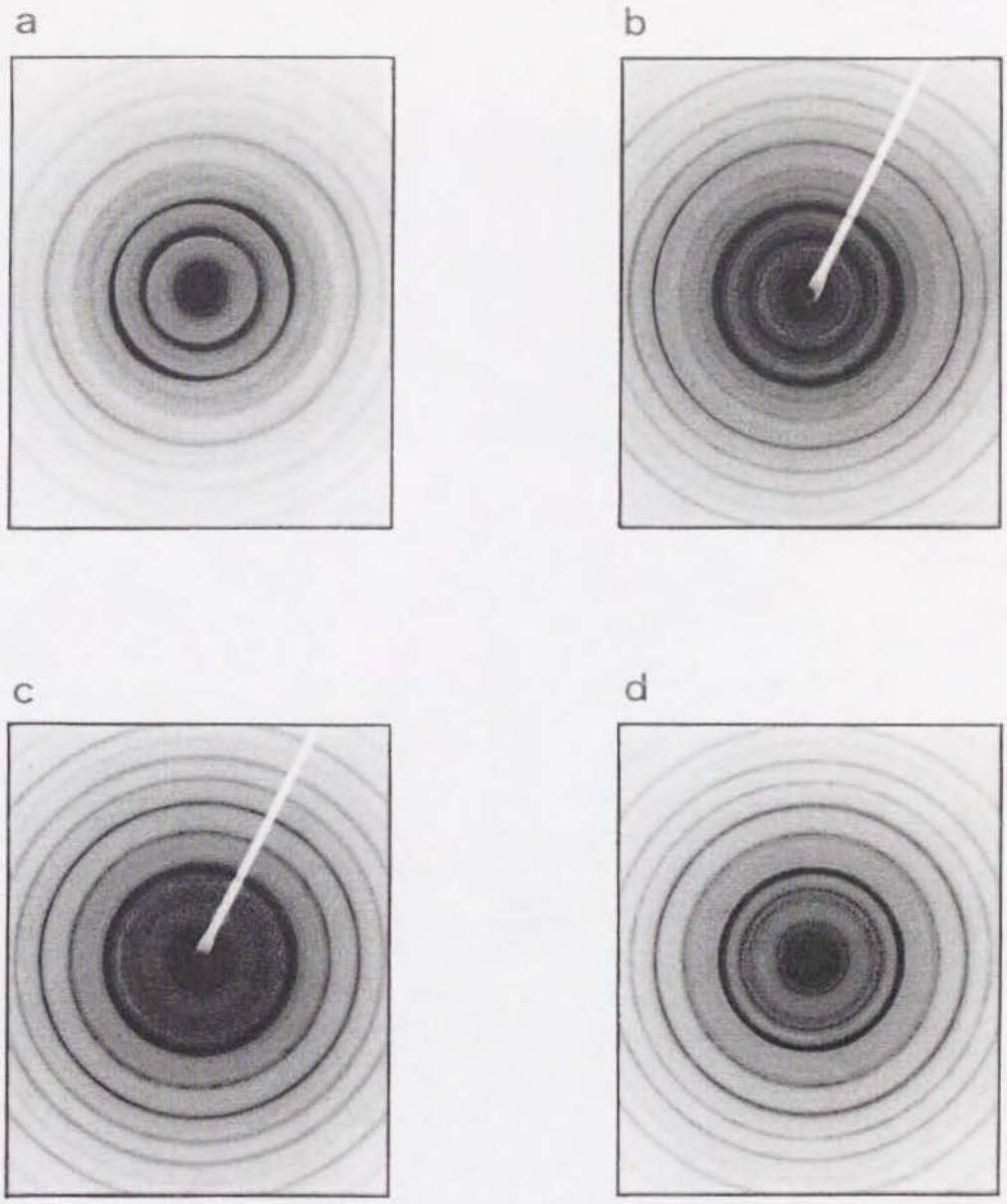

Fig. 11. Electron diffraction patterns for Fe/Nd multilayers with the Fe layer thickness of 39Å. (a) [Fe(39Å)/Nd(46Å)], (b) [Fe(39Å)/Nd(28Å)], (c) [Fe(39Å)/Nd(10Å)], and (d) [Fe(39Å)/Nd(7Å)].

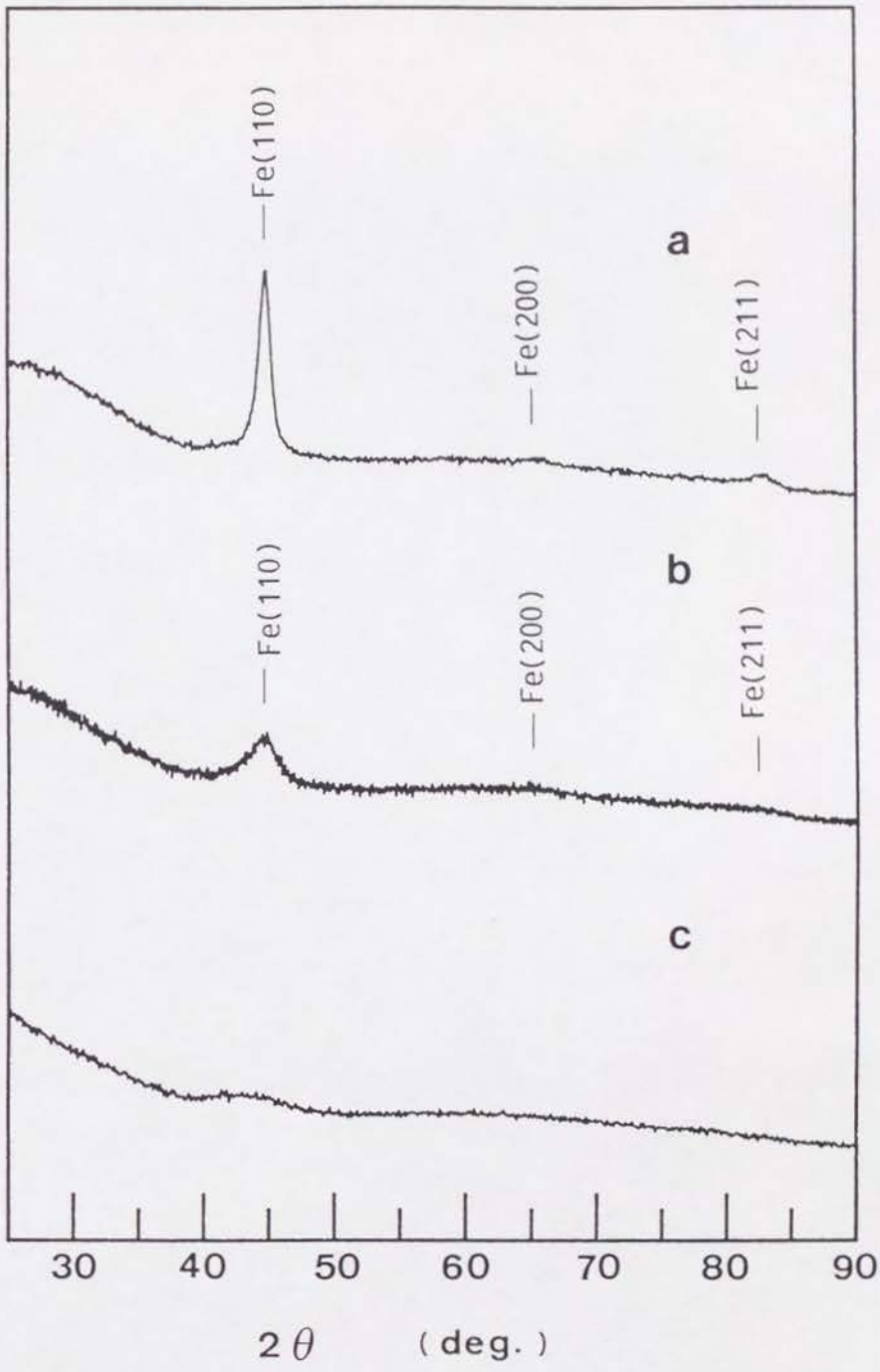

Fig. 12. High angle X-ray patterns for Fe/Nd multilayers with the Nd layer thickness of 7Å. (a) [Fe(39Å)/Nd(7Å)], (b) [Fe(26Å)/Nd(7Å)], and (c) [Fe(13Å)/Nd(7Å)]. The peak positions for bulk bcc Fe are shown for comparison.

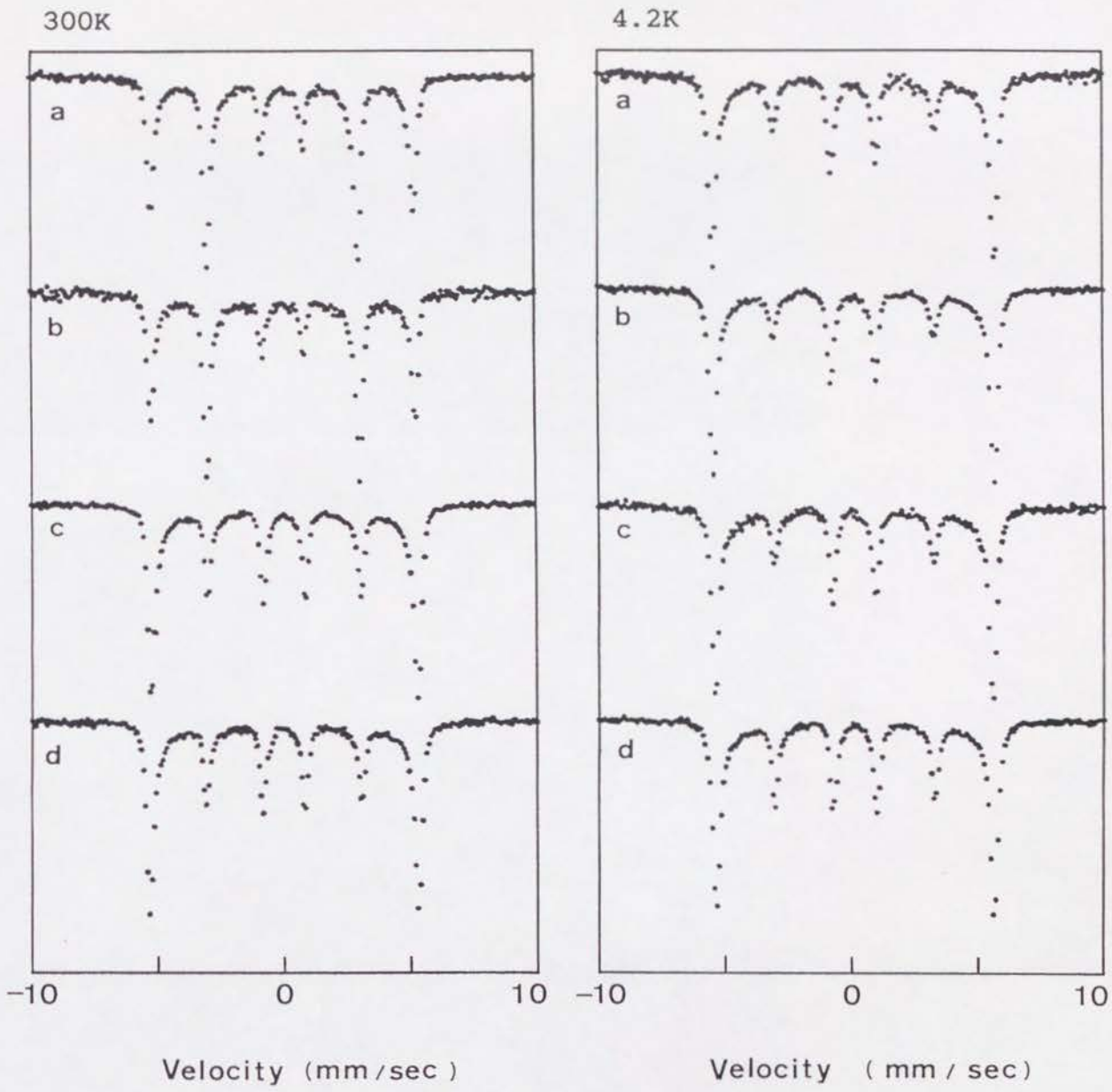

Fig. 13. Mössbauer spectra for Fe/Nd multilayers with the Fe layer thickness of 39Å at 300K and 4.2K. (a) [Fe(39Å)/Nd(46Å)], (b) [Fe(39Å)/Nd(28Å)], (c) [Fe(39Å)/Nd(10Å)], and (d) [Fe(39Å)/Nd(7Å)].

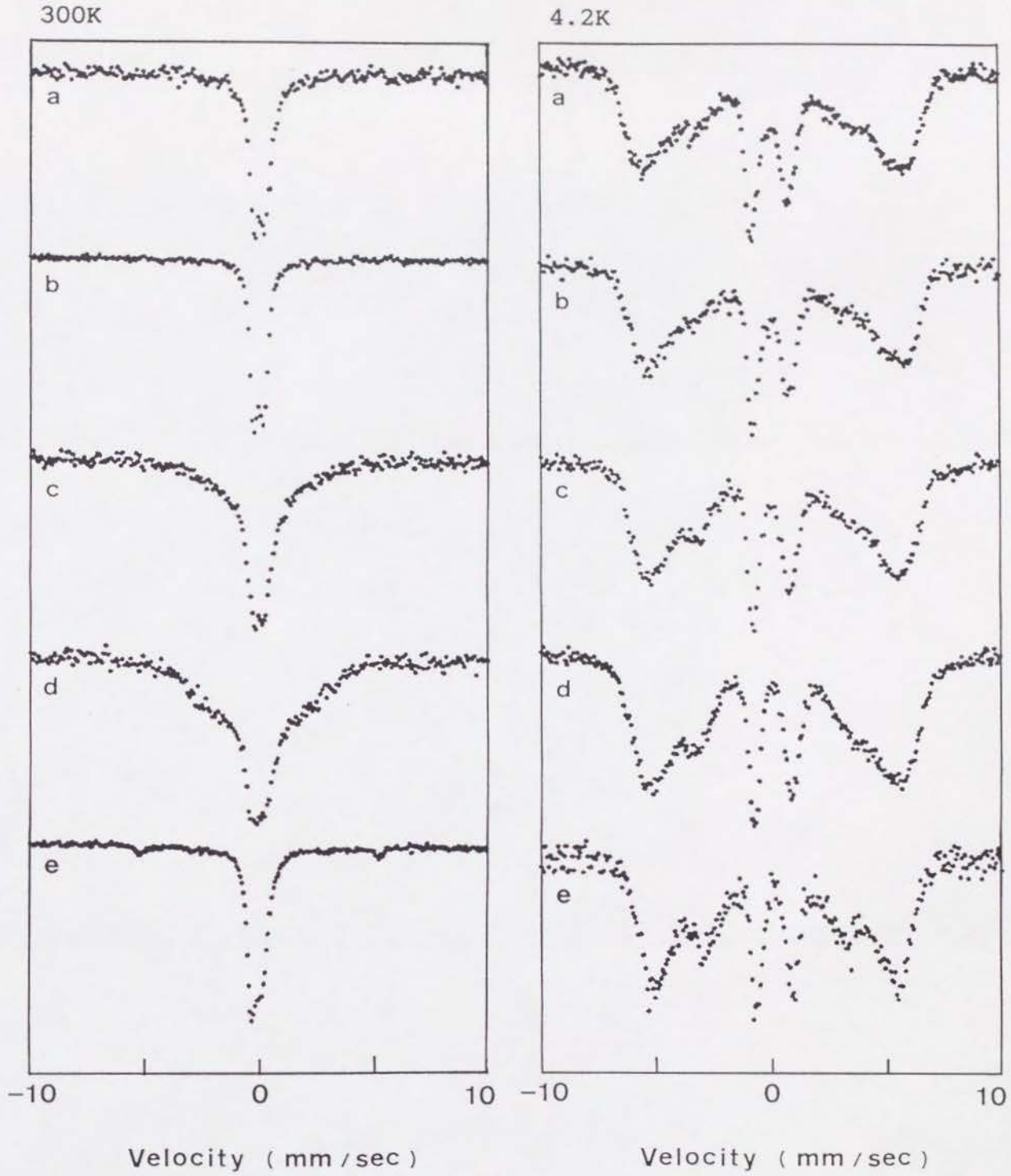

Fig. 14. Mössbauer spectra for Fe/Nd multilayers with the Fe layer thickness of 13Å at 300K and 4.2K. (a) [Fe(13Å)/Nd(46Å)], (b) [Fe(13Å)/Nd(28Å)], (c) [Fe(13Å)/Nd(14Å)], (d) [Fe(13Å)/Nd(7Å)], and (e) [Fe(13Å)/Nd(3Å)].

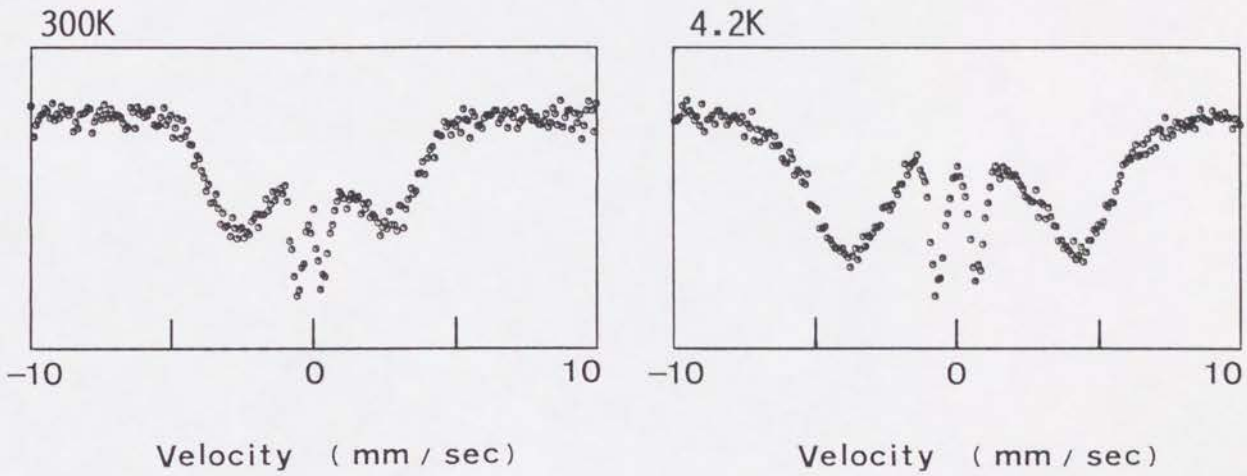

Fig. 15. Mössbauer spectra for an amorphous Fe-Nd alloy, which was prepared by alternate deposition of monatomic Fe (2Å) and Nd (3Å) layers, at 300K and 4.2K.

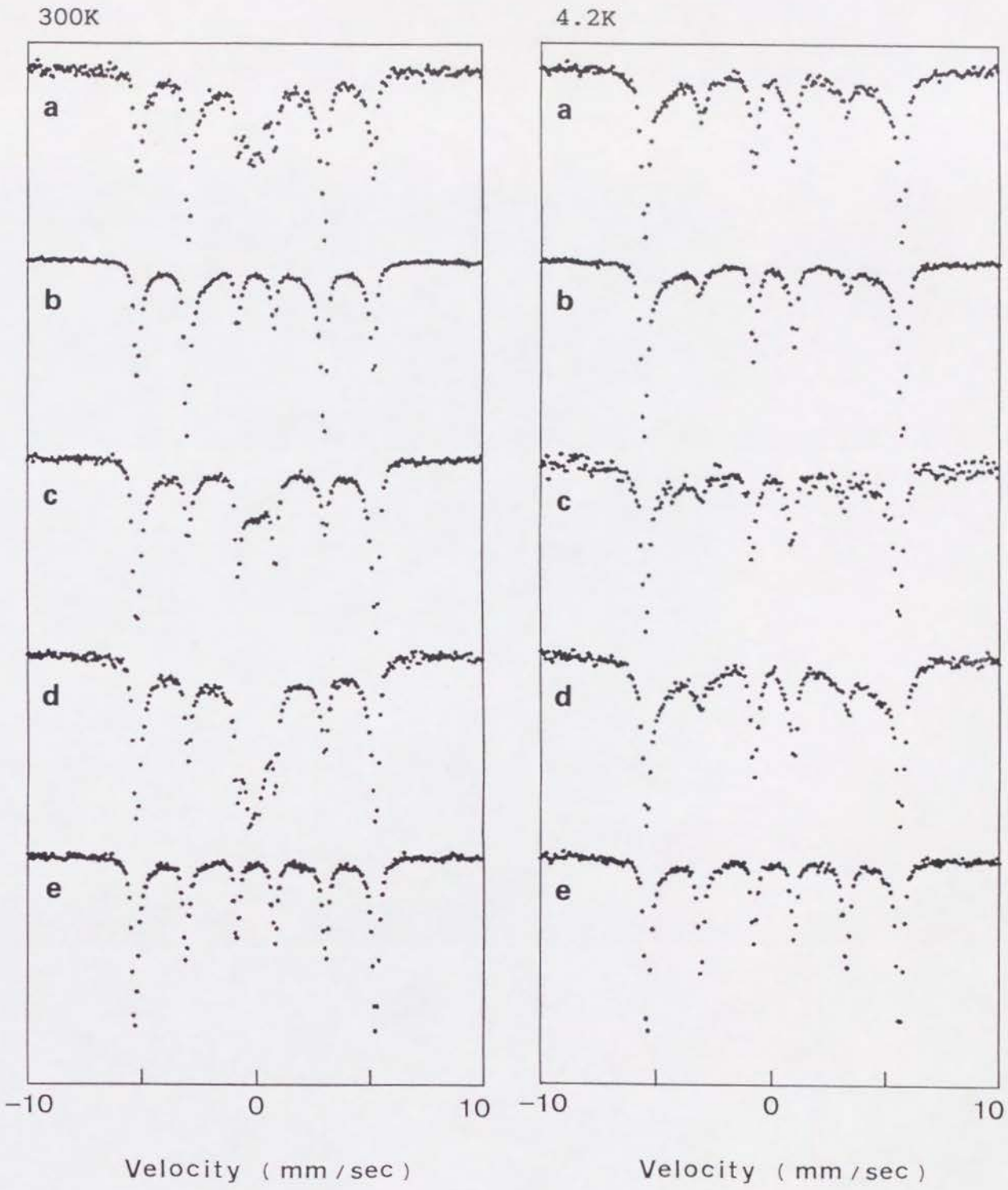

Fig. 16. Mössbauer spectra for Fe/Nd multilayers with the Fe layer thickness of 26Å at 300K and 4.2K. (a) [Fe(26Å)/Nd(35Å)], (b) [Fe(26Å)/Nd(28Å)], (c) [Fe(26Å)/Nd(14Å)], (d) [Fe(26Å)/Nd(10Å)], and (e) [Fe(26Å)/Nd(3Å)].

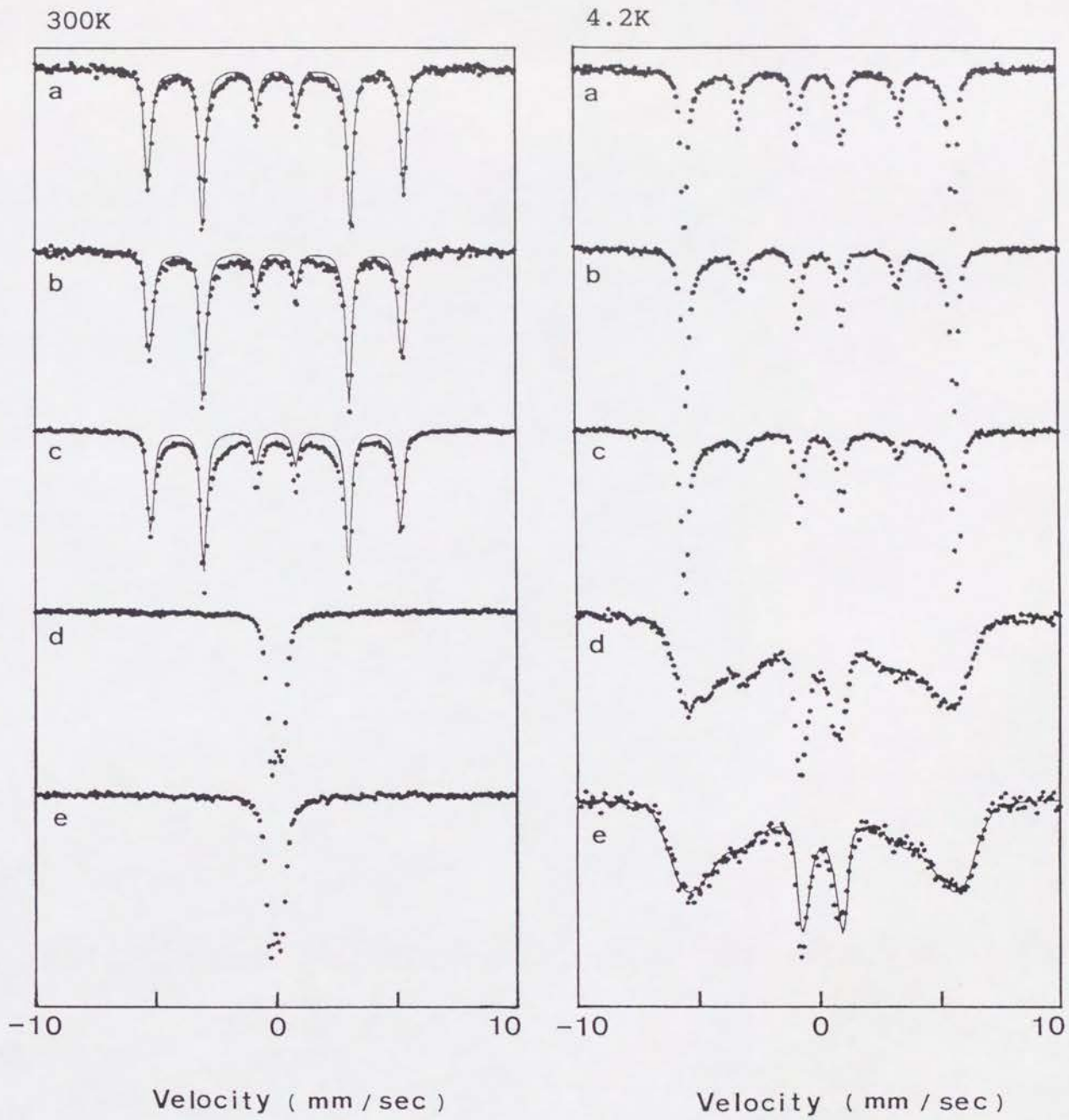

Fig. 17. Mössbauer spectra for Fe/Nd multilayers with the Nd layer thickness of 28Å at 300K and 4.2K. (a) [Fe(52Å)/Nd(28Å)], (b) [Fe(39Å)/Nd(28Å)], (c) [Fe(26Å)/Nd(28Å)], (d) [Fe(19Å)/Nd(28Å)], and (e) [Fe(13Å)/Nd(28Å)].

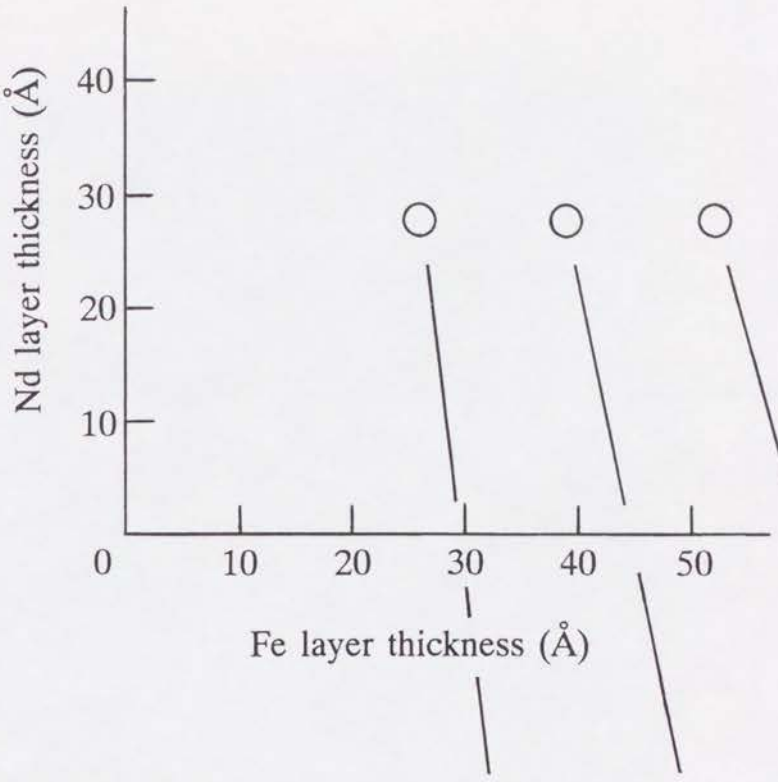

Fe layer thickness	26Å	39Å	52Å
The relative ratio of the interface component	35.5%	20.1%	15.1%
The corresponding thickness of the interface component	9.2Å	7.8Å	7.9Å

Fig. 18. Estimation of the Fe thickness which corresponds to the interface component in Mössbauer spectra.

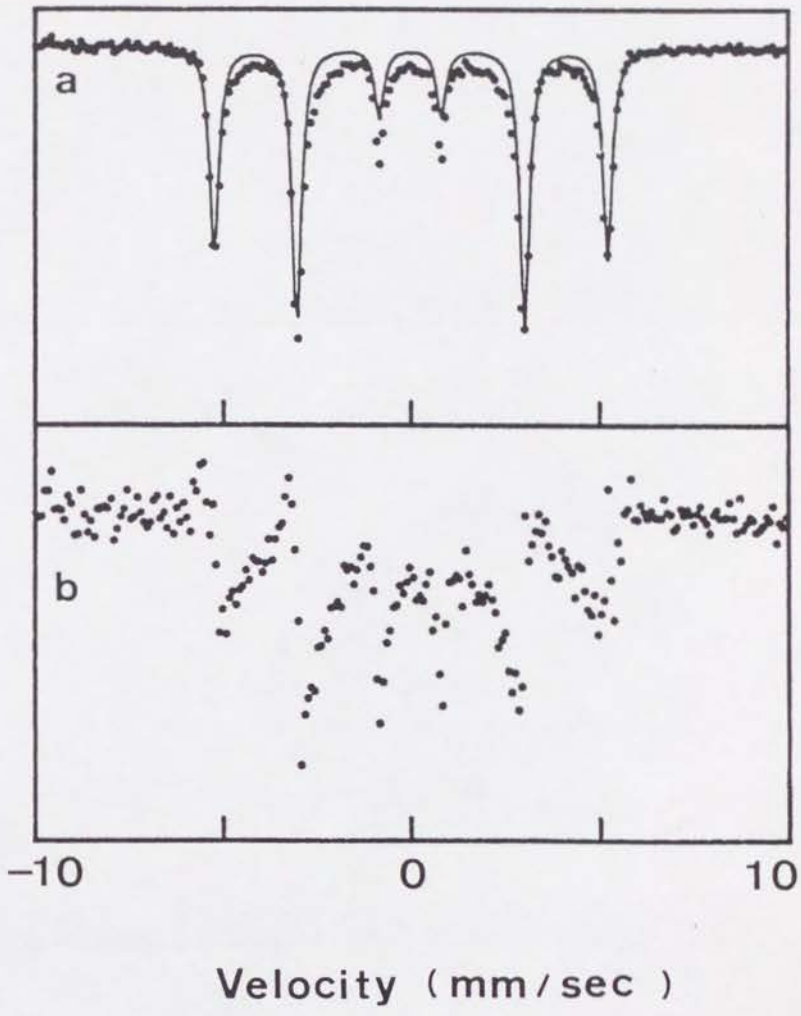

Fig. 19. Separation of two components in the Mössbauer spectrum for [Fe(39Å)/Nd(46Å)]. (a) The component from the inner Fe atoms (the solid line composed of six Lorentzians). (b) The residual component, which is due to the interface Fe atoms.

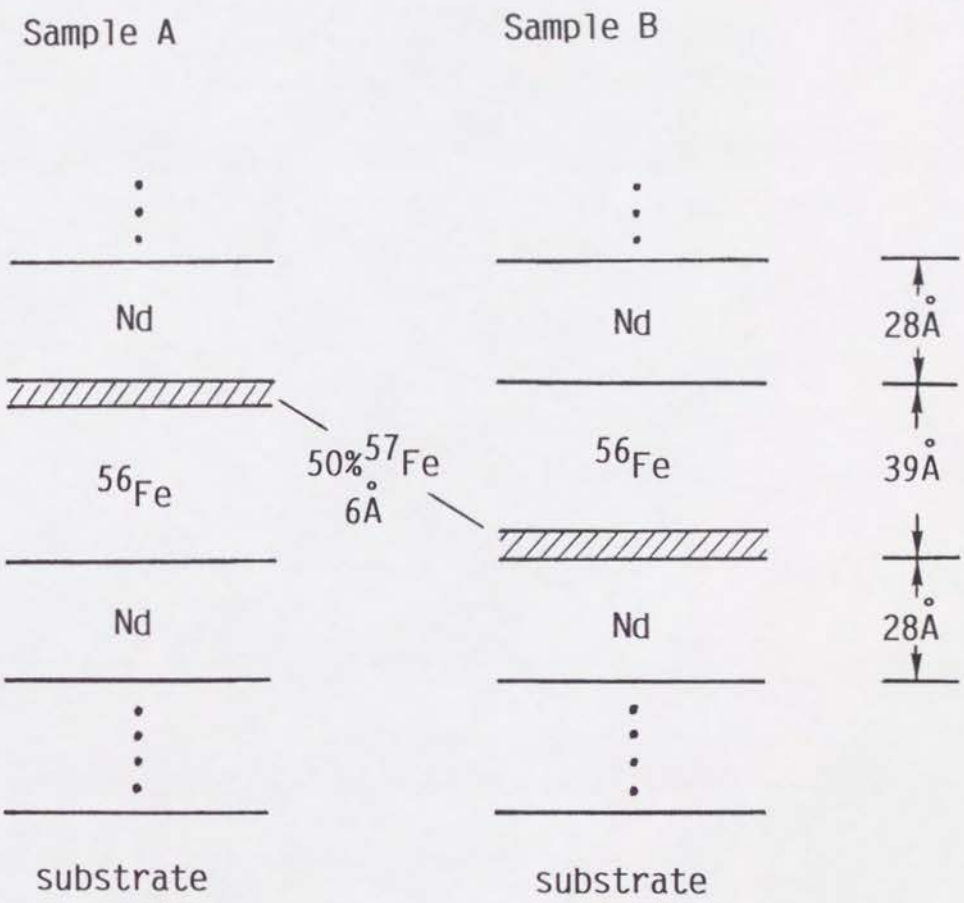

Fig. 20. Structures of two samples with ^{57}Fe enriched interfaces.

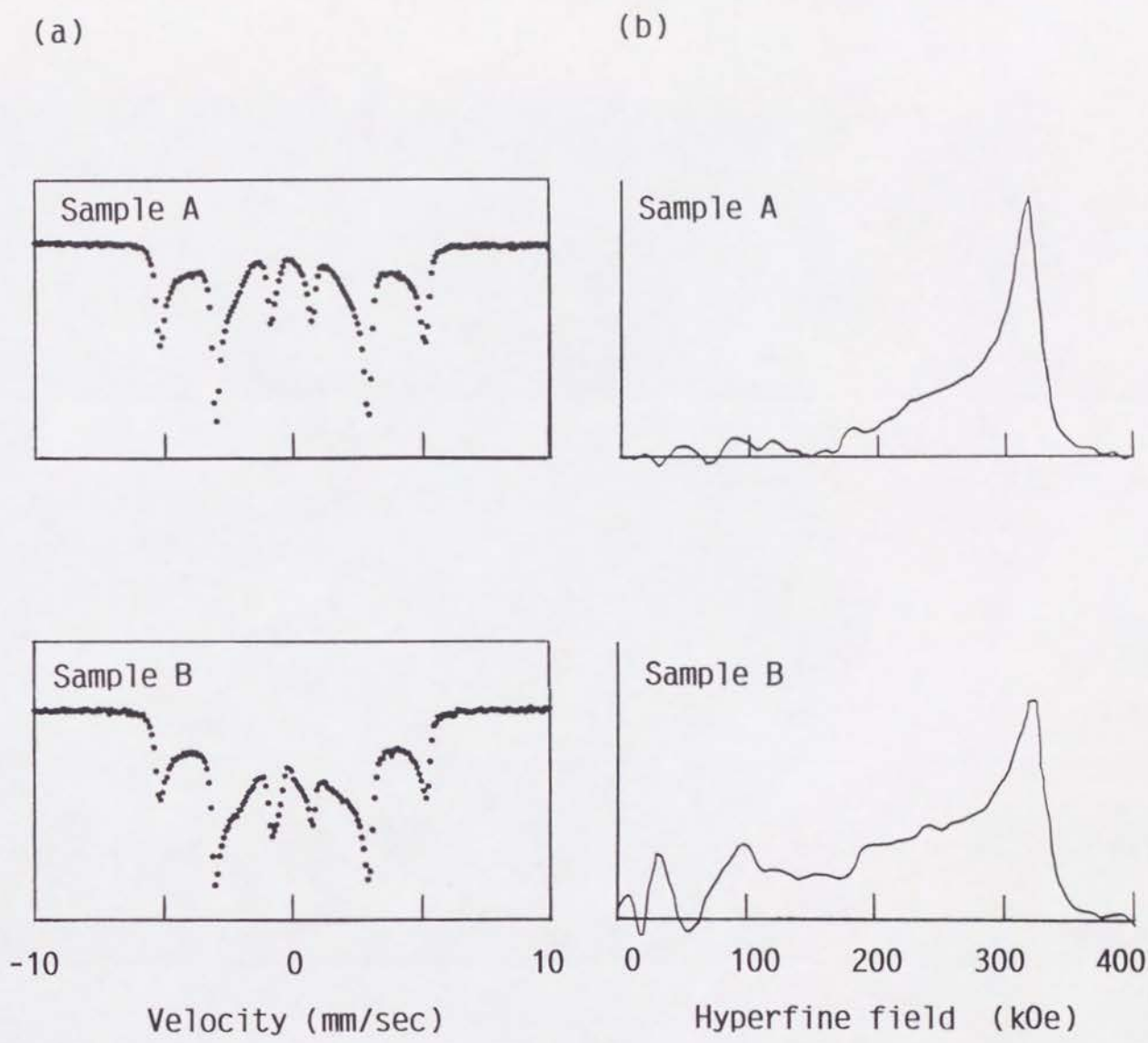

Fig. 21. (a) Mössbauer spectra for Samples A and B at 300K. (b) Distribution of the hyperfine fields derived from the spectra. The direction of the hyperfine fields is assumed to be parallel to the film plane.

[Fe(19Å)/Nd(28Å)]

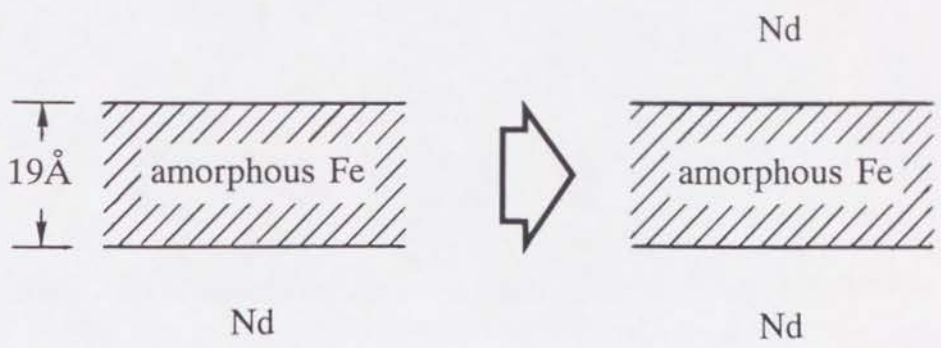

[Fe(26Å)/Nd(28Å)]

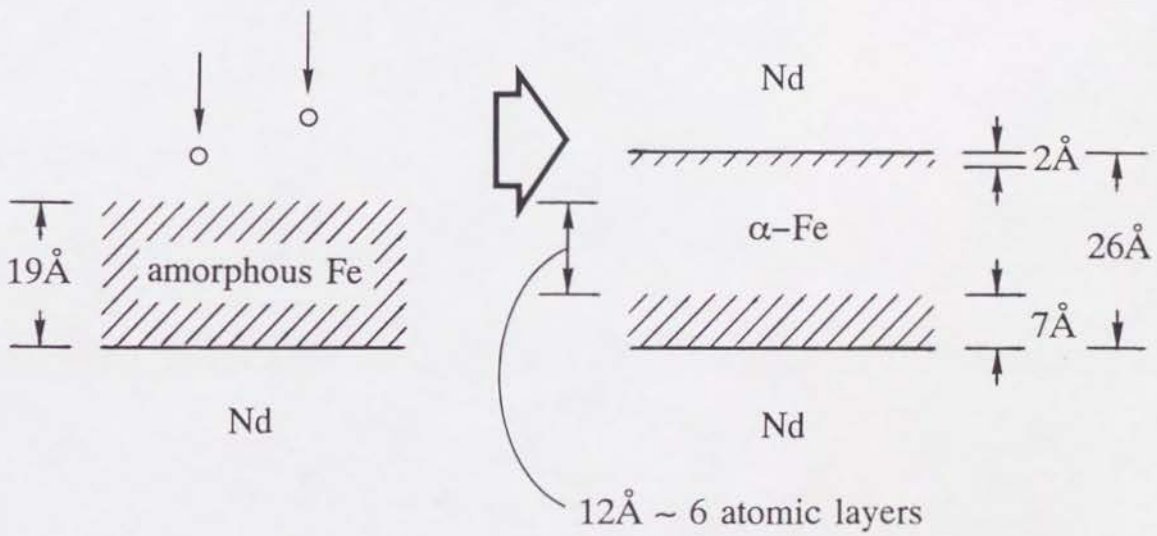

Fig. 22. Illustration of amorphous-to-bcc transformation in an Fe layer.

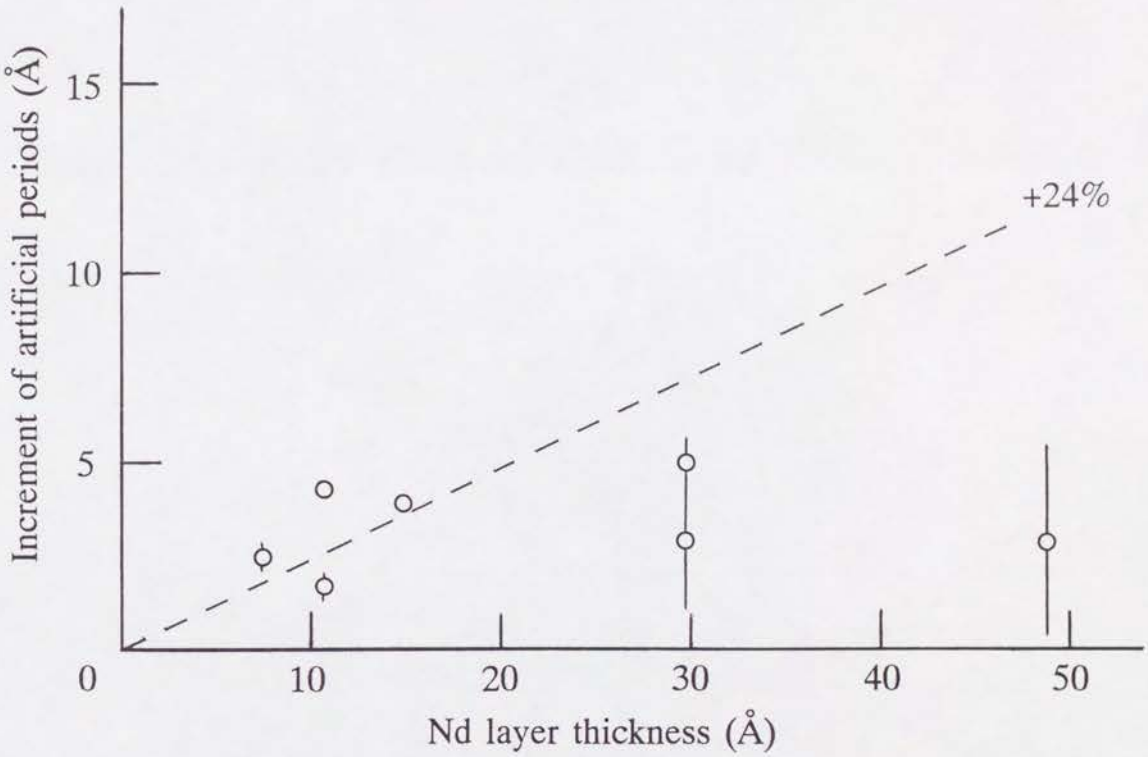

Fig. 23. Increment of artificial periods after annealing in 10^{-6} Torr at 200°C for 24 hours. The Nd layers are expected to expand by 24% if they are oxidized to be cubic Nd_2O_3.

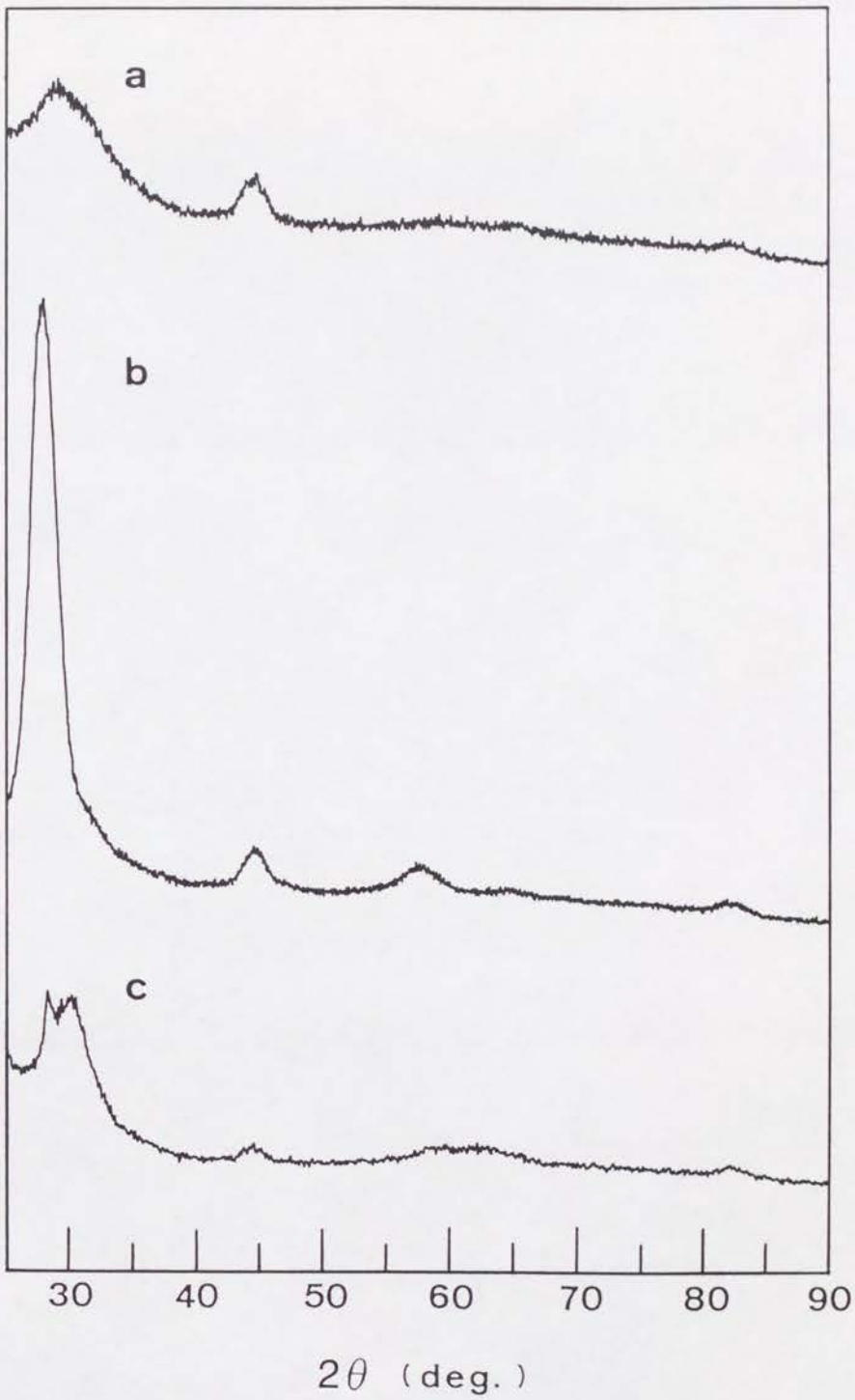

Fig. 24. High angle X-ray patterns for [Fe(39Å)/Nd(28Å)] (a) before annealing and after annealing in (b) 10^{-6}Torr or (c) 10^{-8} Torr at 200°C for 24 hours.

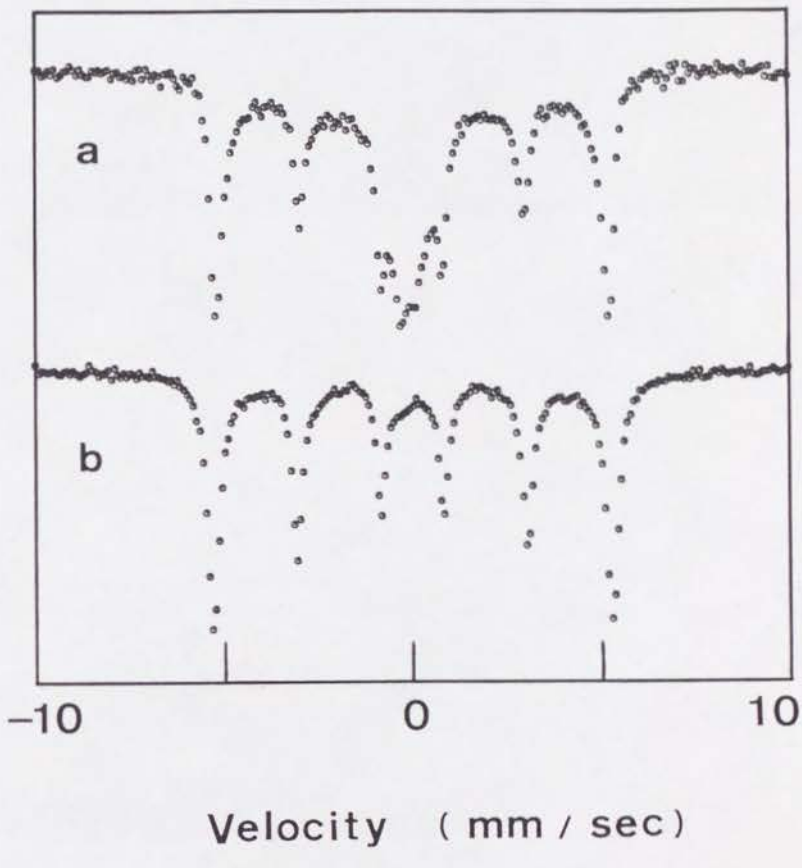

Fig. 25. Mössbauer spectra for [Fe(26Å)/Nd(10Å)] at 300K, (a) before and (b) after annealing in 10^{-6}Torr at 200°C for 24 hours.

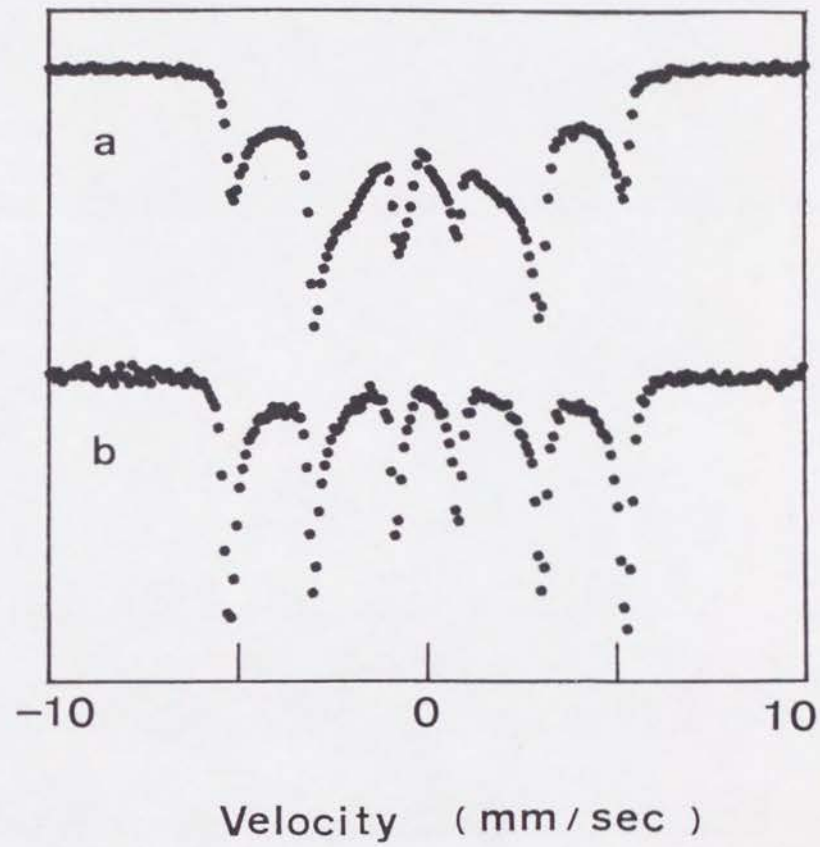

Fig. 26. Mössbauer spectra for the sample with ^{57}Fe enriched interfaces (Sample B) at 300K, (a) before and (b) after annealing in 10^{-8}Torr at 200°C for 24 hours.

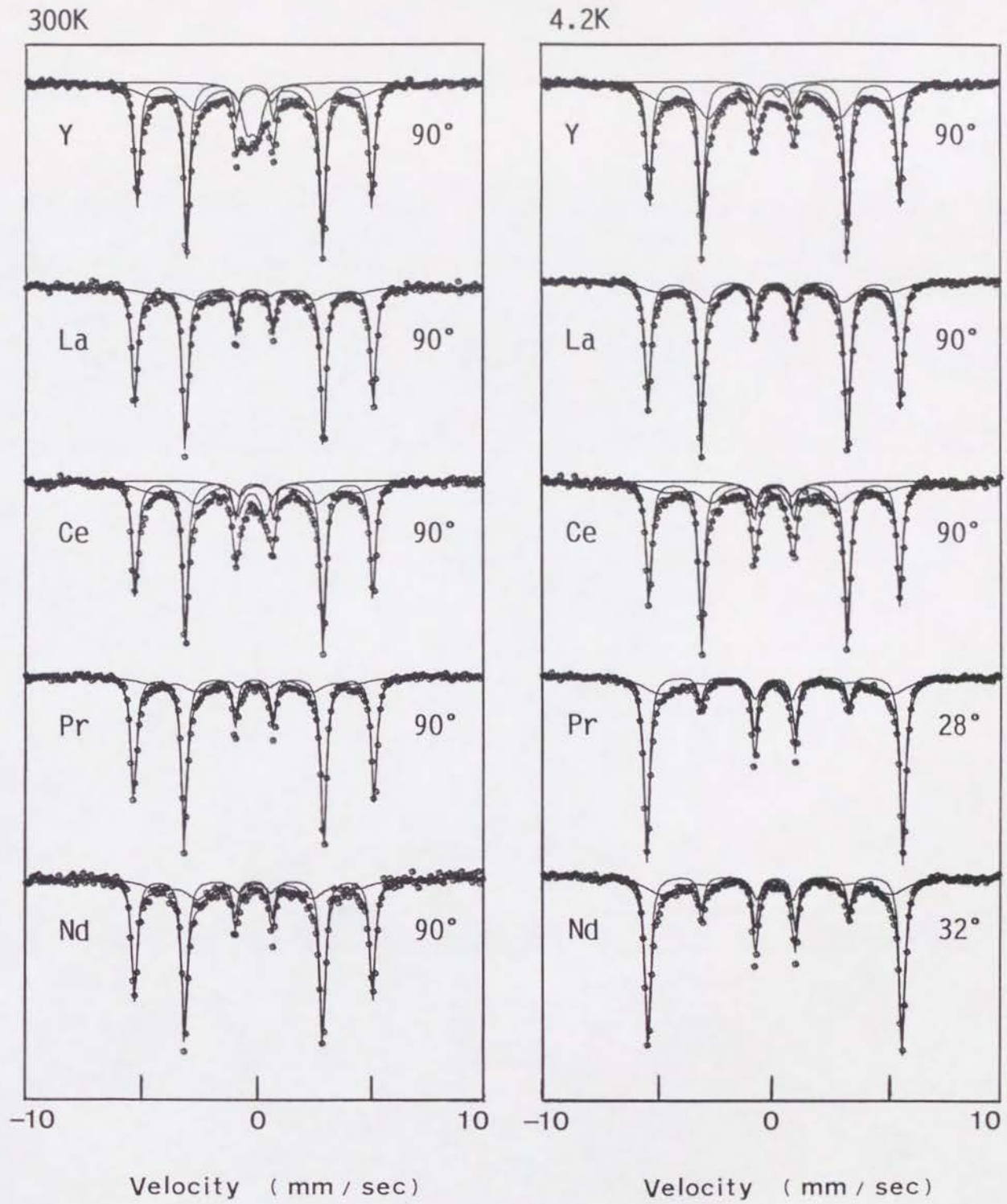

Fig. 27. Mössbauer spectra for [Fe(40Å)/RE(30Å)] (RE=Y, La, Ce, Pr, and Nd) at 300K and 4.2K. The average direction of the Fe magnetic moments relative to the plane normal is also shown in the figure.

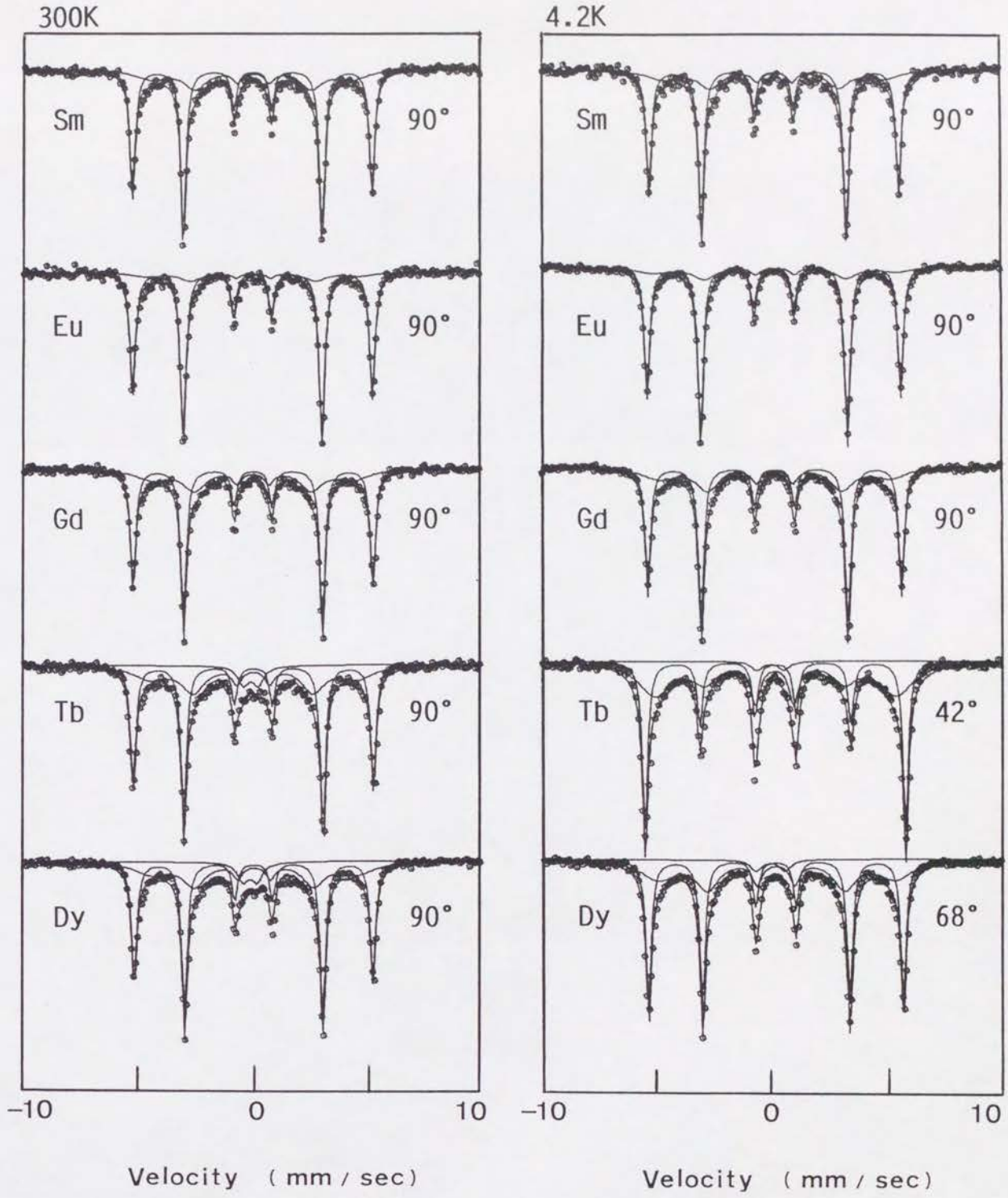

Fig. 28. Mössbauer spectra for [Fe(40Å)/RE(30Å)] (RE=Sm, Eu Gd, Tb, and Dy) at 300K and 4.2K. The average direction of the Fe magnetic moments relative to the plane normal is also shown in the figure.

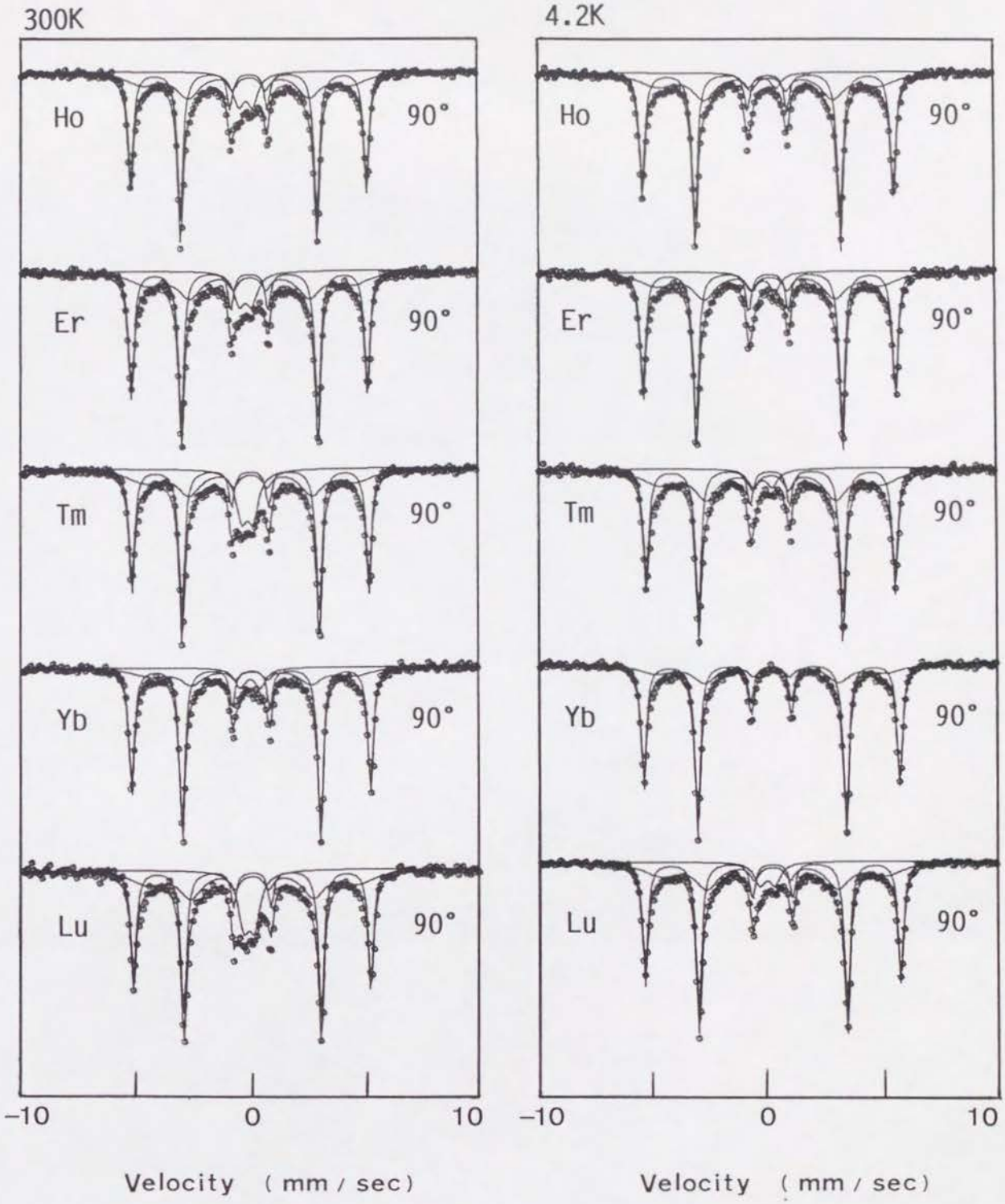

Fig. 29. Mössbauer spectra for [Fe(40Å)/RE(30Å)] (RE=Ho, Er, Tm, Yb, and Lu) at 300K and 4.2K. The average direction of the Fe magnetic moments relative to the plane normal is also shown in the figure.

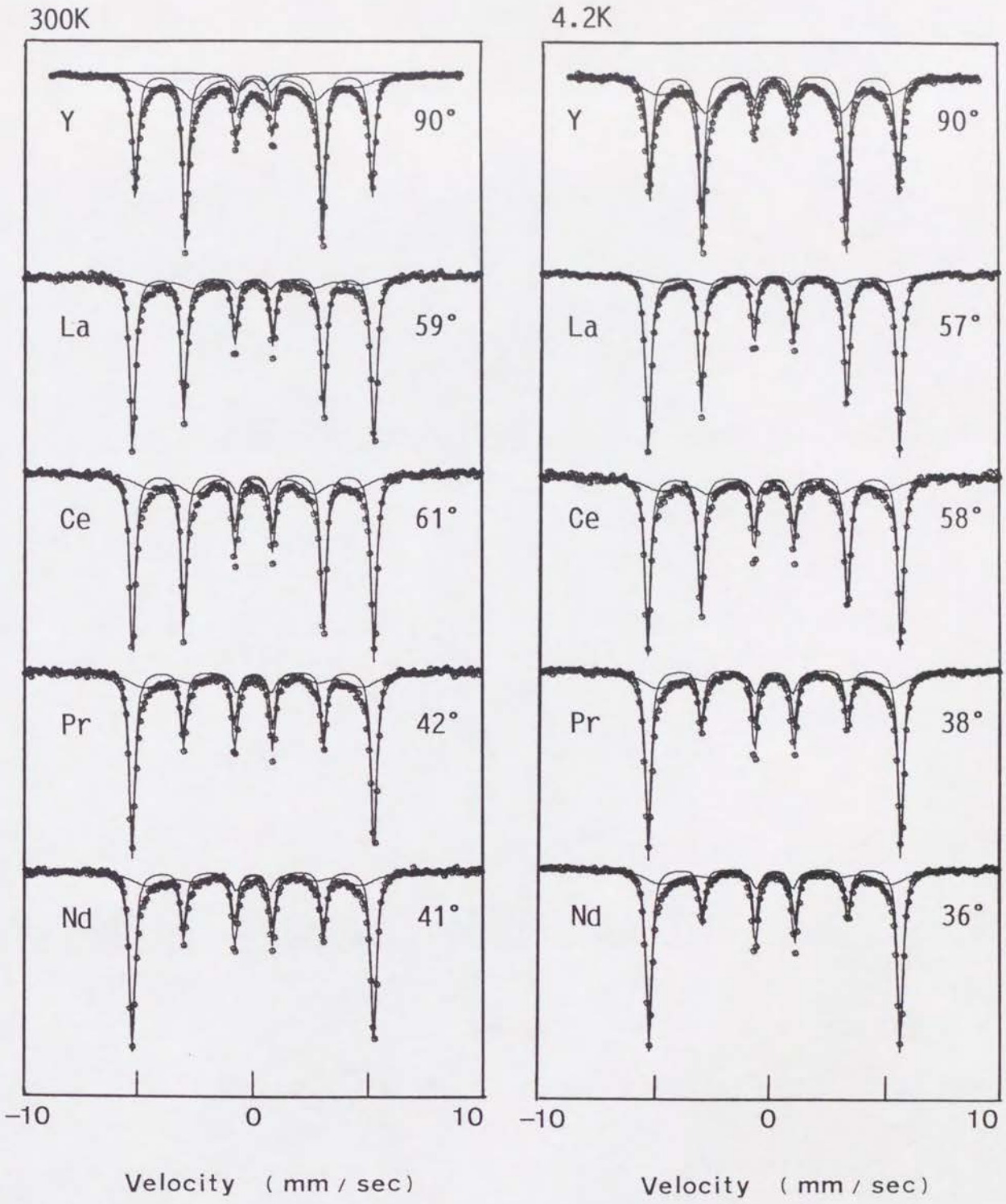

Fig. 30. Mössbauer spectra for [Fe(40Å)/RE(10Å)] (RE=Y, La, Ce, Pr, and Nd) at 300K and 4.2K. The average direction of the Fe magnetic moments relative to the plane normal is also shown in the figure.

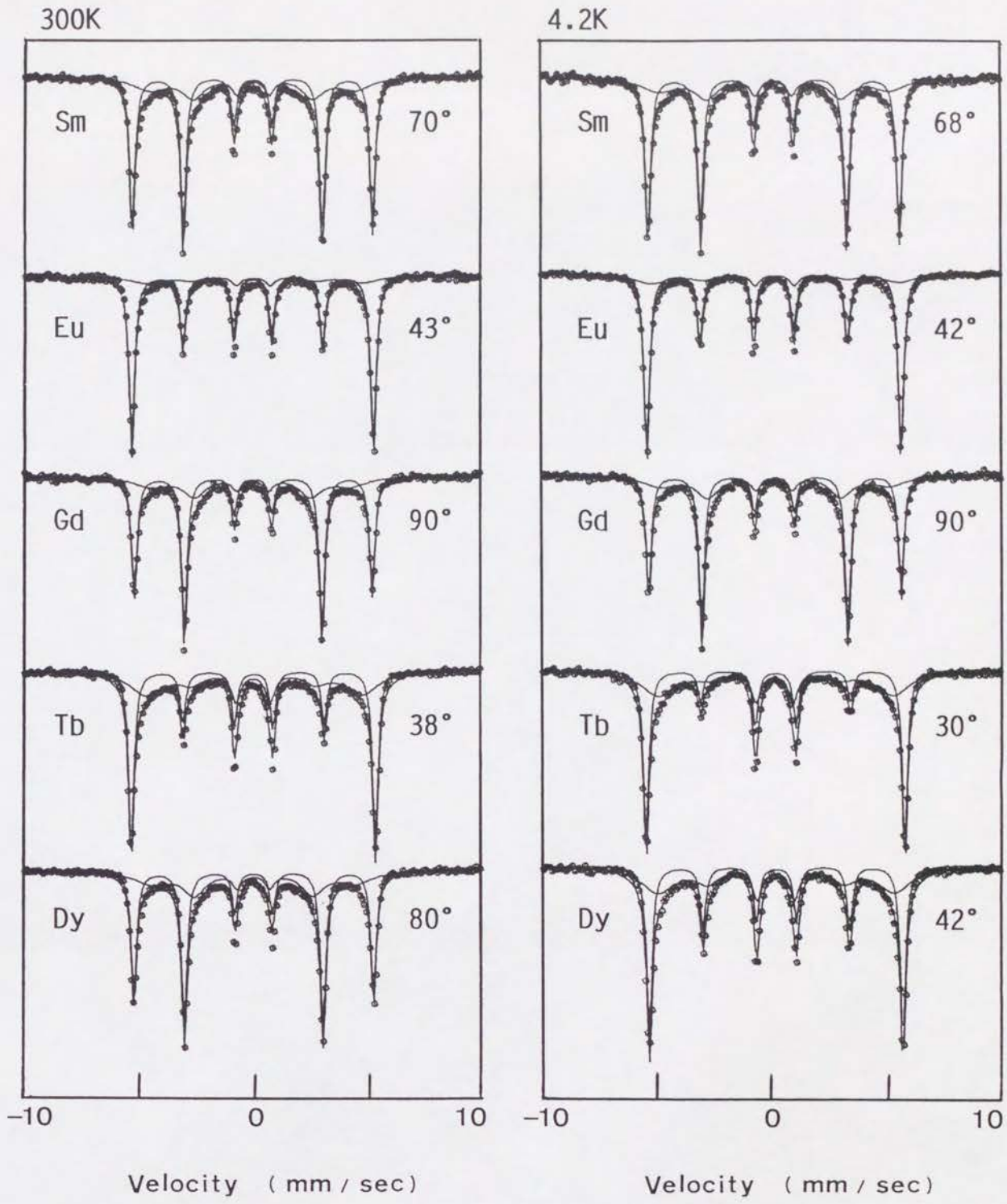

Fig. 31. Mössbauer spectra for [Fe(40Å)/RE(10Å)] (RE=Sm, Eu Gd, Tb, and Dy) at 300K and 4.2K. The average direction of the Fe magnetic moments relative to the plane normal is also shown in the figure.

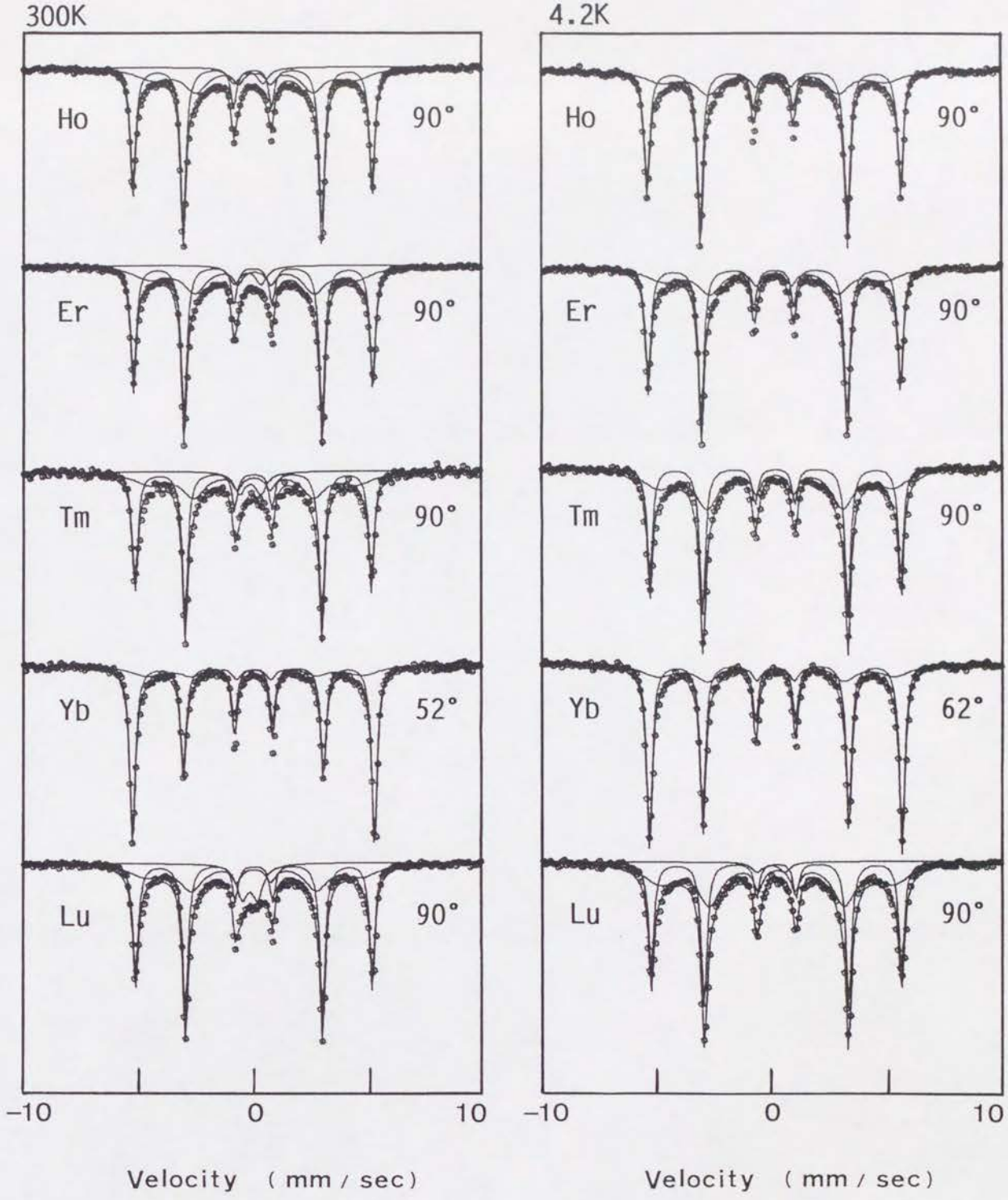

Fig. 32. Mössbauer spectra for [Fe(40Å)/RE(10Å)] (RE=Ho, Er, Tm, Yb, and Lu) at 300K and 4.2K. The average direction of the Fe magnetic moments relative to the plane normal is also shown in the figure.

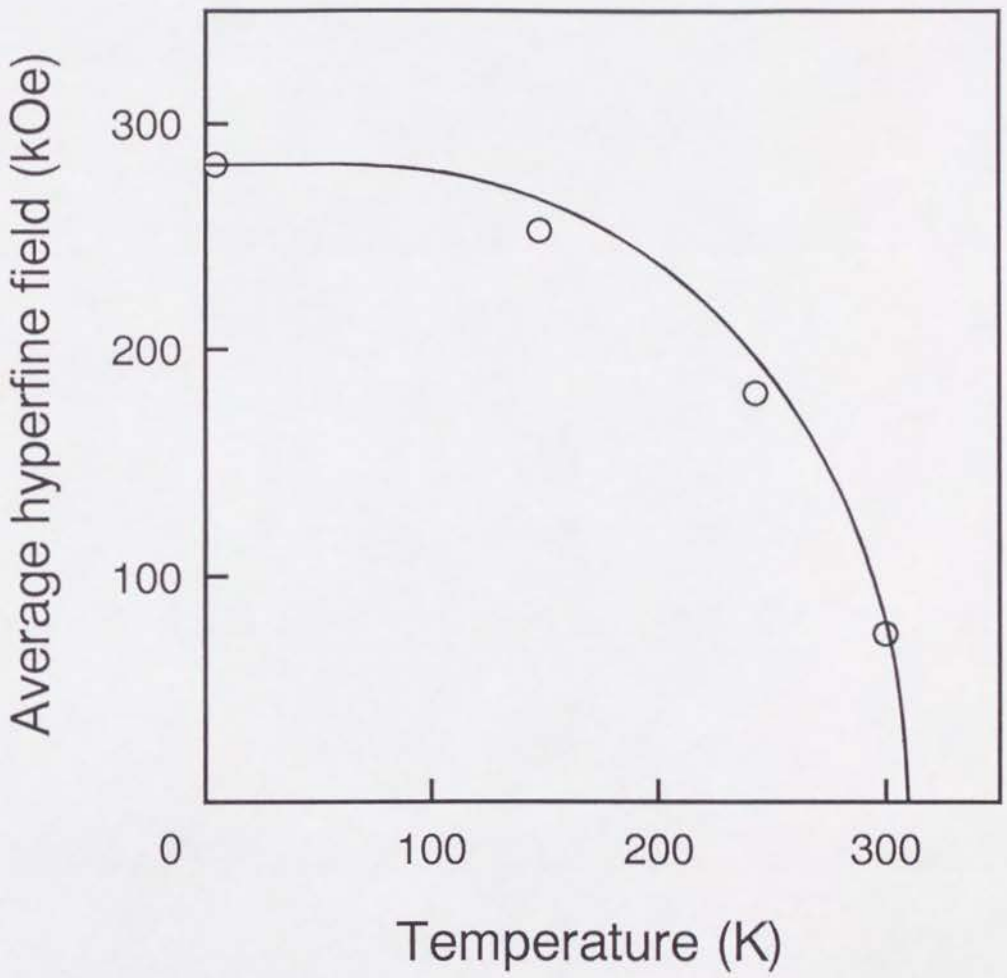

Fig. 33. Temperature dependence of the average hyperfine field for [Fe(13Å)/Nd(14Å)]. The Brillouin curve for S=1 is shown for comparison.

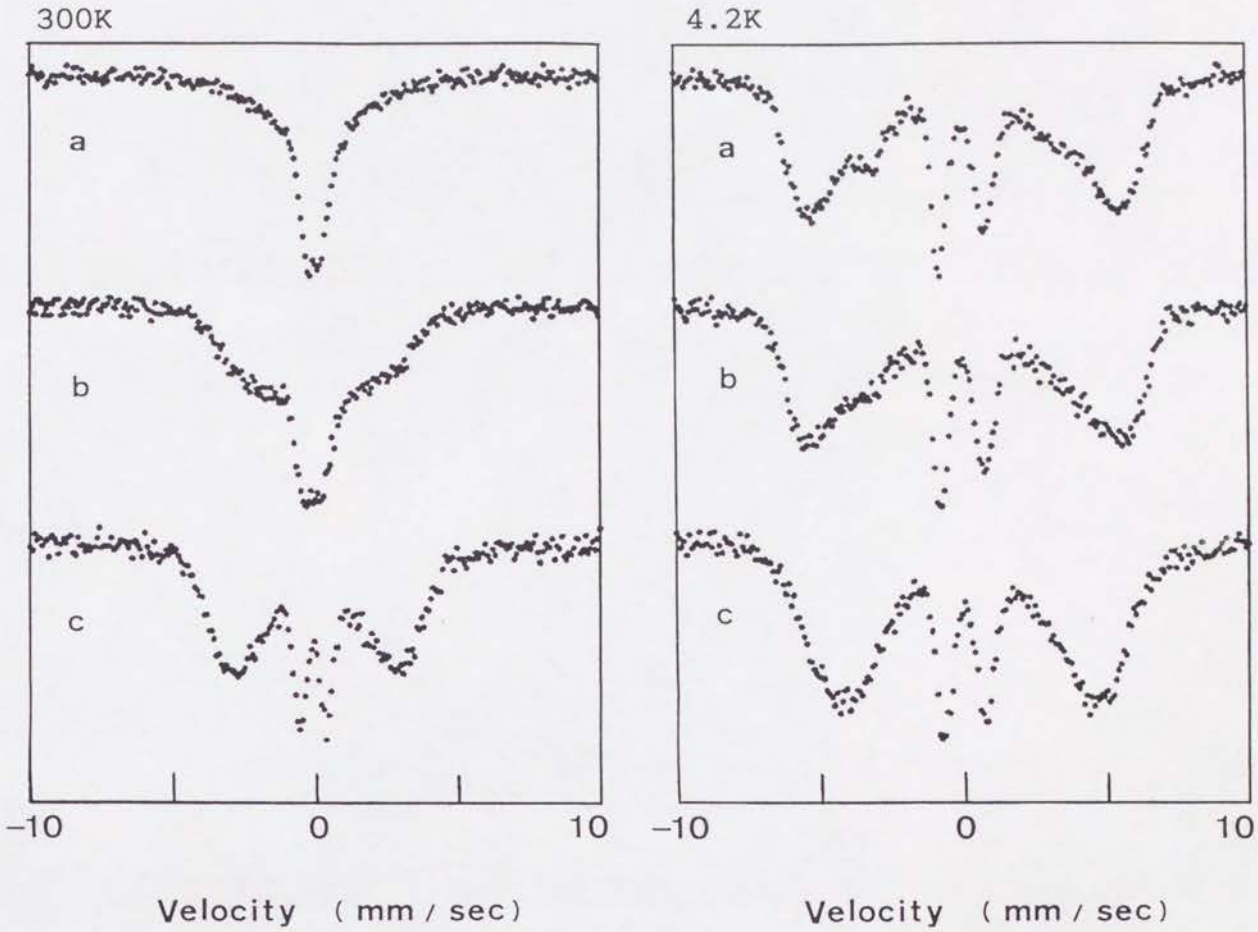

Fig. 34. Substrate temperature dependence of Mössbauer spectra for [Fe(13Å)/Nd(14Å)]. (a) T_{sub}=-50°C, (b) T_{sub}=25°C, and (c) T_{sub}=150°C.

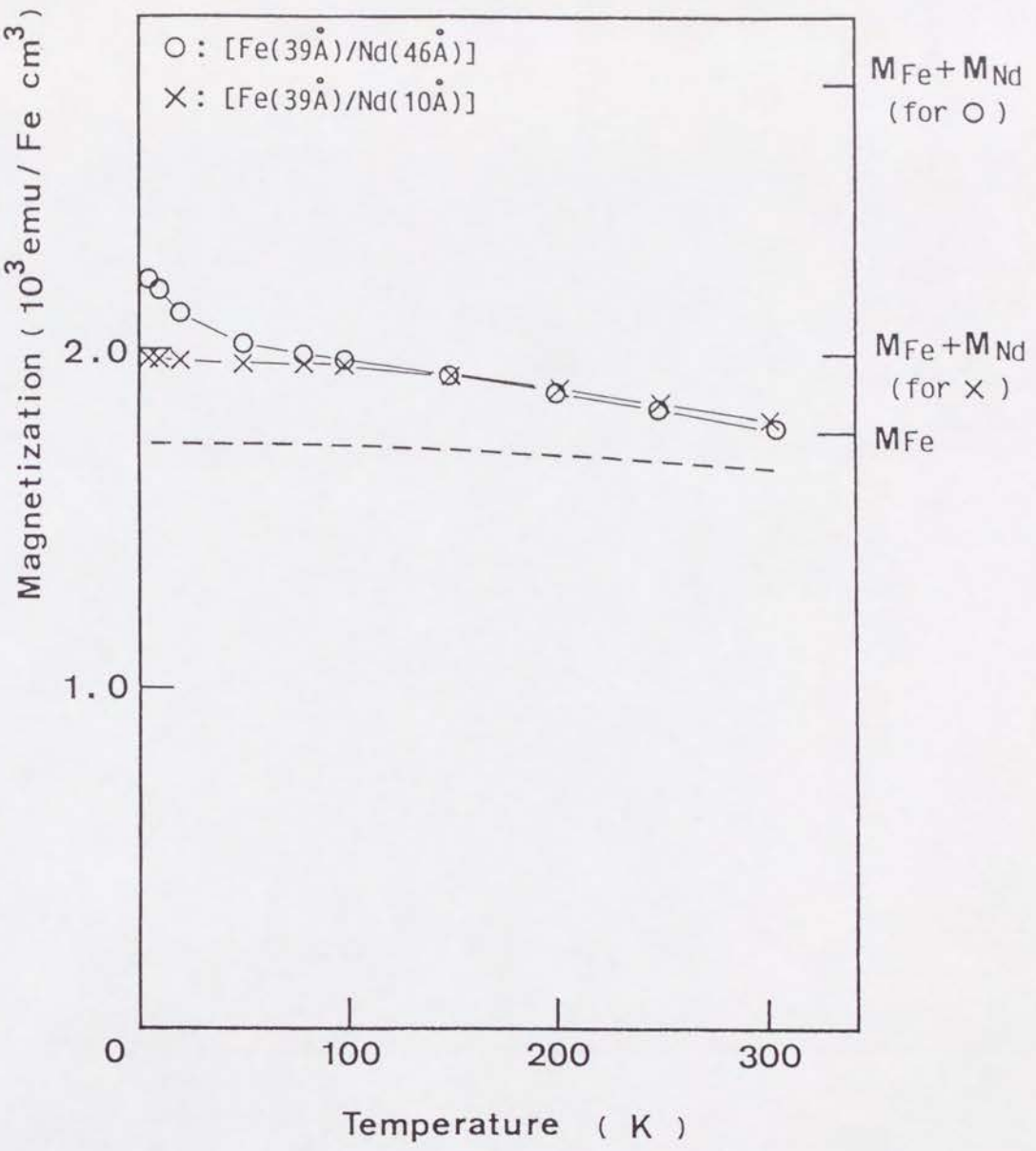

Fig. 35. Temperature dependence of magnetization for [Fe(39Å)/Nd(10Å)] and [Fe(39Å)/Nd(46Å)] in 24kOe. The broken line shows expected temperature dependence of the Fe layer magnetization. The full magnetization for the Fe layers (M_{Fe}) and Nd layers (M_{Nd}) are calculated with an assumption that the Fe and Nd atoms have magnetic moments of $2.22\mu_B$ and $3.27\mu_B$, respectively.

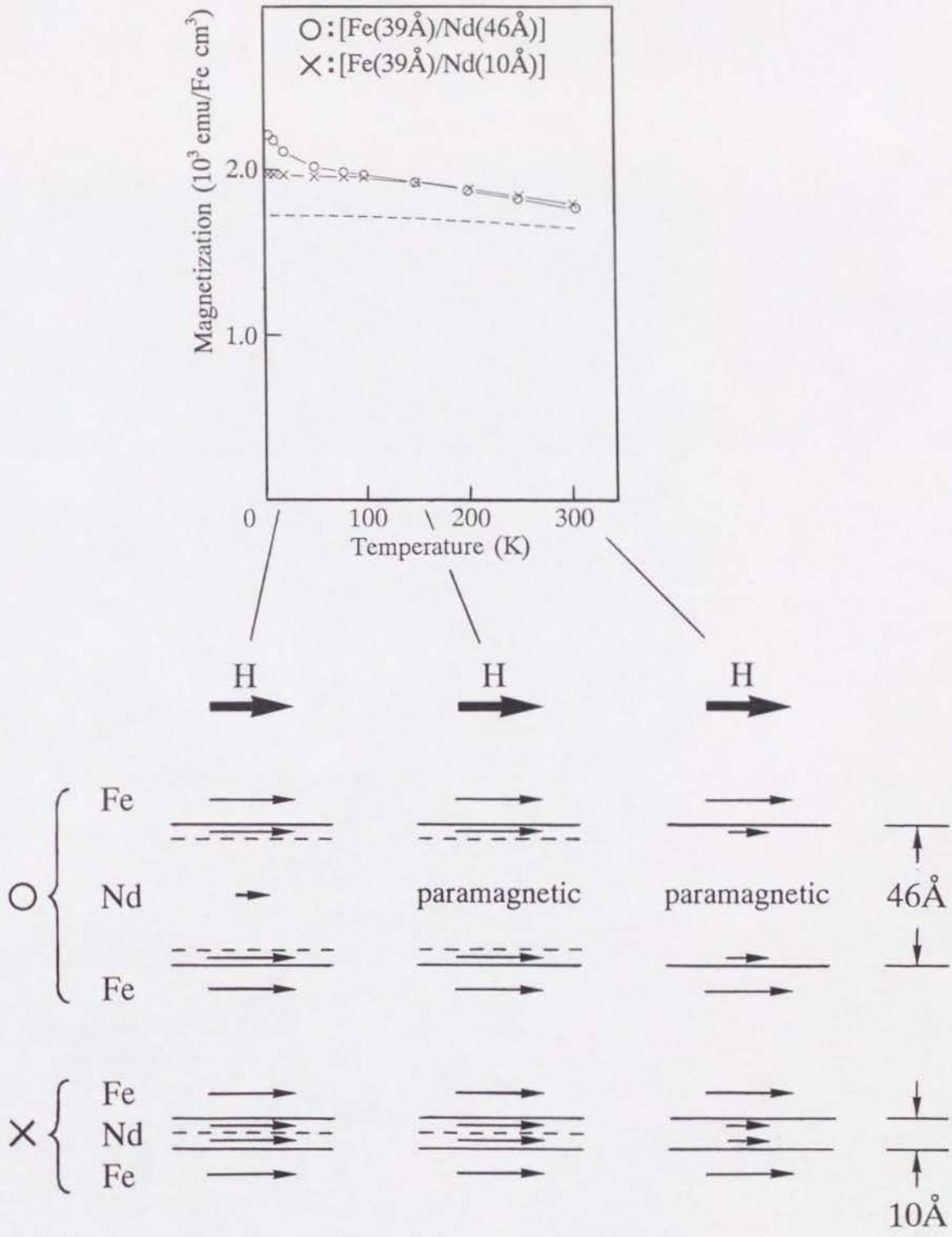

Fig. 36. Illustration of the magnetic structures for [Fe(39Å)/Nd(10Å)] and [Fe(39Å)/Nd(46Å)] in 24kOe at various temperatures.

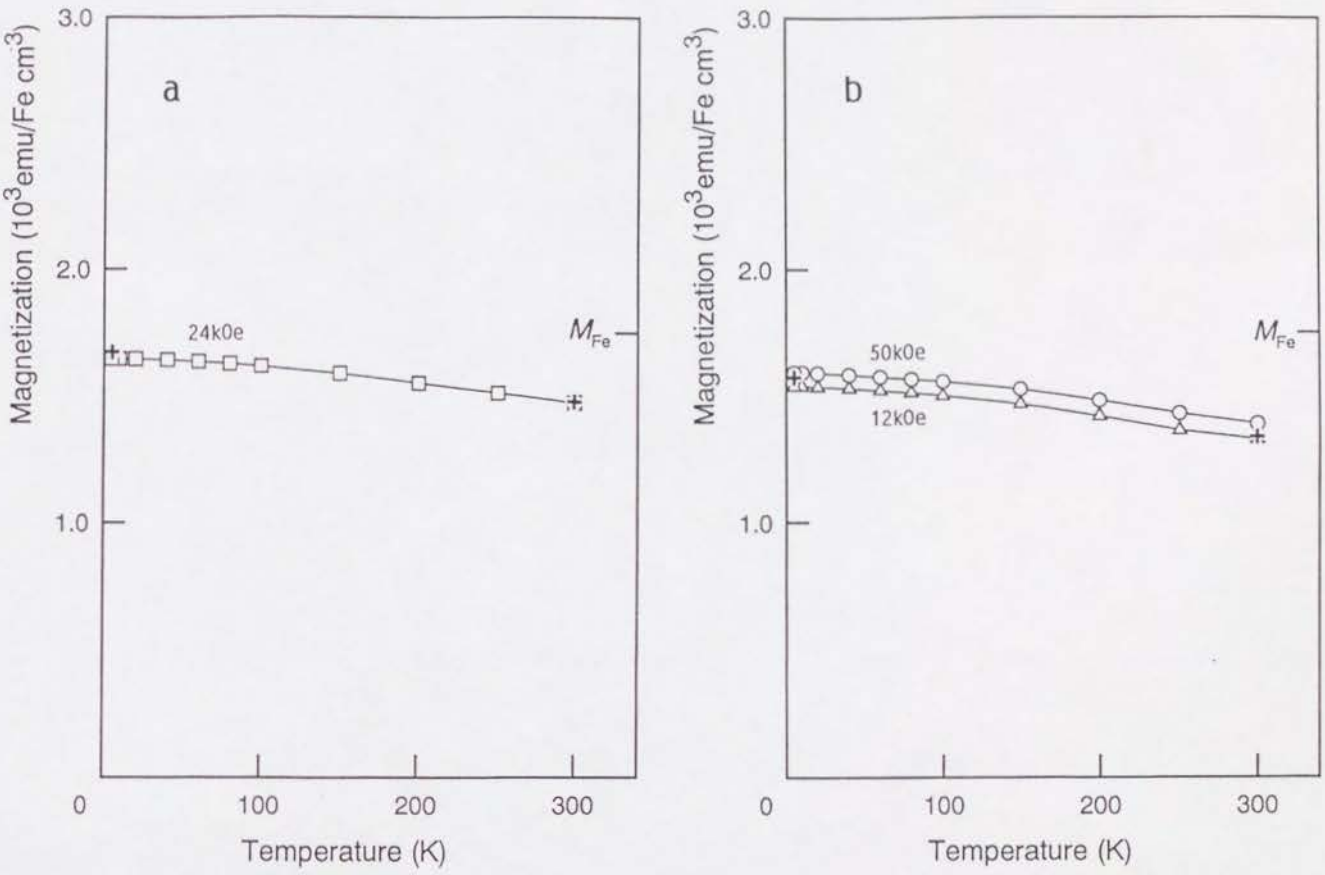

Fig. 37. Temperature dependence of magnetization for (a) [Fe(40Å)/Y(10Å)] and (b) [Fe(40Å)/Y(30Å)]. The Fe layer magnetization estimated from the average hyperfine field is shown at 4.2K and 300K (+). The calculated full magnetization of the Fe layers is expressed as M_{Fe}.

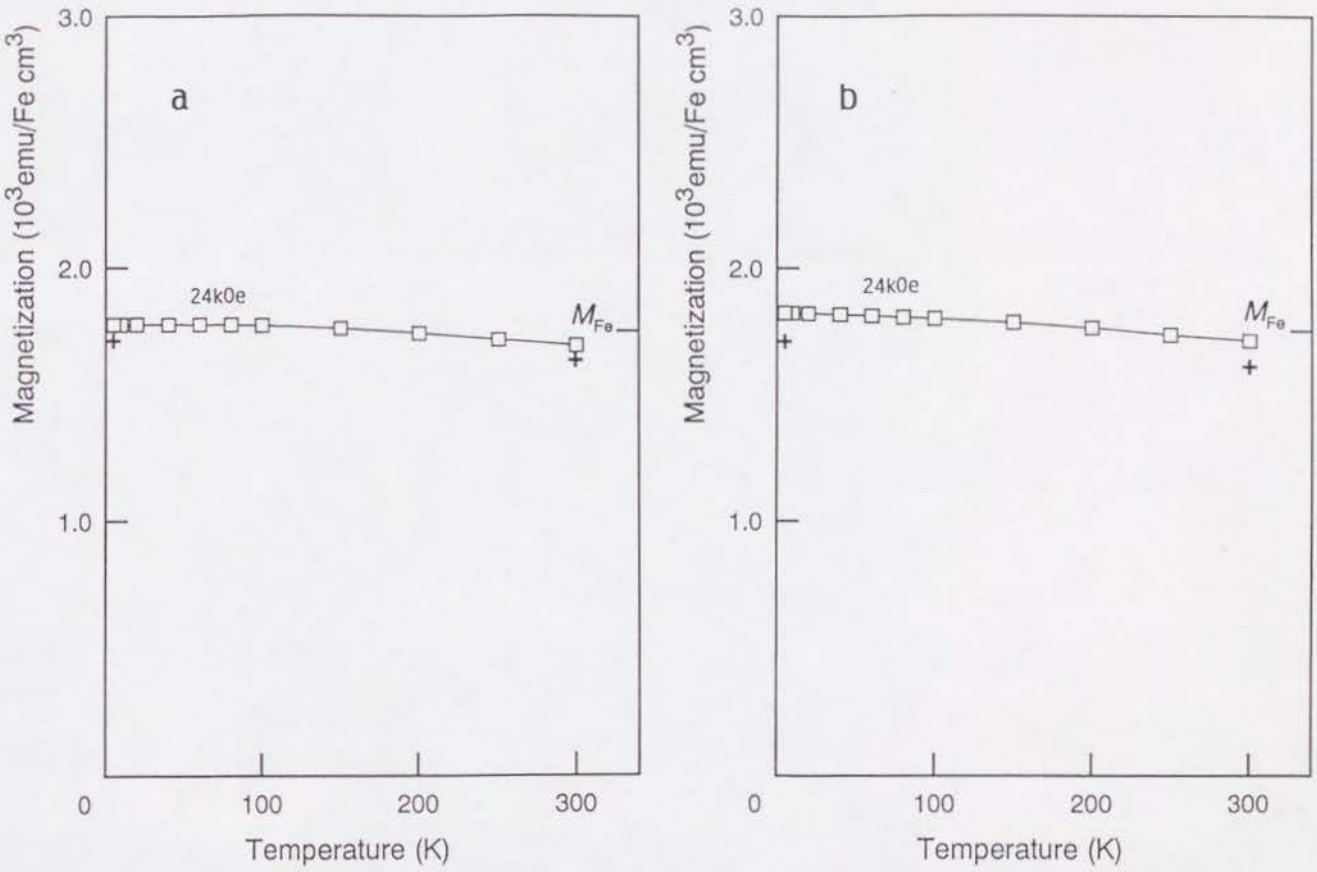

Fig. 38. Temperature dependence of magnetization for (a) [Fe(40Å)/La(10Å)] and (b) [Fe(40Å)/La(30Å)]. The Fe layer magnetization estimated from the average hyperfine field is shown at 4.2K and 300K (+). The calculated full magnetization of the Fe layers is expressed as M_{Fe}.

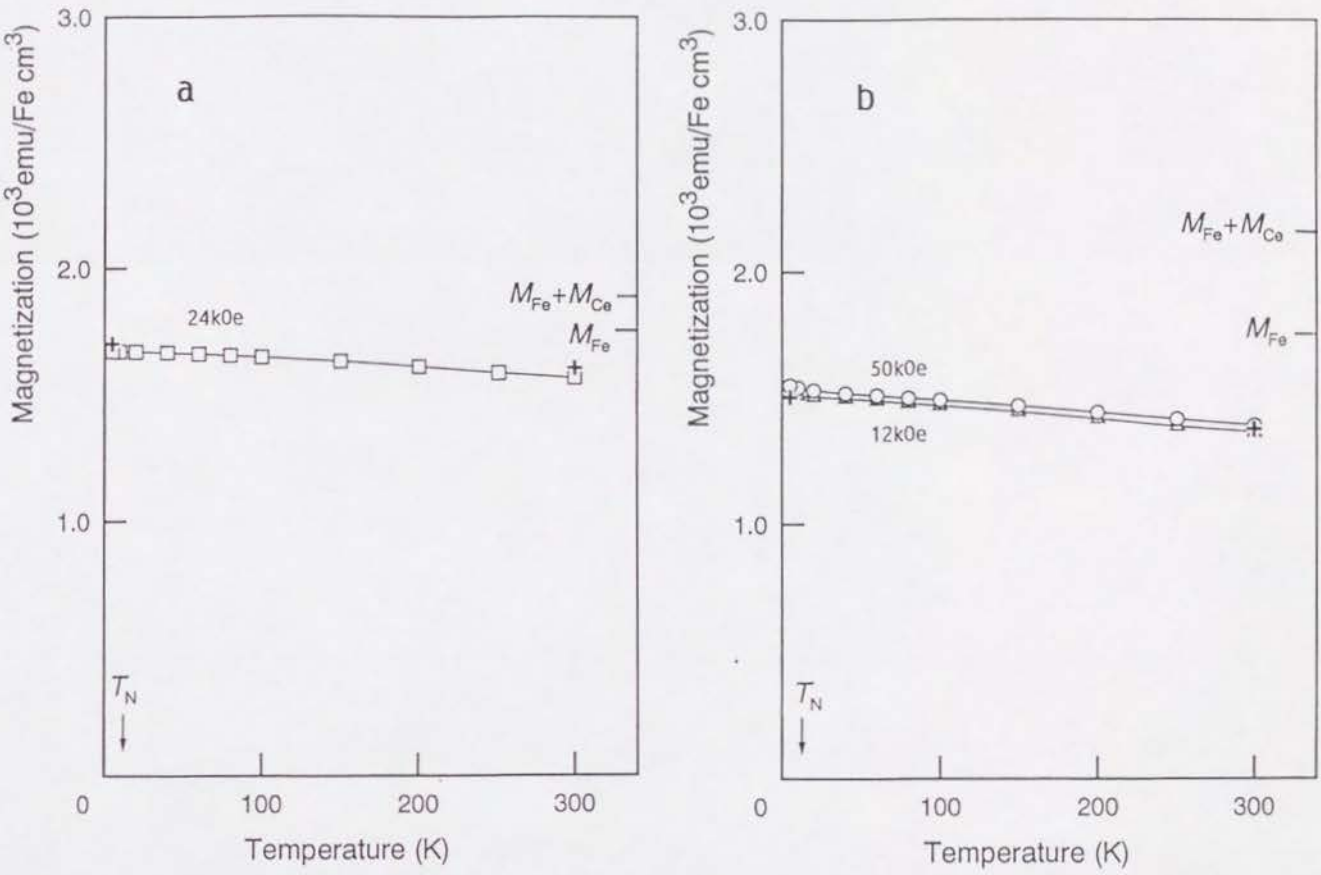

Fig. 39. Temperature dependence of magnetization for (a) [Fe(40Å)/Ce(10Å)] and (b) [Fe(40Å)/Ce(30Å)]. The Fe layer magnetization estimated from the average hyperfine field is shown at 4.2K and 300K (+). The calculated full magnetization of the Fe and Ce layers is expressed as M_{Fe} and M_{Ce}. The Néel temperature of bulk Ce metal is also shown in the figure.

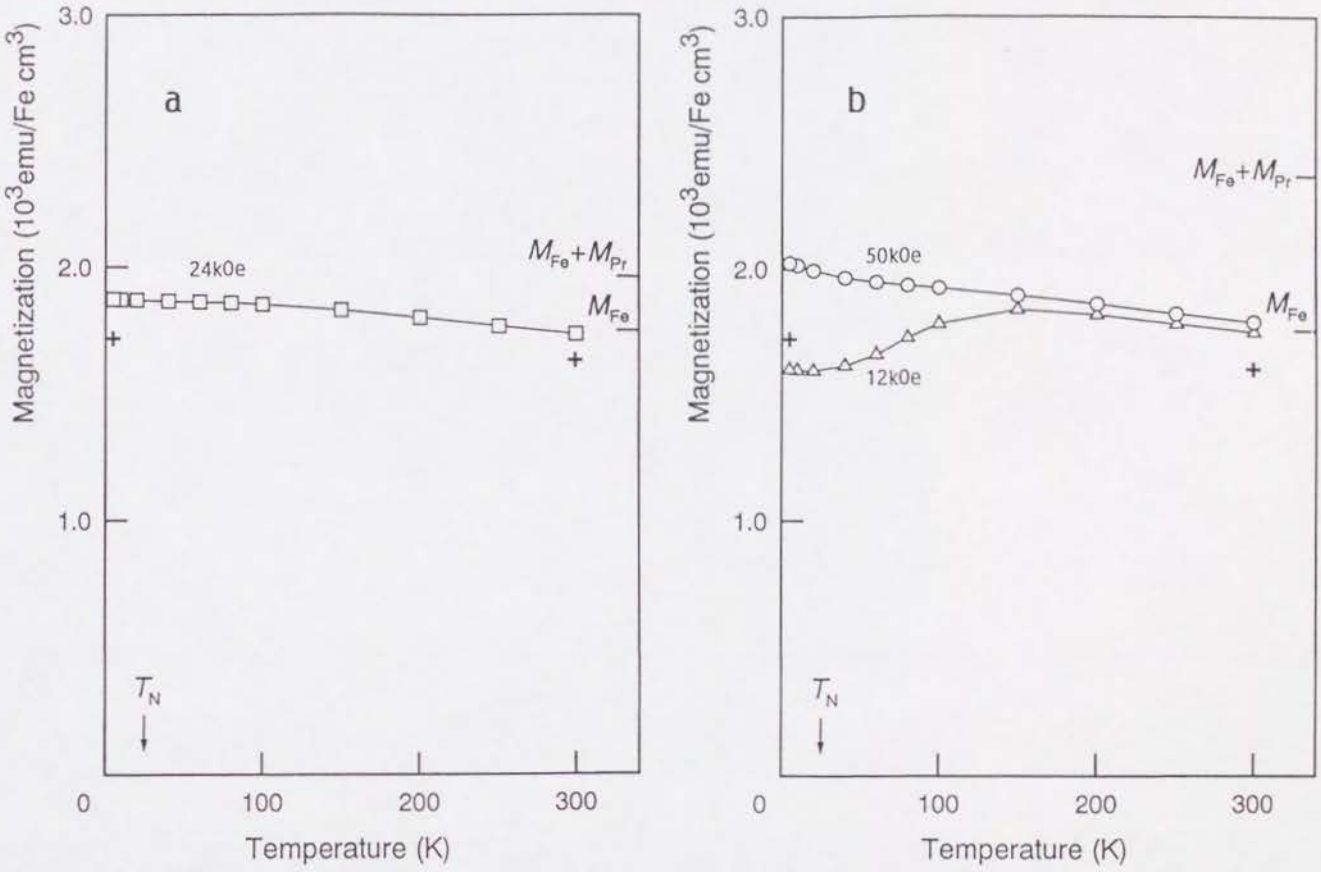

Fig. 40. Temperature dependence of magnetization for (a) [Fe(40Å)/Pr(10Å)] and (b) [Fe(40Å)/Pr(30Å)]. The Fe layer magnetization estimated from the average hyperfine field is shown at 4.2K and 300K (+). The calculated full magnetization of the Fe and Pr layers is expressed as M_{Fe} and M_{Pr}. The Néel temperature of bulk Pr metal is also shown in the figure.

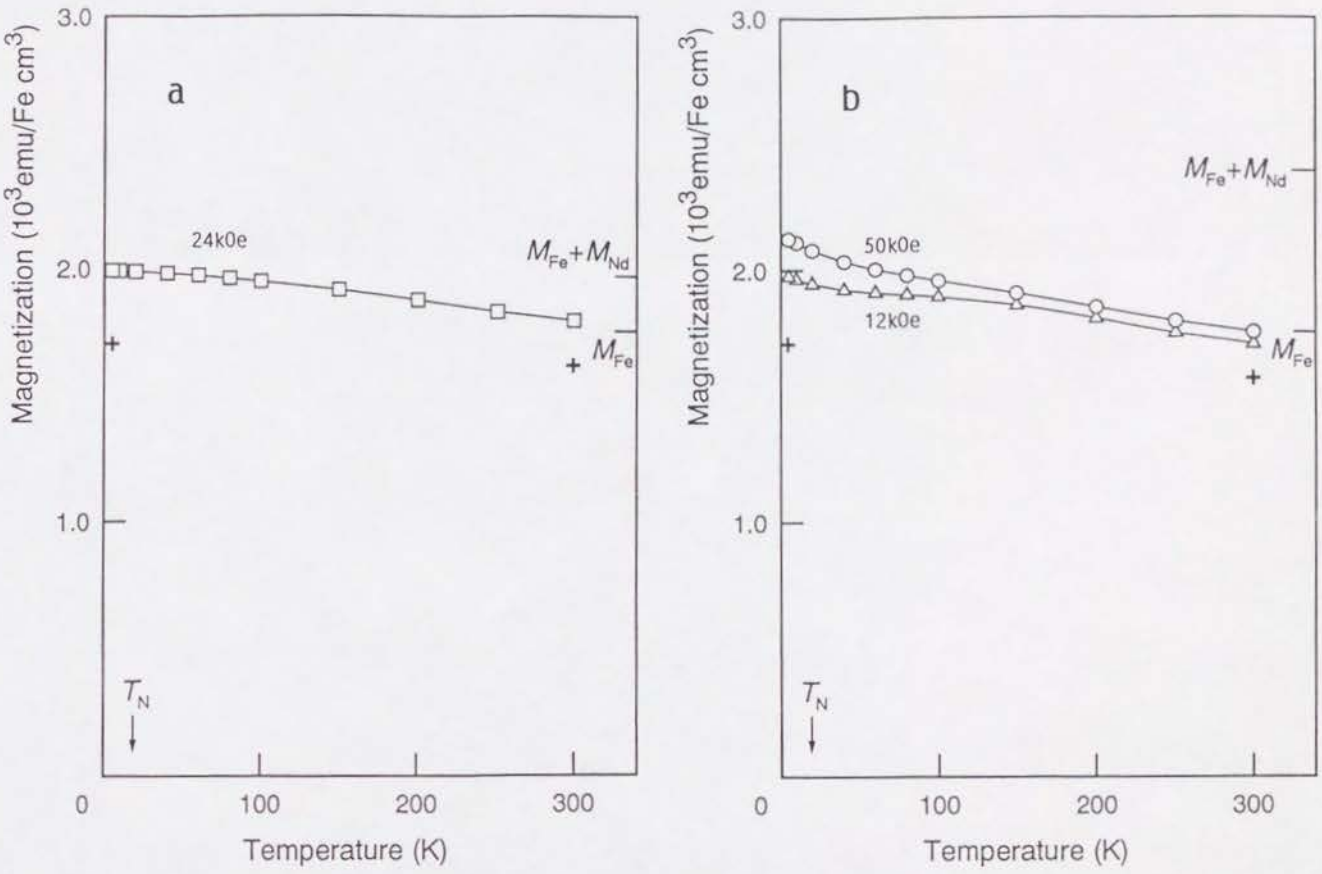

Fig. 41. Temperature dependence of magnetization for (a) [Fe(40Å)/Nd(10Å)] and (b) [Fe(40Å)/Nd(30Å)]. The Fe layer magnetization estimated from the average hyperfine field is shown at 4.2K and 300K (+). The calculated full magnetization of the Fe and Nd layers is expressed as M_{Fe} and M_{Nd}. The Néel temperature of bulk Nd metal is also shown in the figure.

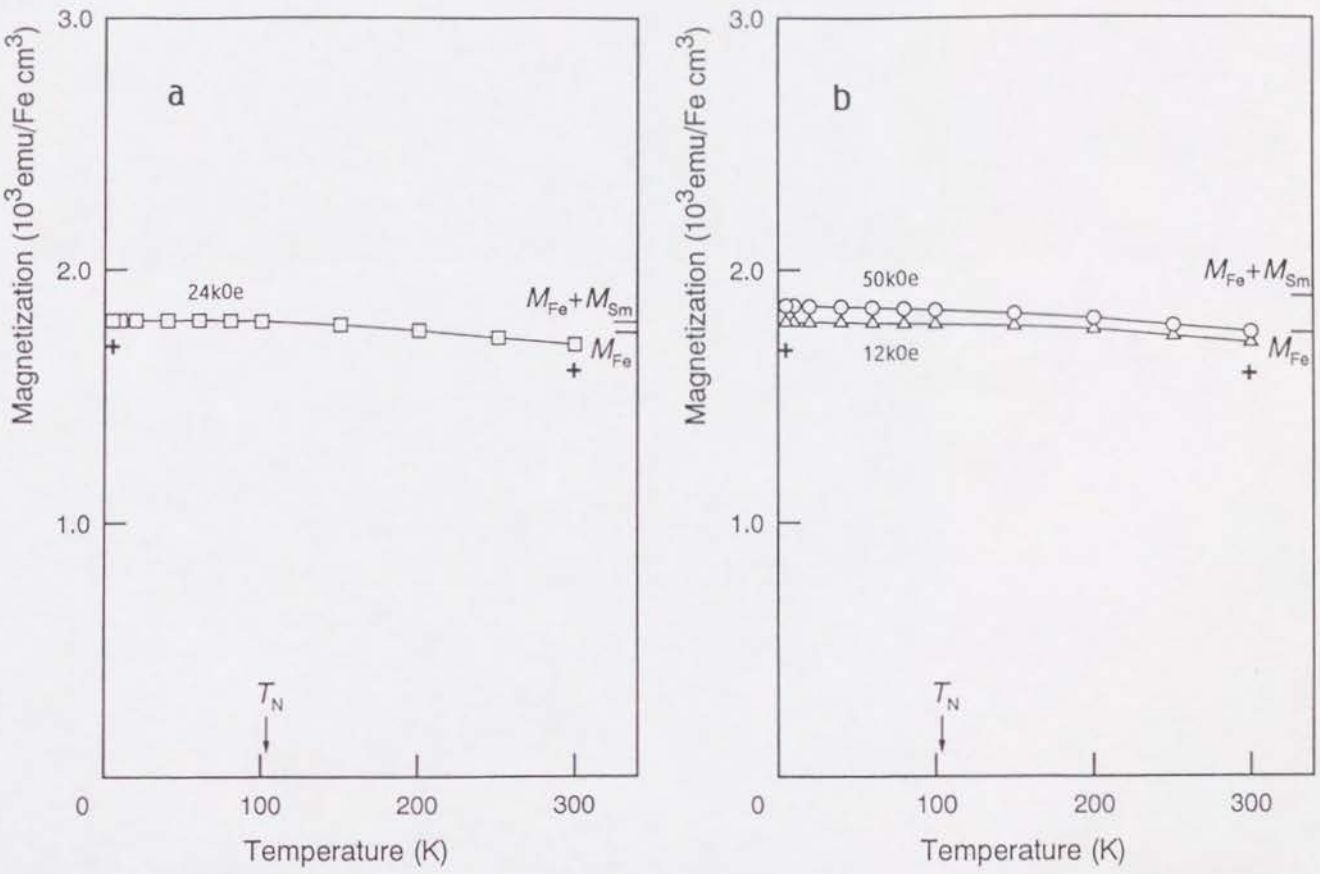

Fig. 42. Temperature dependence of magnetization for (a) [Fe(40Å)/Sm(10Å)] and (b) [Fe(40Å)/Sm(30Å)]. The Fe layer magnetization estimated from the average hyperfine field is shown at 4.2K and 300K (+). The calculated full magnetization of the Fe and Sm layers is expressed as M_{Fe} and M_{Sm}. The Néel temperature of bulk Sm metal is also shown in the figure.

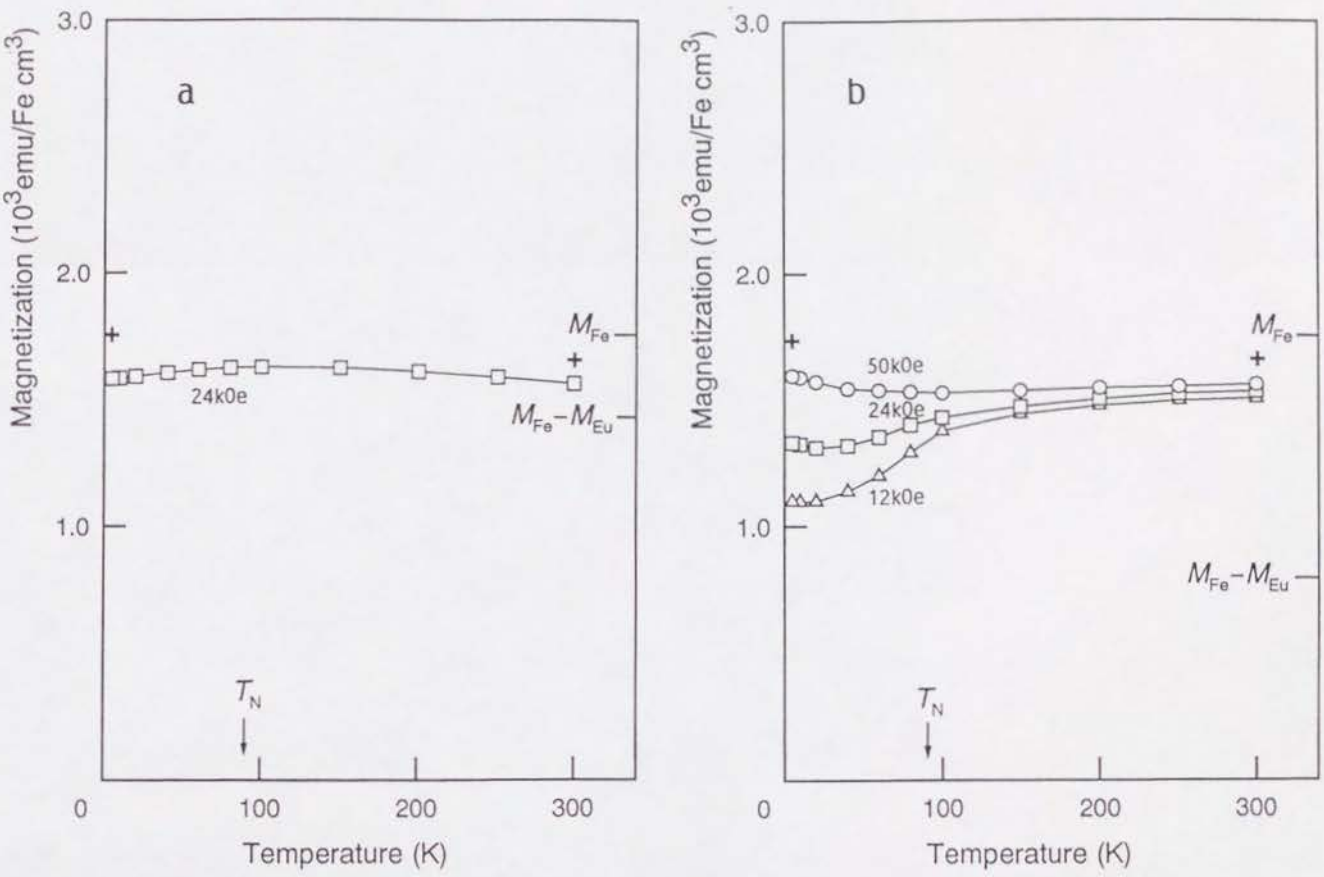

Fig. 43. Temperature dependence of magnetization for (a) [Fe(40Å)/Eu(10Å)] and (b) [Fe(40Å)/Eu(30Å)]. The Fe layer magnetization estimated from the average hyperfine field is shown at 4.2K and 300K (+). The calculated full magnetization of the Fe and Eu layers is expressed as M_{Fe} and M_{Eu}. The Néel temperature of bulk Eu metal is also shown in the figure.

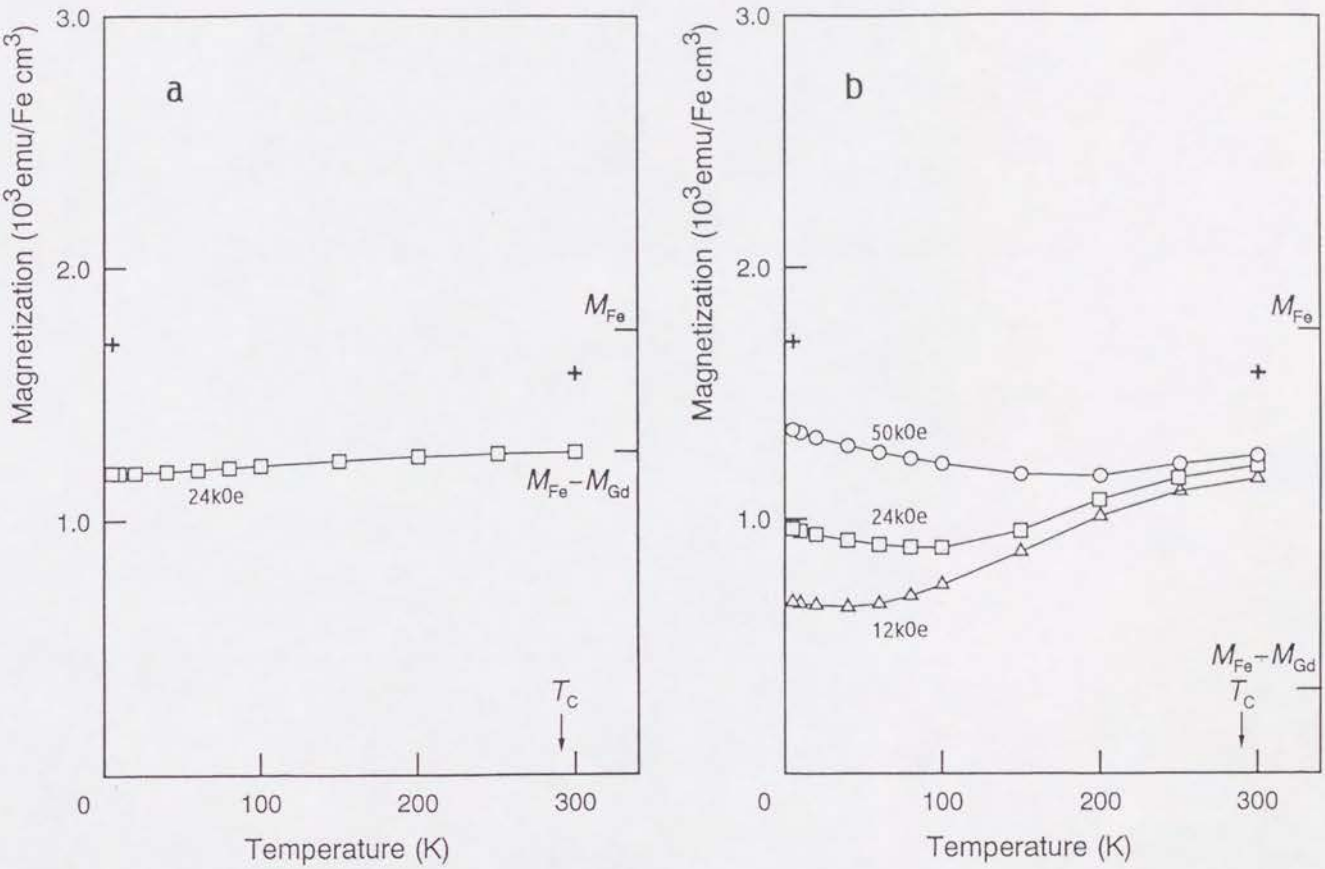

Fig. 44. Temperature dependence of magnetization for (a) [Fe(40Å)/Gd(10Å)] and (b) [Fe(40Å)/Gd(30Å)]. The Fe layer magnetization estimated from the average hyperfine field is shown at 4.2K and 300K (+). The calculated full magnetization of the Fe and Gd layers is expressed as M_{Fe} and M_{Gd}. The Curie temperature of bulk Gd metal is also shown in the figure.

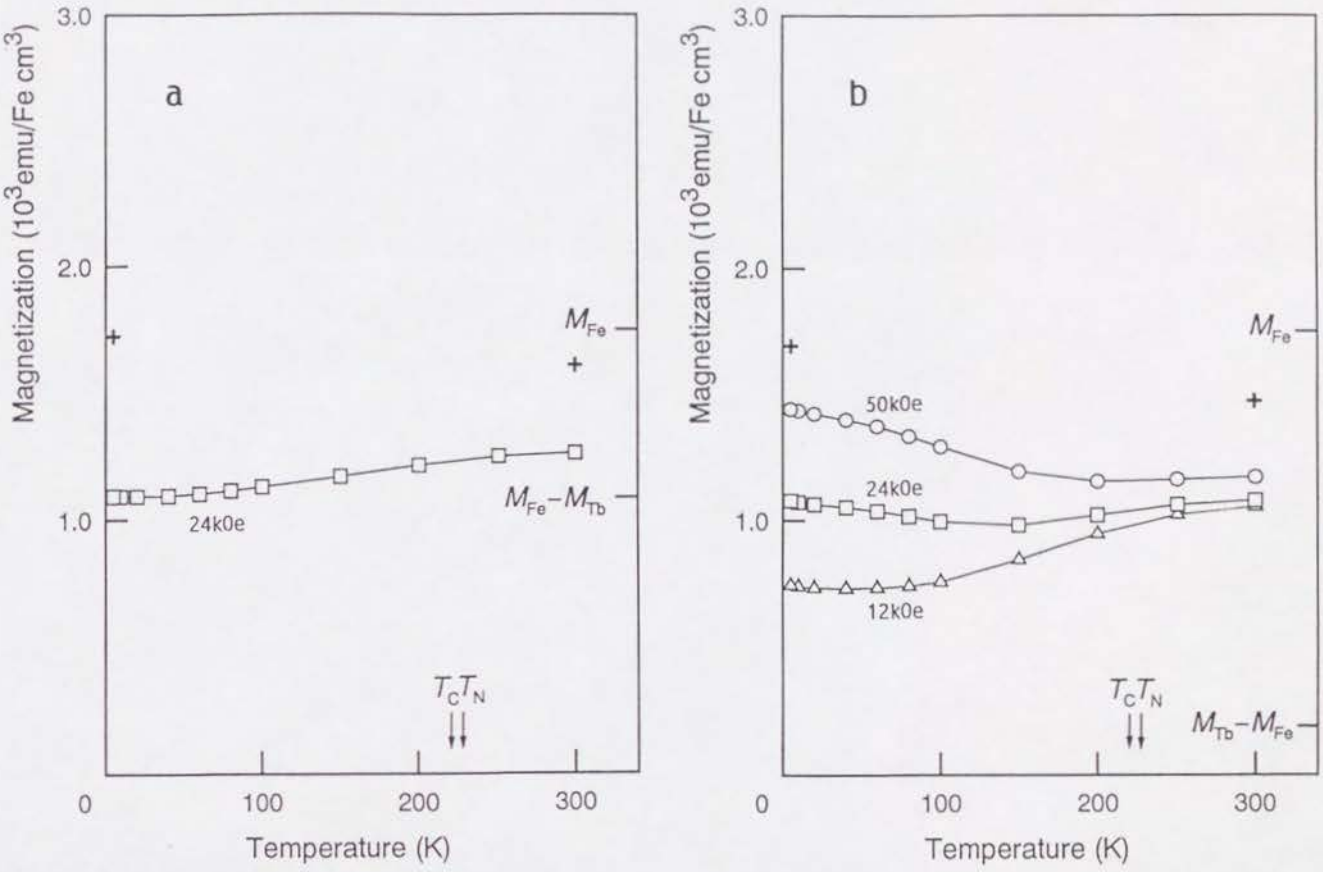

Fig. 45. Temperature dependence of magnetization for (a) [Fe(40Å)/Tb(10Å)] and (b) [Fe(40Å)/Tb(30Å)]. The Fe layer magnetization estimated from the average hyperfine field is shown at 4.2K and 300K (+). The calculated full magnetization of the Fe and Tb layers is expressed as M_{Fe} and M_{Tb}. The Néel and Curie temperatures of bulk Tb metal are also shown in the figure.

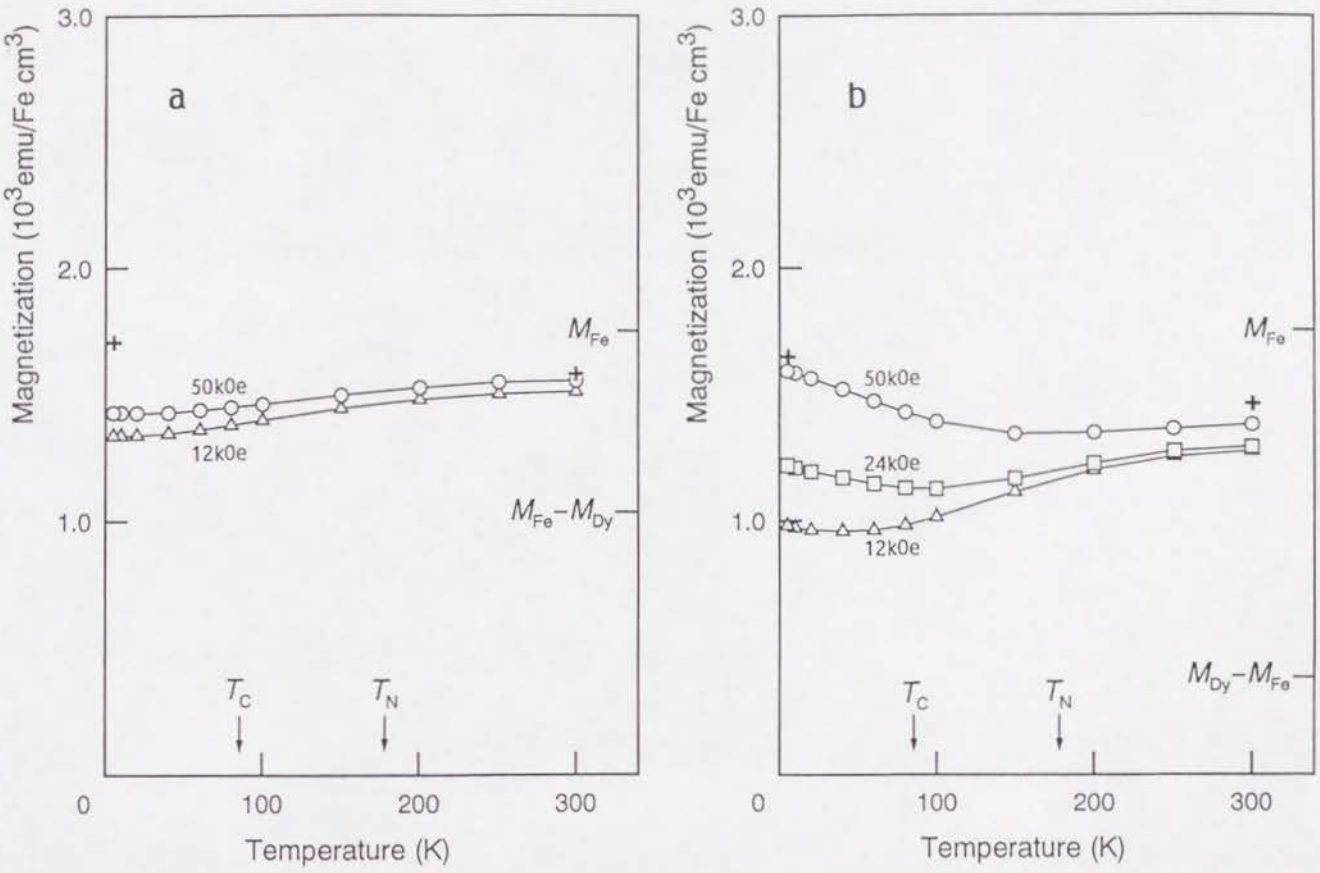

Fig. 46. Temperature dependence of magnetization for (a) [Fe(40Å)/Dy(10Å)] and (b) [Fe(40Å)/Dy(30Å)]. The Fe layer magnetization estimated from the average hyperfine field is shown at 4.2K and 300K (+). The calculated full magnetization of the Fe and Dy layers is expressed as M_{Fe} and M_{Dy}. The Néel and Curie temperatures of bulk Dy metal are also shown in the figure.

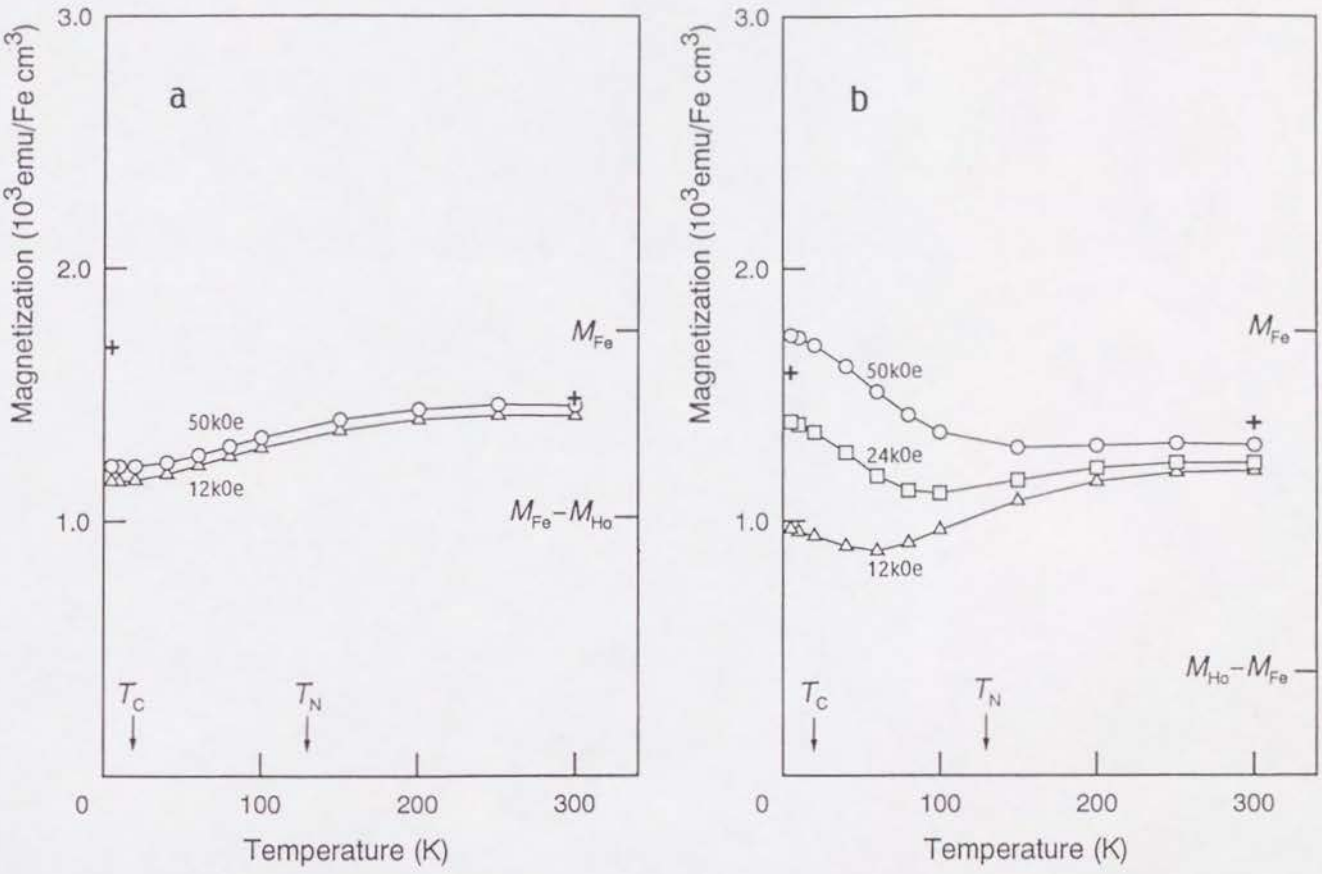

Fig. 47. Temperature dependence of magnetization for (a) [Fe(40Å)/Ho(10Å)] and (b) [Fe(40Å)/Ho(30Å)]. The Fe layer magnetization estimated from the average hyperfine field is shown at 4.2K and 300K (+). The calculated full magnetization of the Fe and Ho layers is expressed as M_{Fe} and M_{Ho}. The Néel and Curie temperatures of bulk Ho metal are also shown in the figure.

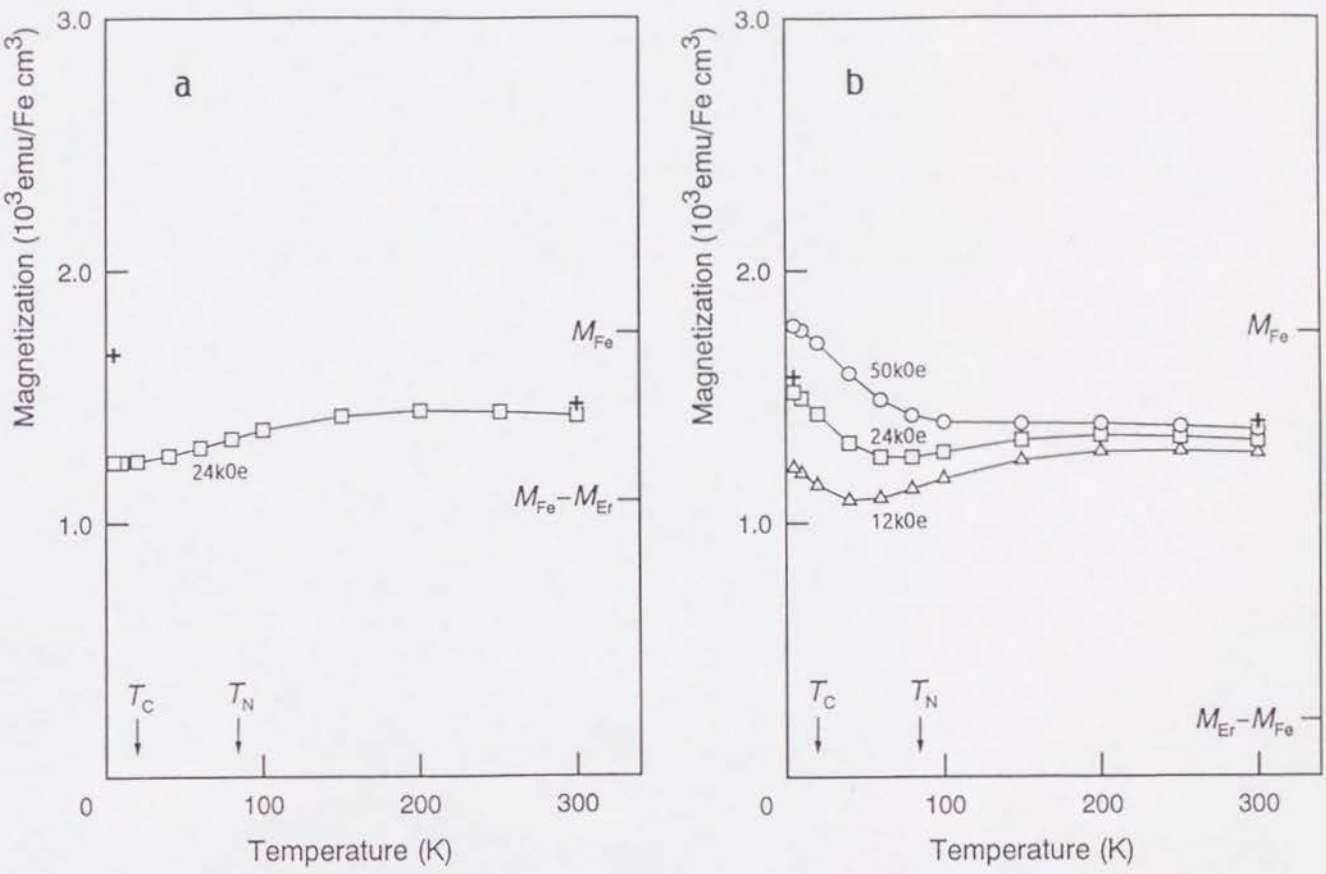

Fig. 48. Temperature dependence of magnetization for (a) [Fe(40Å)/Er(10Å)] and (b) [Fe(40Å)/Er(30Å)]. The Fe layer magnetization estimated from the average hyperfine field is shown at 4.2K and 300K (+). The calculated full magnetization of the Fe and Er layers is expressed as M_{Fe} and M_{Er}. The Néel and Curie temperatures of bulk Er metal are also shown in the figure.

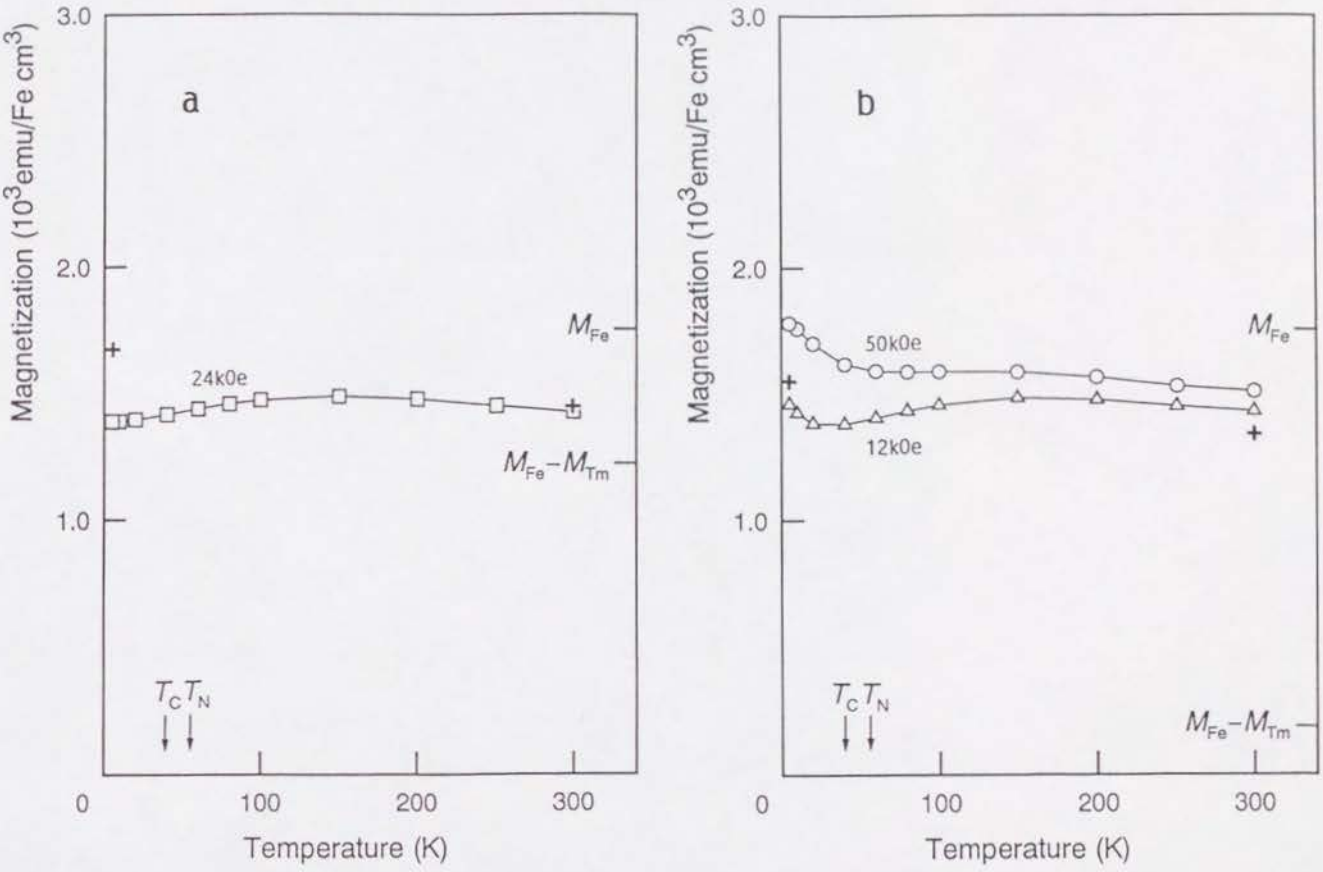

Fig. 49. Temperature dependence of magnetization for (a) [Fe(40Å)/Tm(10Å)] and (b) [Fe(40Å)/Tm(30Å)]. The Fe layer magnetization estimated from the average hyperfine field is shown at 4.2K and 300K (+). The calculated full magnetization of the Fe and Tm layers is expressed as M_{Fe} and M_{Tm}. The Néel and Curie temperatures of bulk Tm metal are also shown in the figure.

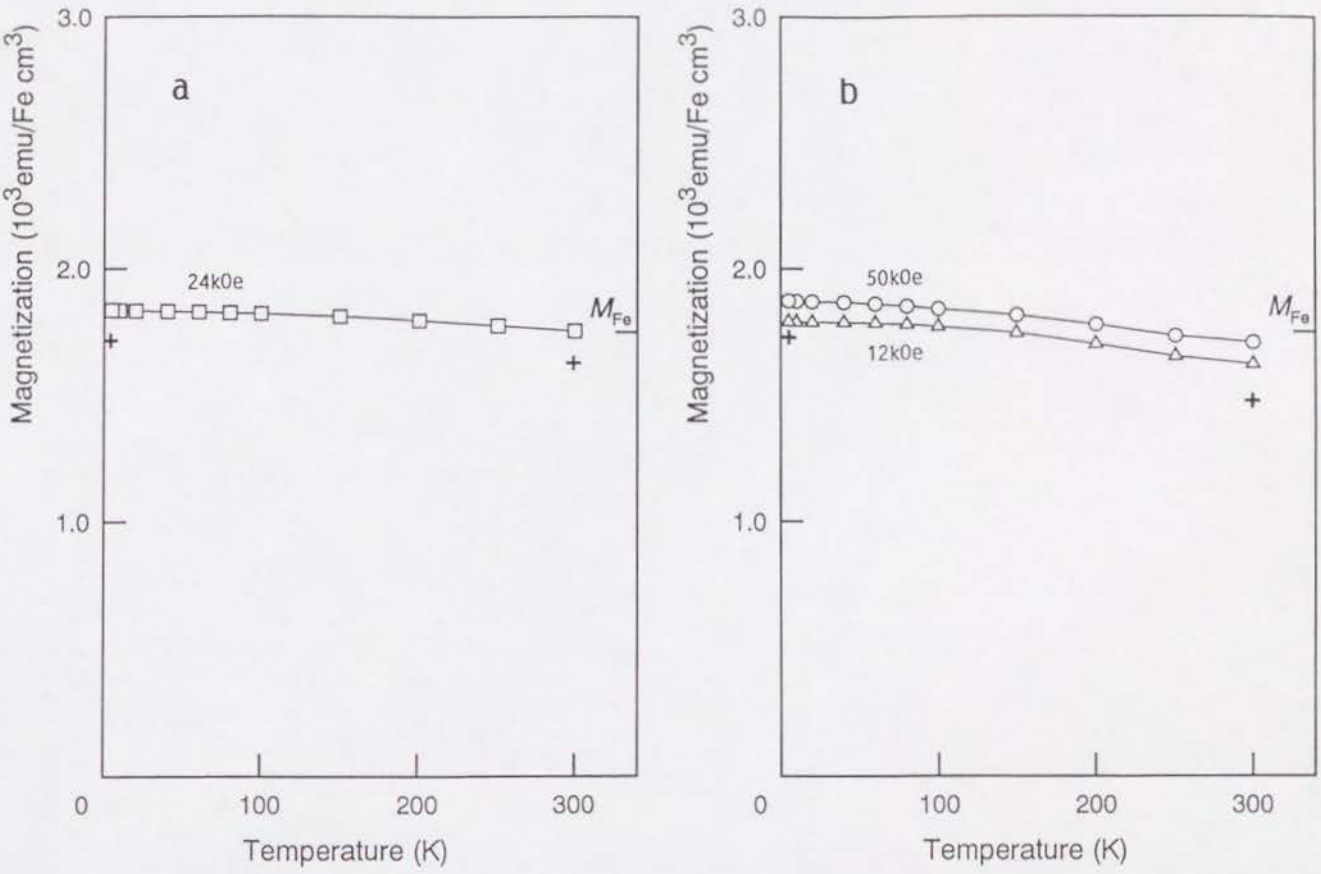

Fig. 50. Temperature dependence of magnetization for (a) [Fe(40Å)/Yb(10Å)] and (b) [Fe(40Å)/Yb(30Å)]. The Fe layer magnetization estimated from the average hyperfine field is shown at 4.2K and 300K (+). The calculated full magnetization of the Fe layers is expressed as M_{Fe}.

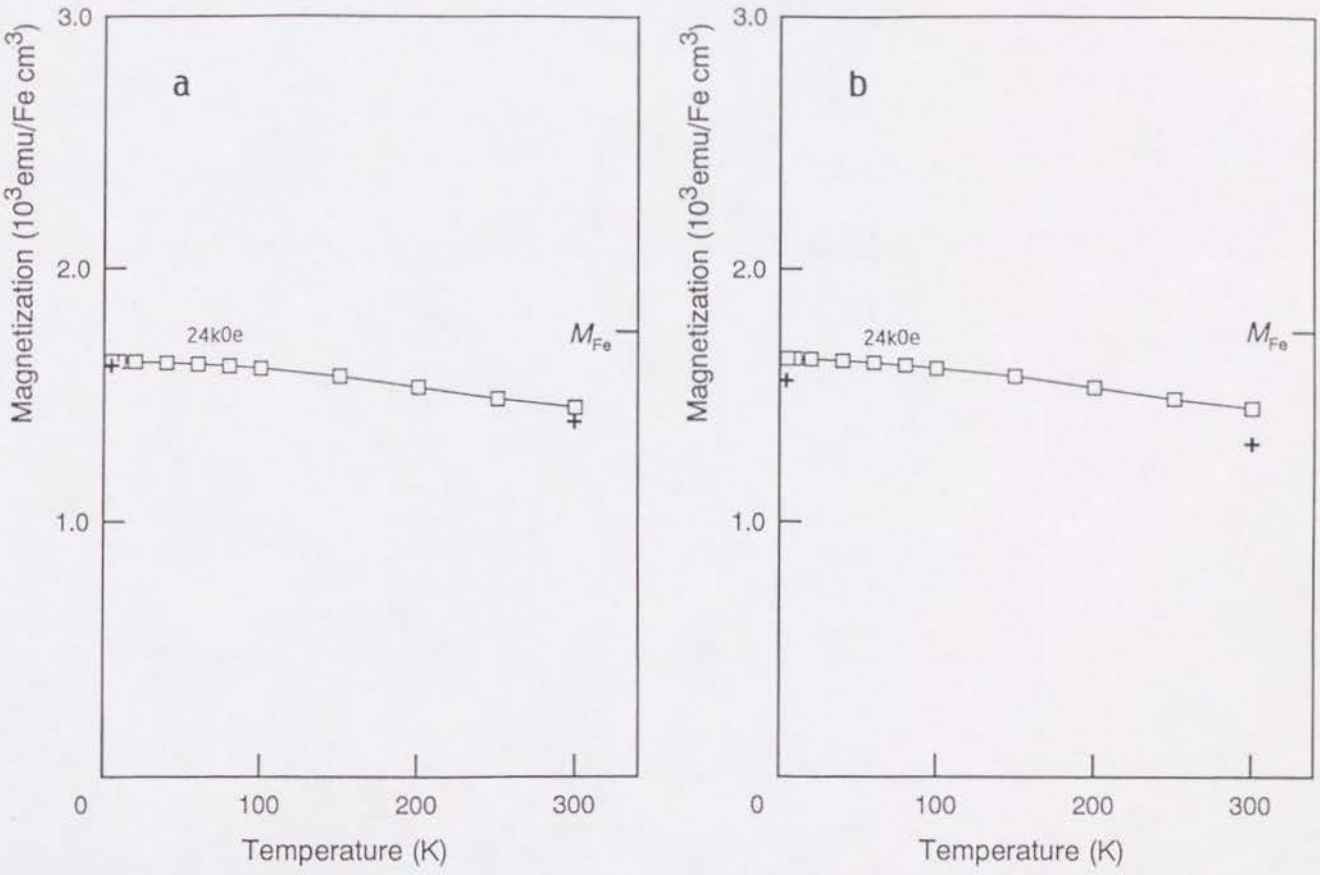

Fig. 51. Temperature dependence of magnetization for (a) [Fe(40Å)/Lu(10Å)] and (b) [Fe(40Å)/Lu(30Å)]. The Fe layer magnetization estimated from the average hyperfine field is shown at 4.2K and 300K (+). The calculated full magnetization of the Fe layers is expressed as M_{Fe}.

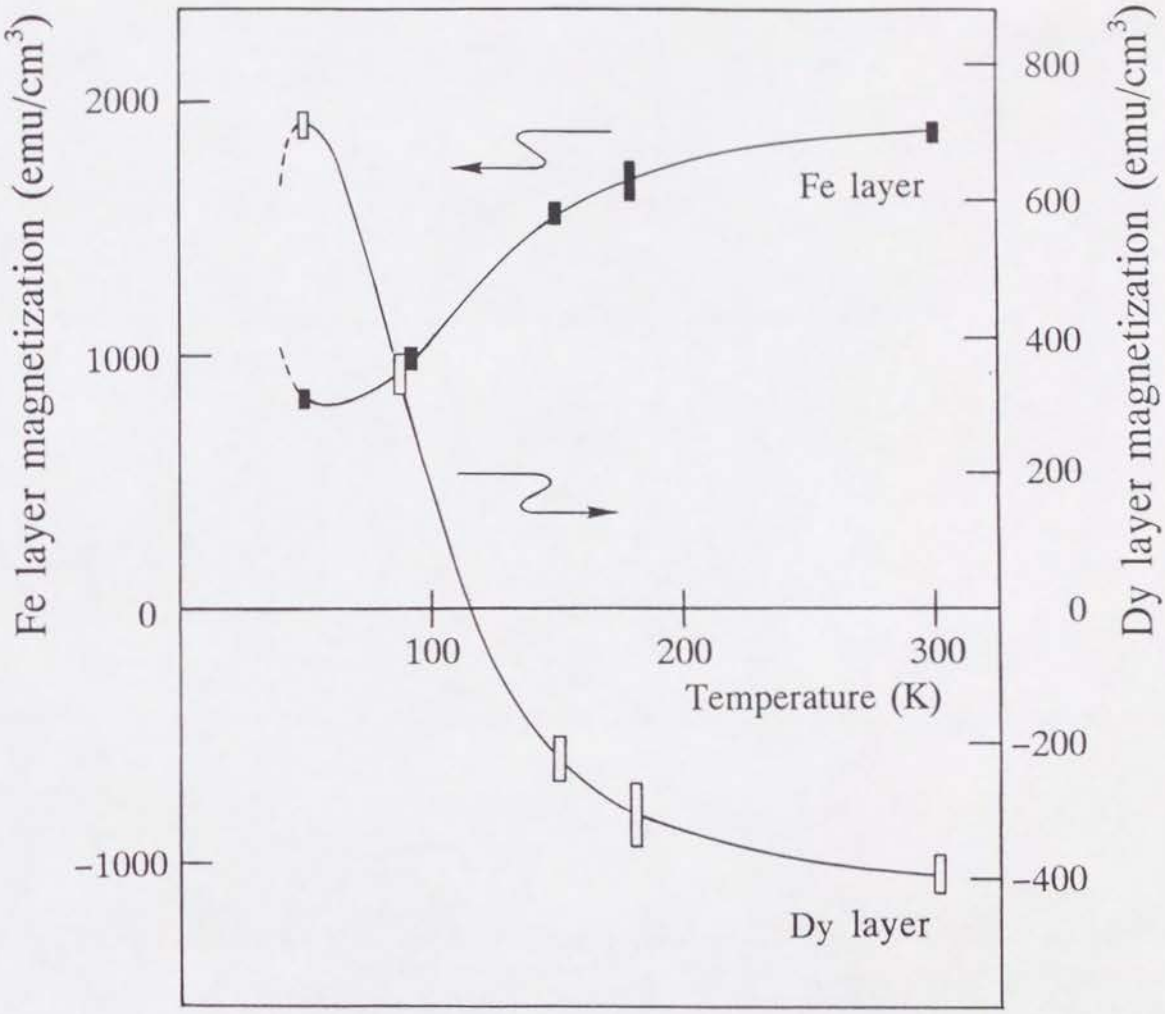

Fig. 52. Temperature dependence of the Fe and Dy layer magnetization for [Fe(40Å)/Dy(60Å)] in 9.8kOe derived from neutron diffraction measurement.

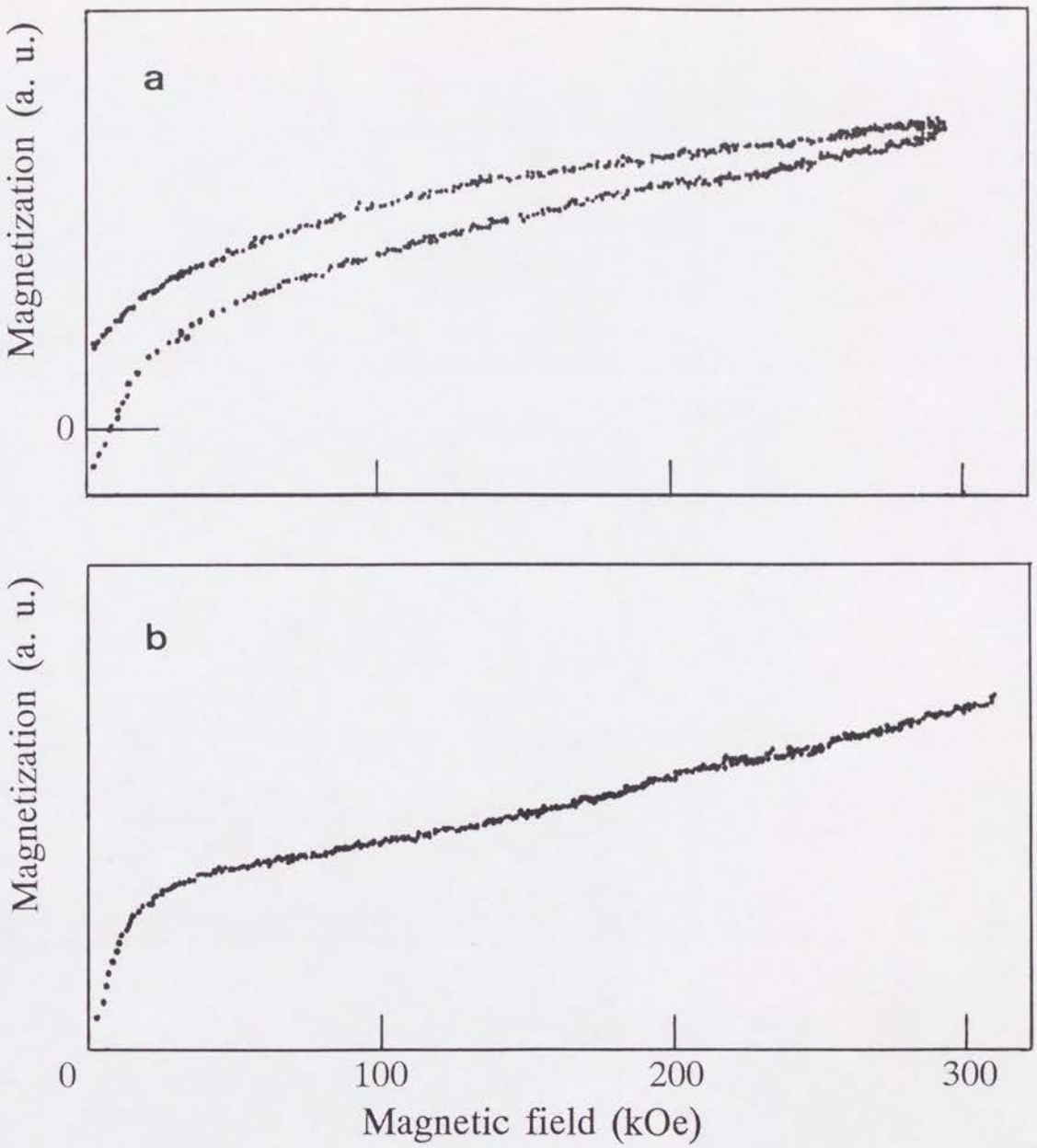

Fig. 53. Magnetization curves for (a) [Fe(40Å)/Dy(40Å)] and (b) [Fe(44Å)/Dy(12Å)] measured in pulsed high magnetic fields at 4.2K. (After M. Motokawa *et al.*: the 45th Annual Meeting of the Physical Society of Japan, Osaka, Mar. 30, 1990.)

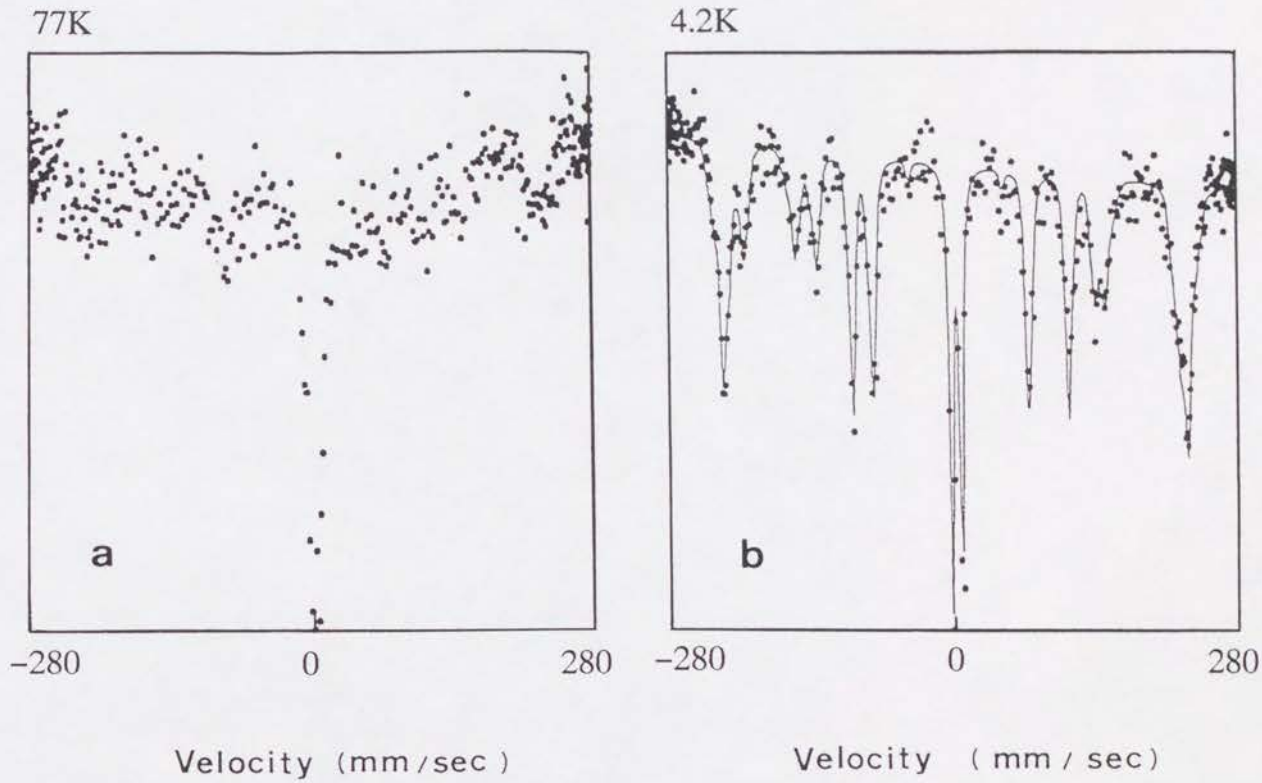

Fig. 54. ^{161}Dy Mössbauer spectra for [Fe(15Å)/Dy(30Å)] at (a) 77K and (b) 4.2K (ref. 37).

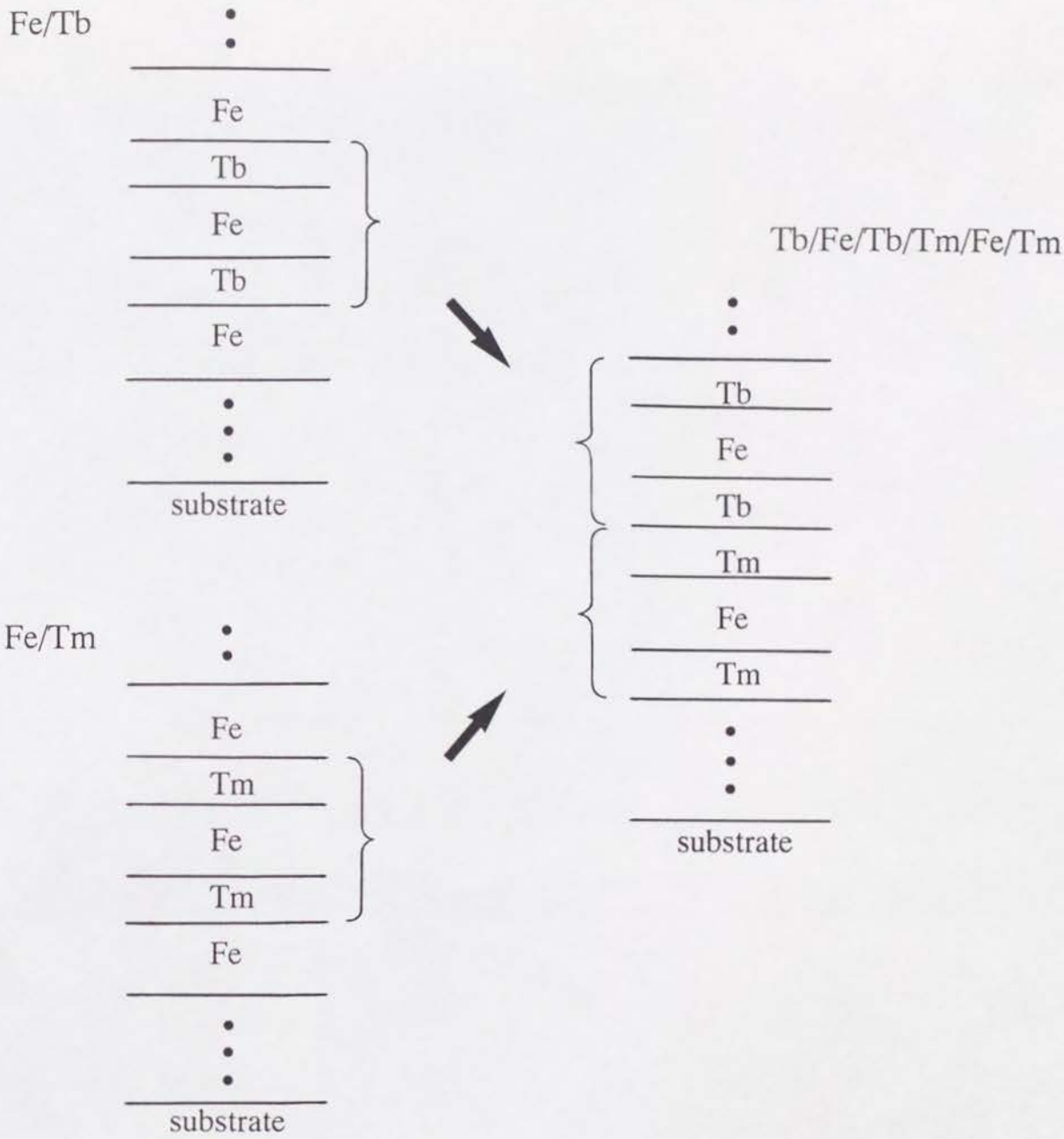

Fig. 55. Structure of a Tb/Fe/Tb/Tm/Fe/Tm multilayer, where Fe layers are sandwiched between Tb layers or between Tm layers.

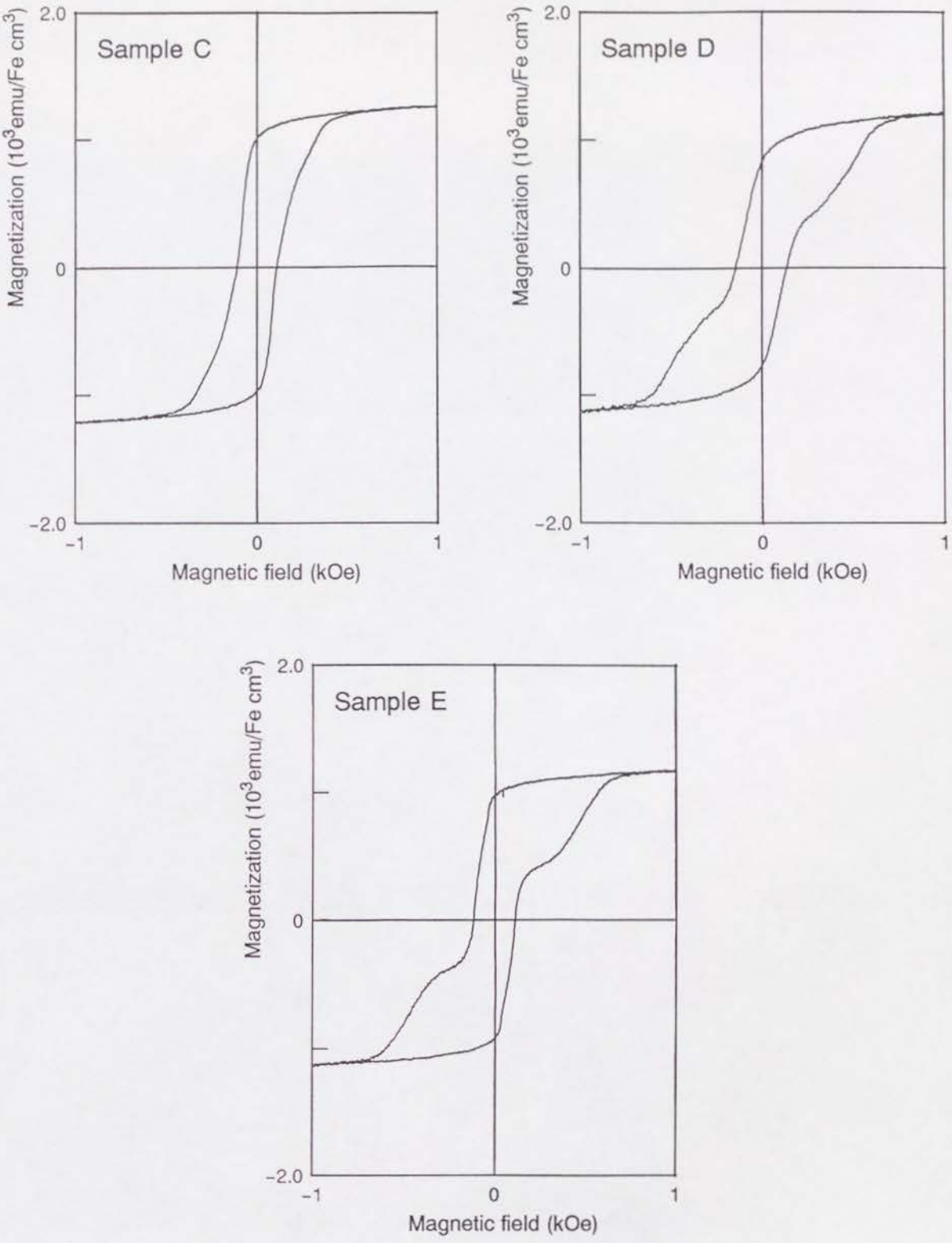

Fig. 56. Magnetization curves for Tb/Fe/Tb/Tm/Fe/Tm multilayers at 300K.

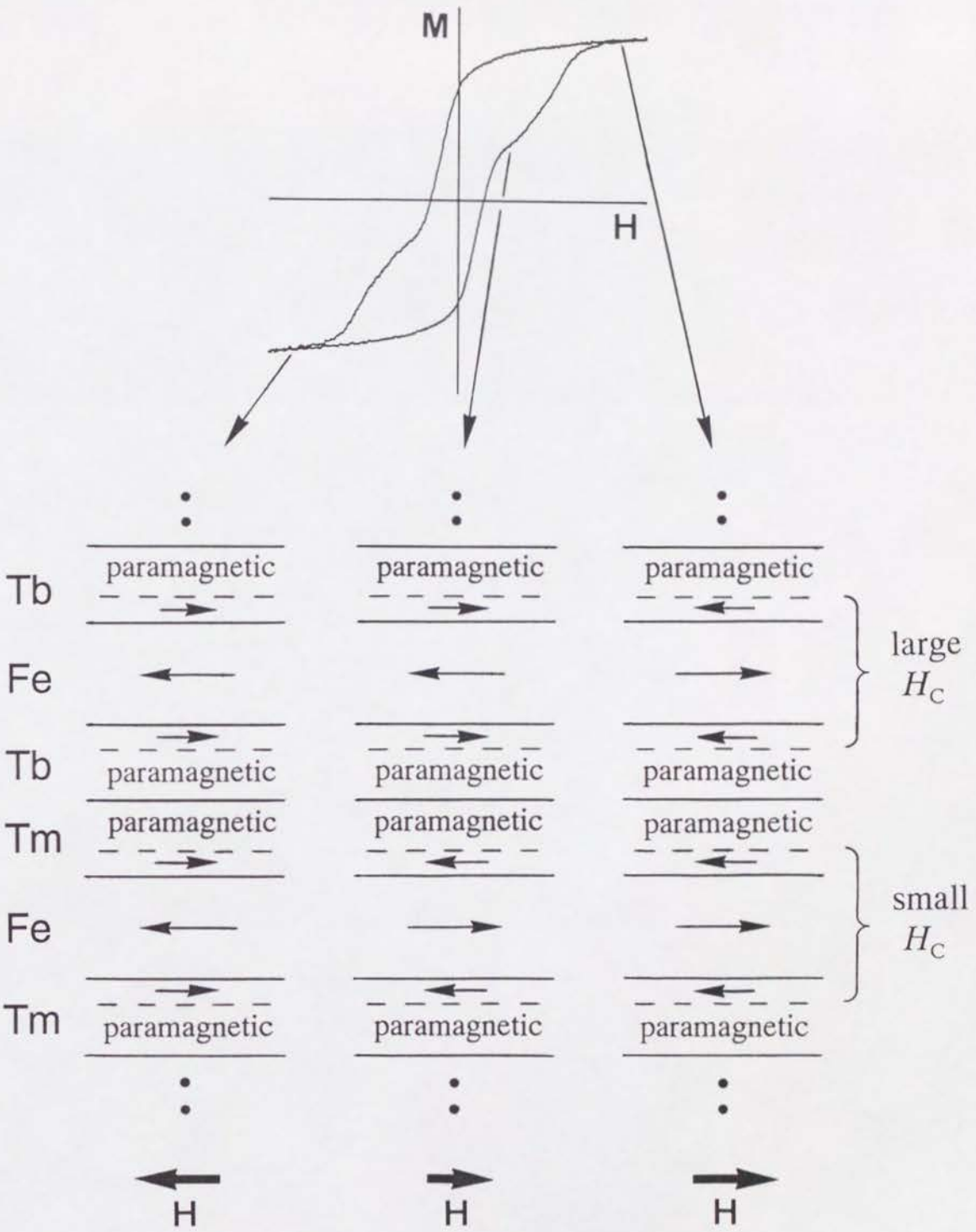

Fig. 57. Illustration of the magnetization process of the Tb/Fe/Tb/Tm/Fe/Tm multilayer (Sample D or E) at 300K.

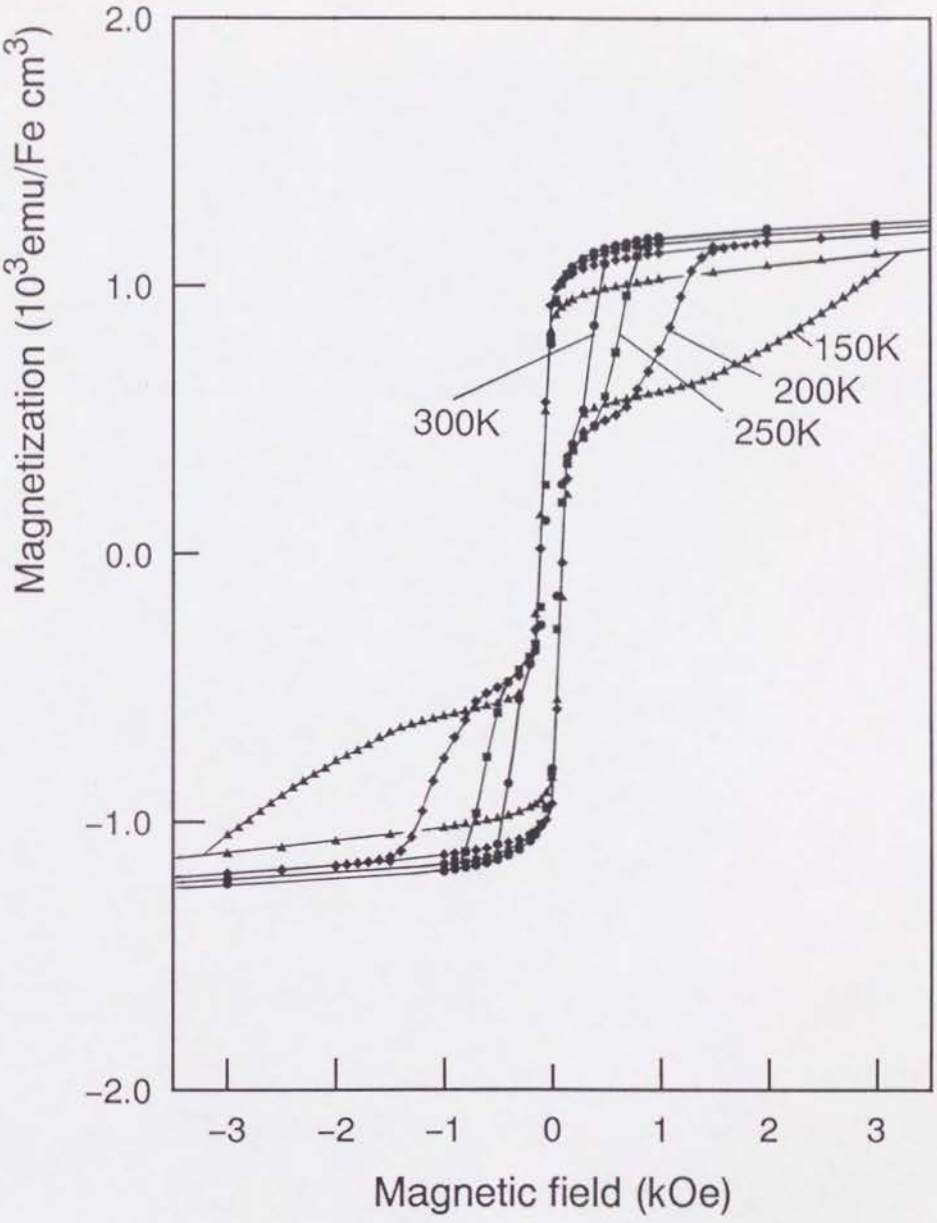

Fig. 58. Temperature dependence of in-plane M-H curves for the Tb/Fe/Tb/Tm/Fe/Tm multilayer (Sample E).

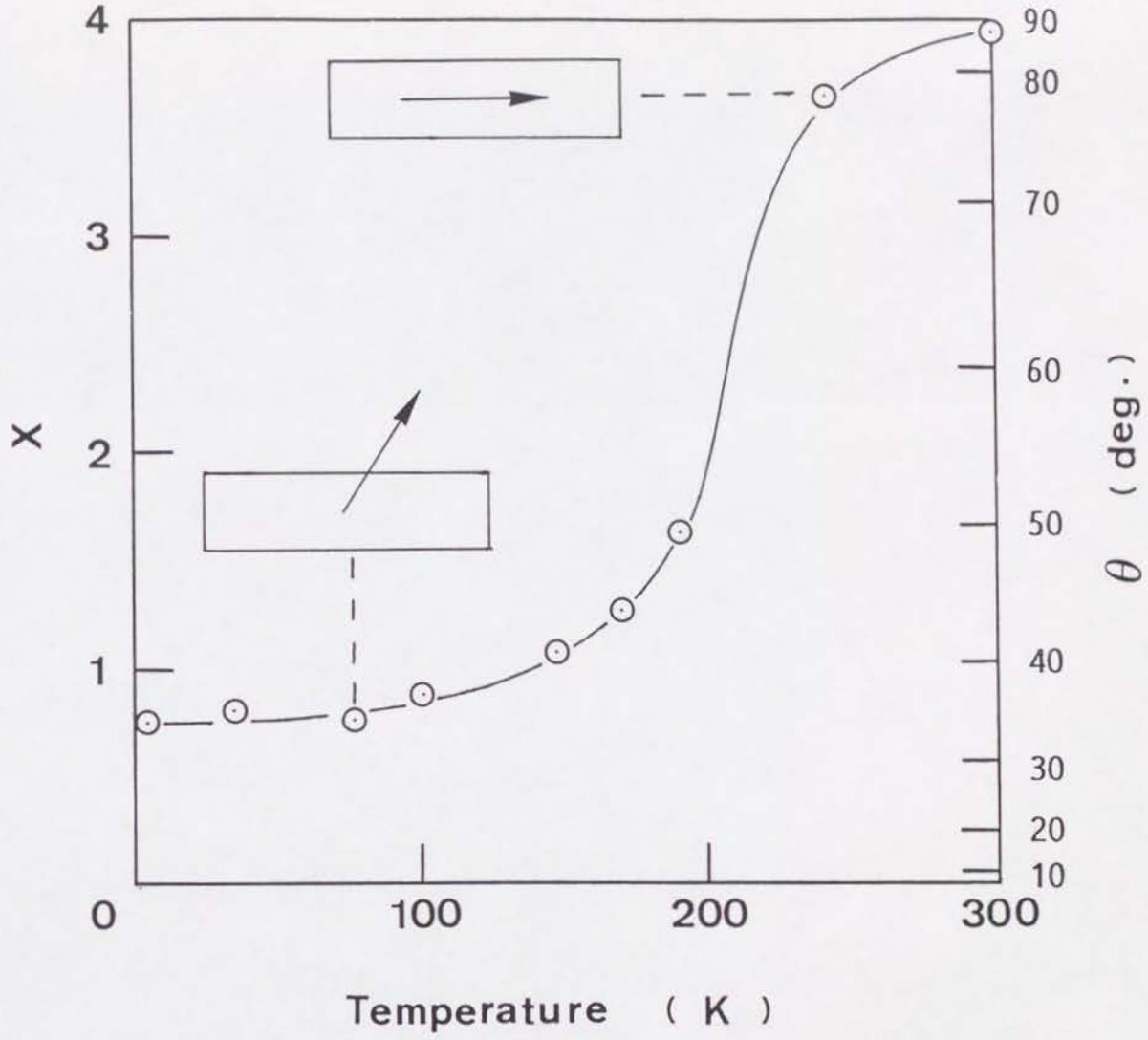

Fig. 59. Temperature dependence of the relative intensity X of the Δm=0 (2nd and 5th) Mössbauer lines for [Fe(39Å)/Nd(28Å)]. The intensity ratio of the six lines is expressed as 3:X:1:1:X:3. The corresponding direction of the Fe magnetic moment relative to the film normal is also shown on the right side of the ordinate.

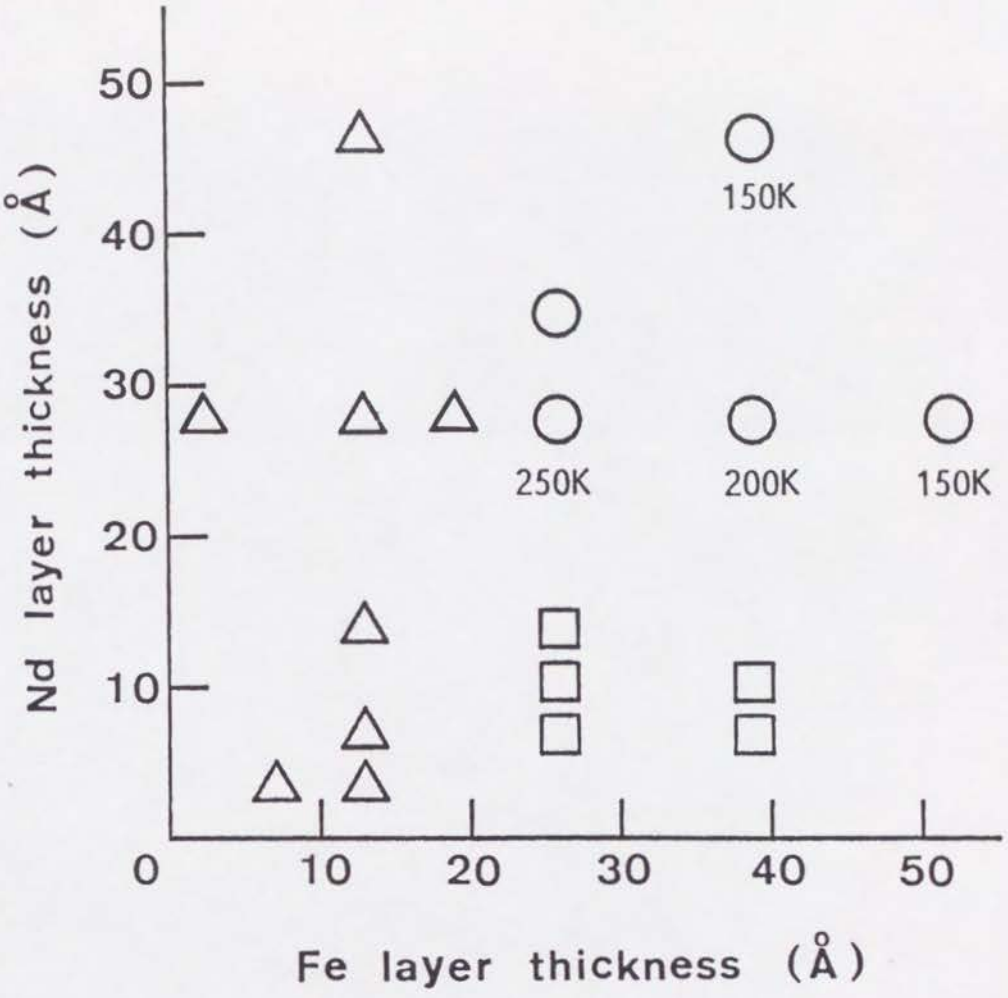

Fig. 60. Grouping of Fe/Nd multilayers according to the feature of the major component of the Mössbauer spectra. ○ : The major component is sharp six lines from α-Fe. The Fe magnetic moment is in the film plane at 300K and is oriented to the perpendicular direction at 4.2K. The temperatures where the spin reorientation occurs are shown in the figure. □ : The major component is six sharp lines from α-Fe. The Fe magnetic moment is oriented to the perpendicular direction at both 300K and 4.2K. △ : The major component is a nonmagnetic doublet at 300K and a magnetic sextet with widely distributed hyperfine fields at 4.2K.

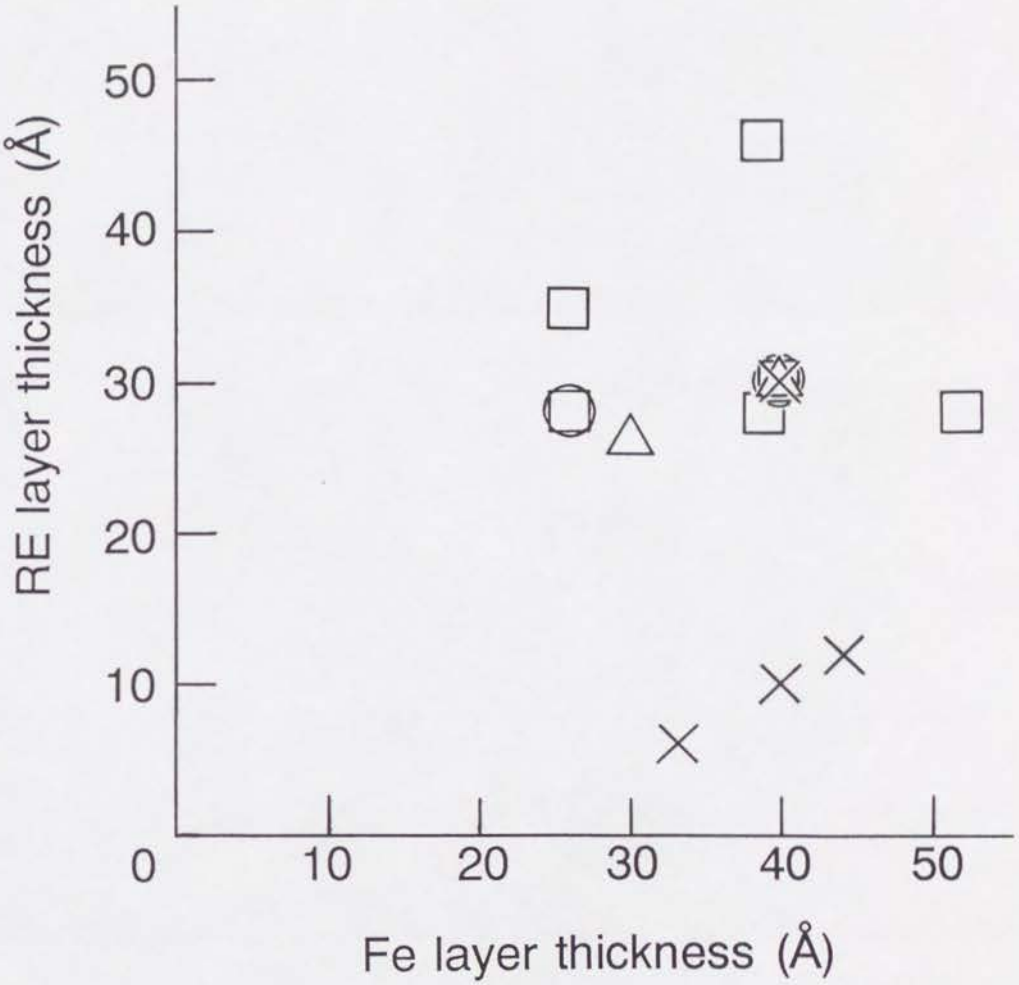

Fig. 61. Thickness region where the Fe spin reorientation occurs in Fe/Pr (○), Fe/Nd (□), Fe/Tb (△), and Fe/Dy (×) multilayers.

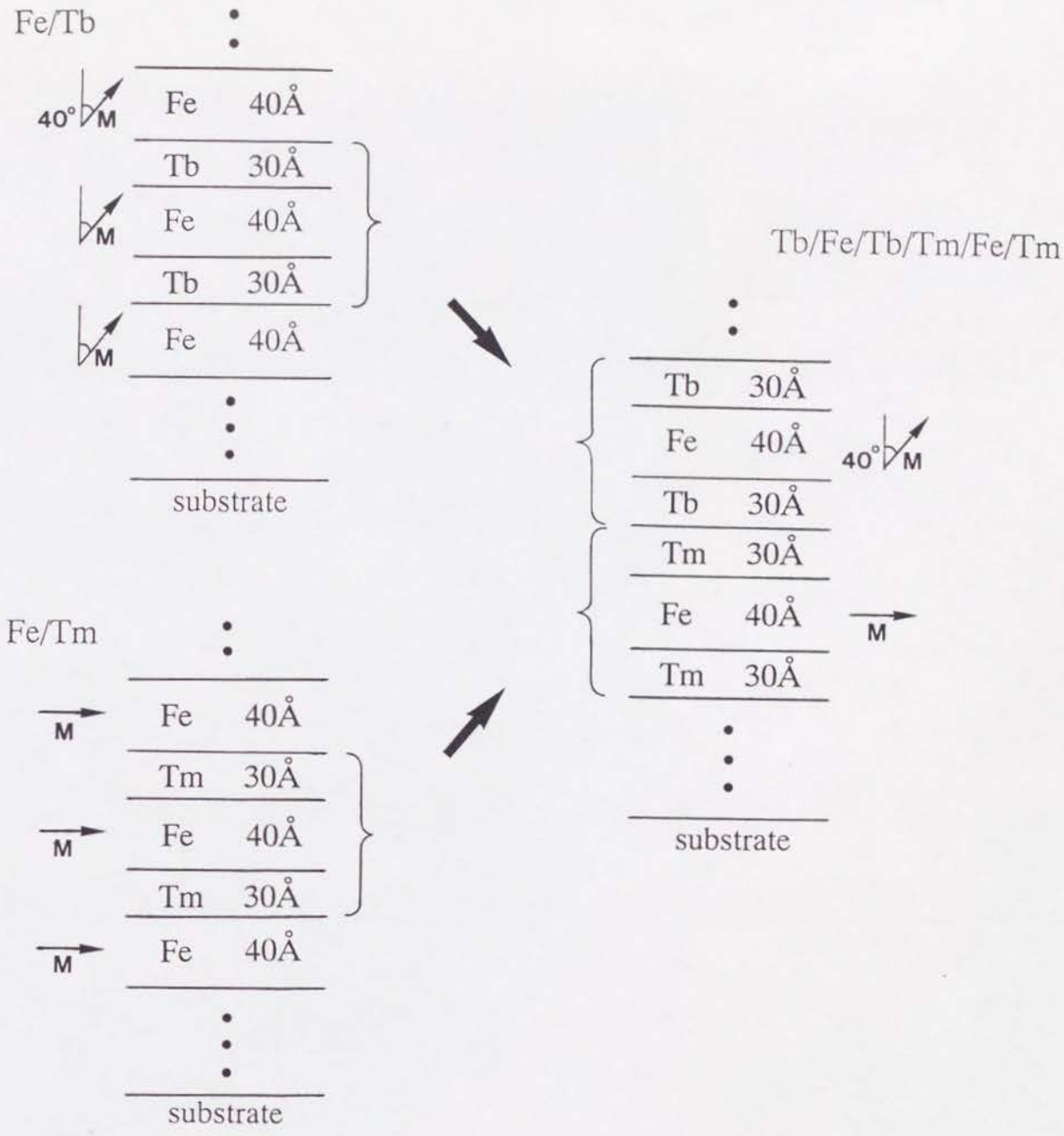

Fig. 62. Illustration of an expected magnetic structure of a Tb/Fe/Tb/Tm/Fe/Tm multilayer in a certain temperature range.

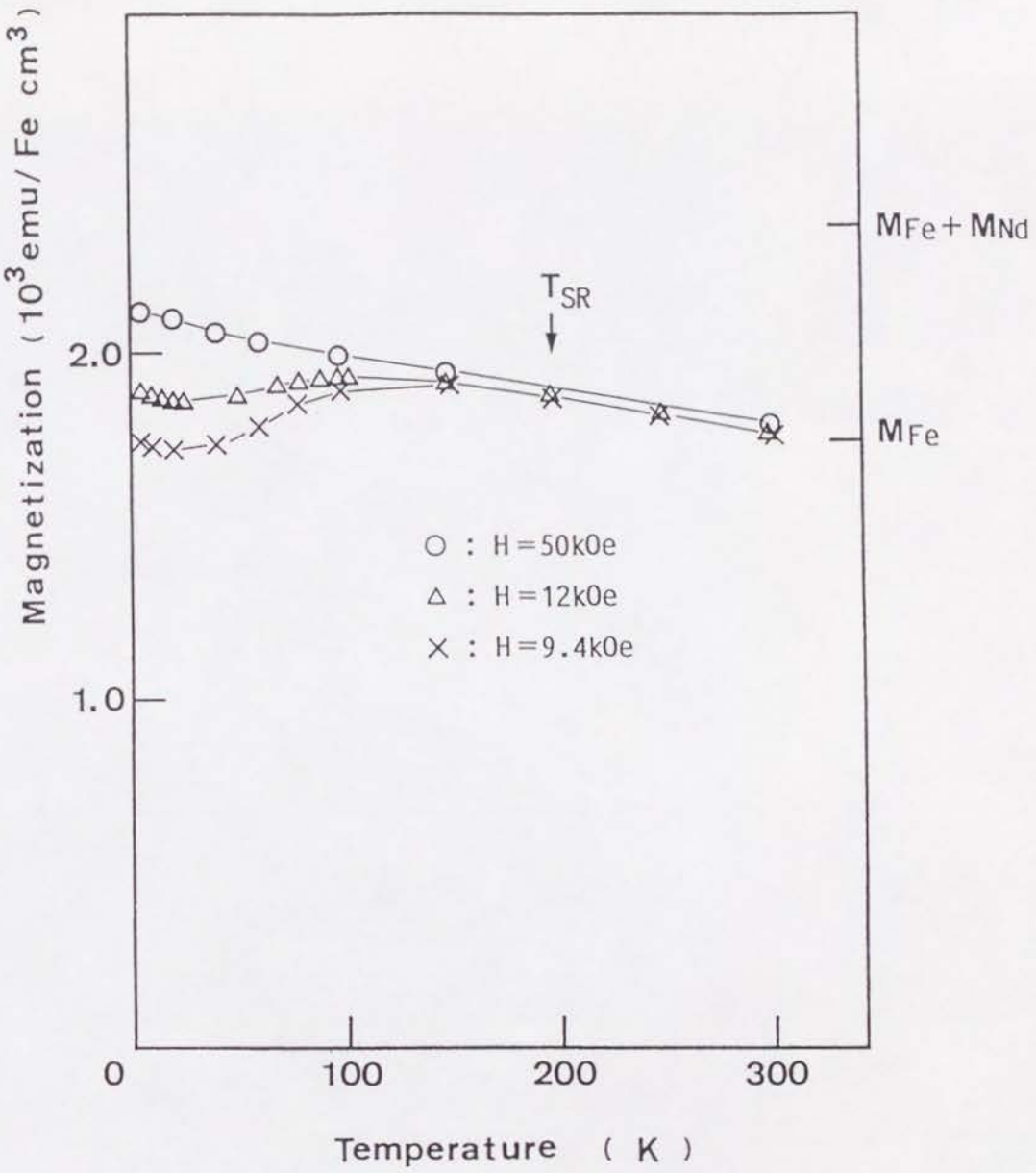

Fig. 63. Temperature dependence of magnetization for [Fe(39Å)/Nd(28Å)]. Magnetic fields of 9.4kOe, 12kOe, and 50kOe are applied parallel to the film plane. The temperature where the spin reorientation is observed in Mössbauer spectra is expressed as T_{SR}.

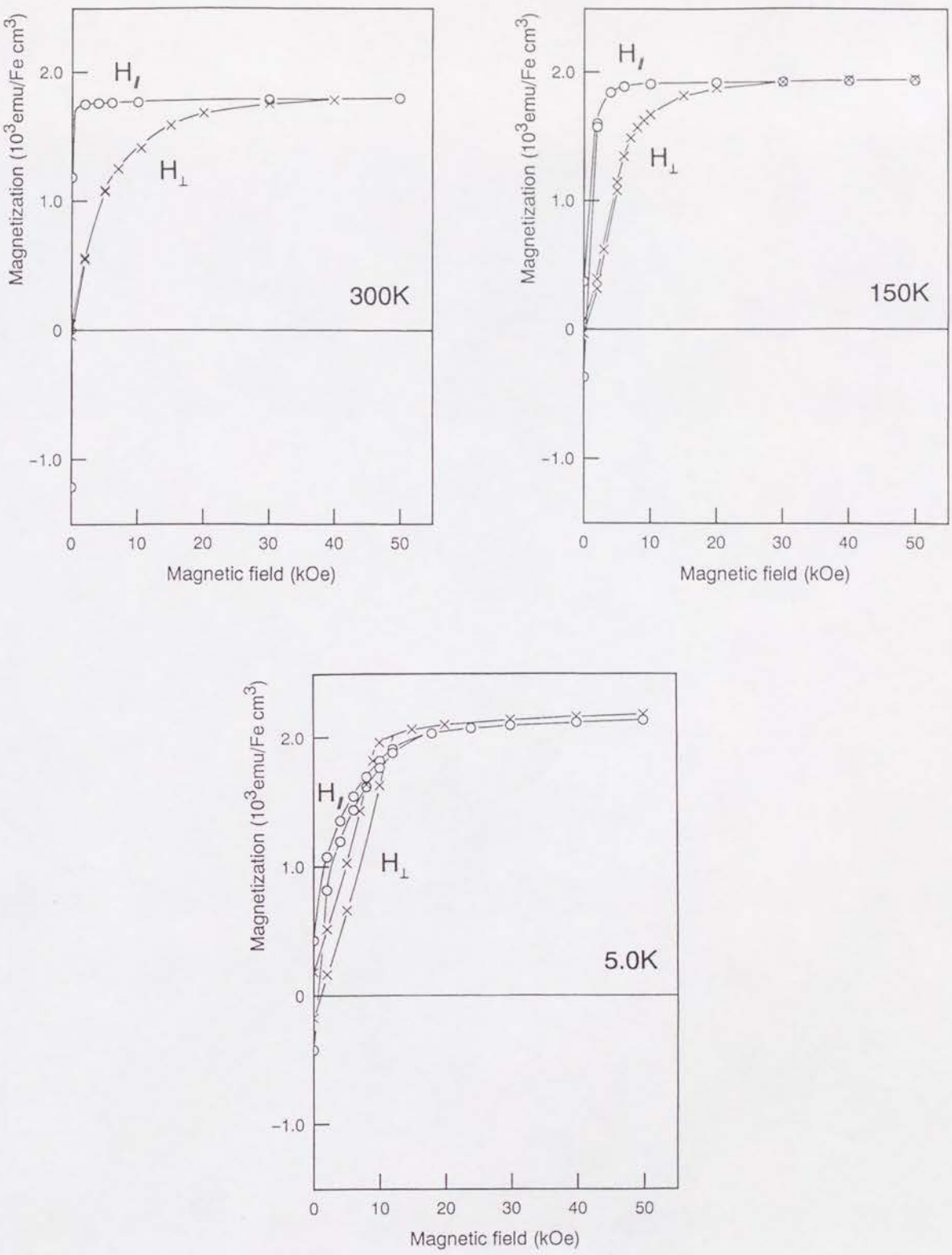

Fig. 64. Magnetization curves for [Fe(39Å)/Nd(28Å)] at 300K, 150K, and 5.0K.

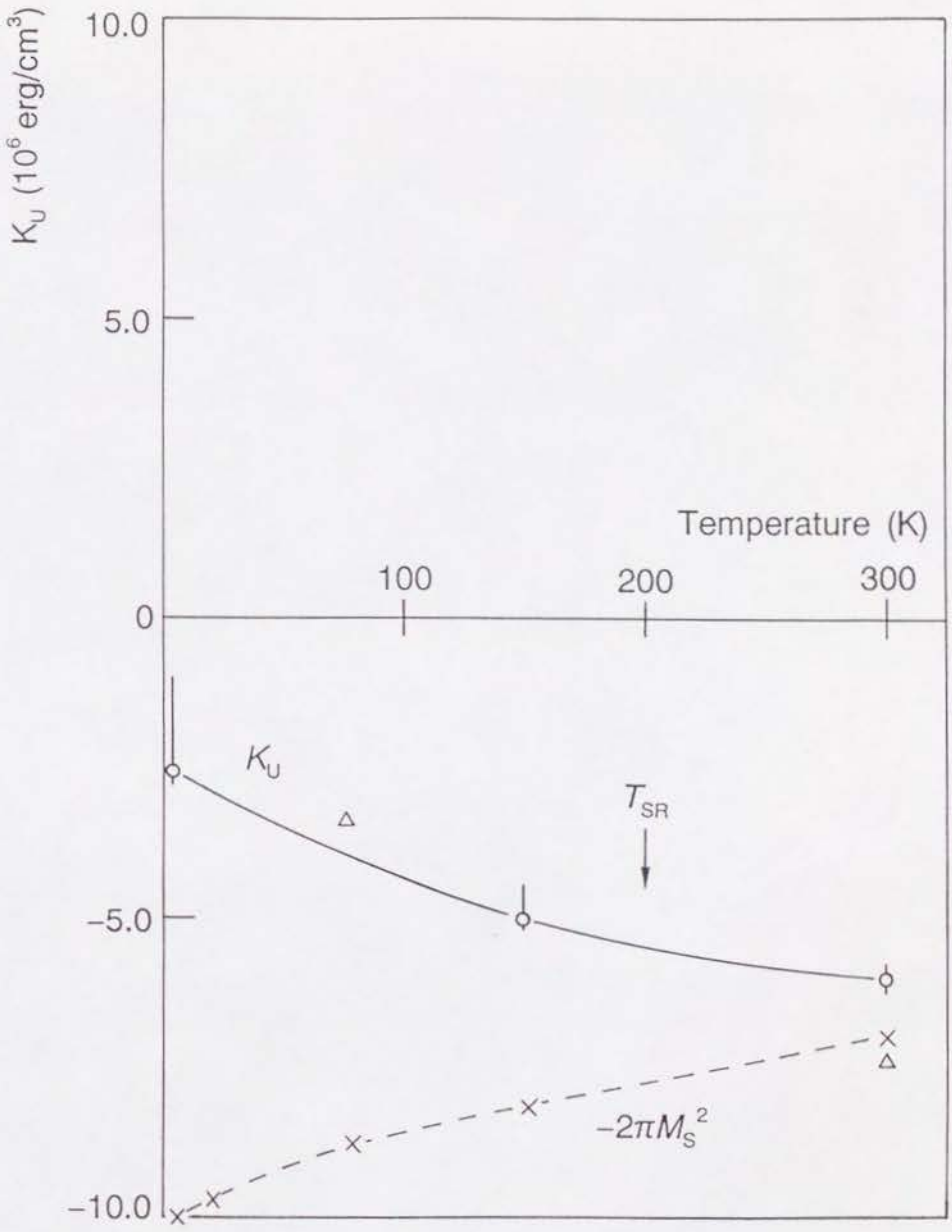

Fig. 65. Temperature dependence of the magnetic anisotropy constant K_u estimated from magnetization measurements (O) and torque measurements (△) for [Fe(39Å)/Nd(28Å)]. The shape anisotropy energy $-2\pi M_s^2$ is also shown for comparison (×). The temperature where the spin reorientation is observed in Mössbauer spectra is expressed as T_{SR}.

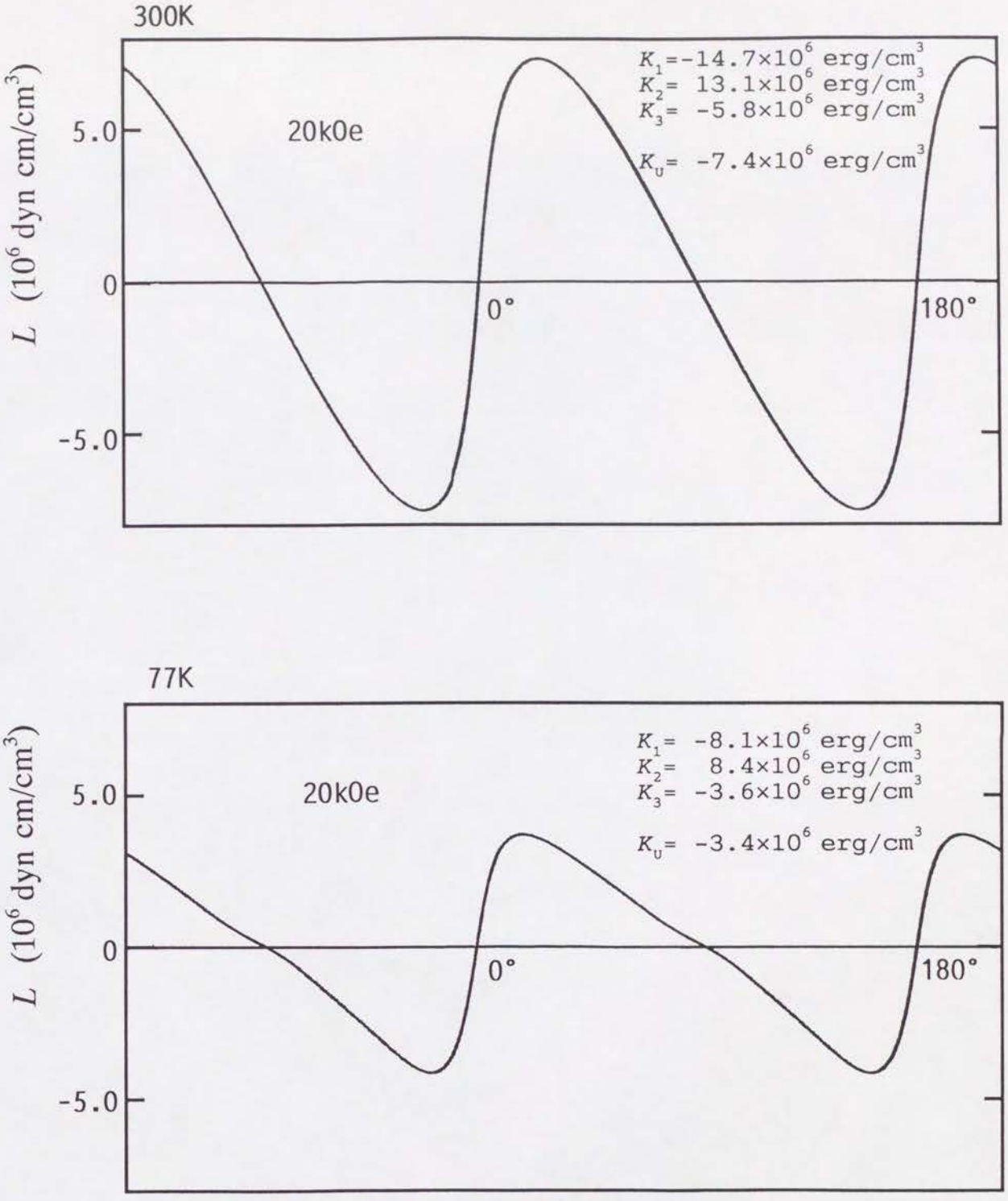

Fig. 66. Torque curves for [Fe(39Å)/Nd(28Å)] at 300K and 77K. For a rough estimation of the anisotropy constants K_1, K_2, K_3, and K_U, the curves were fitted with a single magnetic component with uniaxial anisotropy energy expressed by eq. (6).

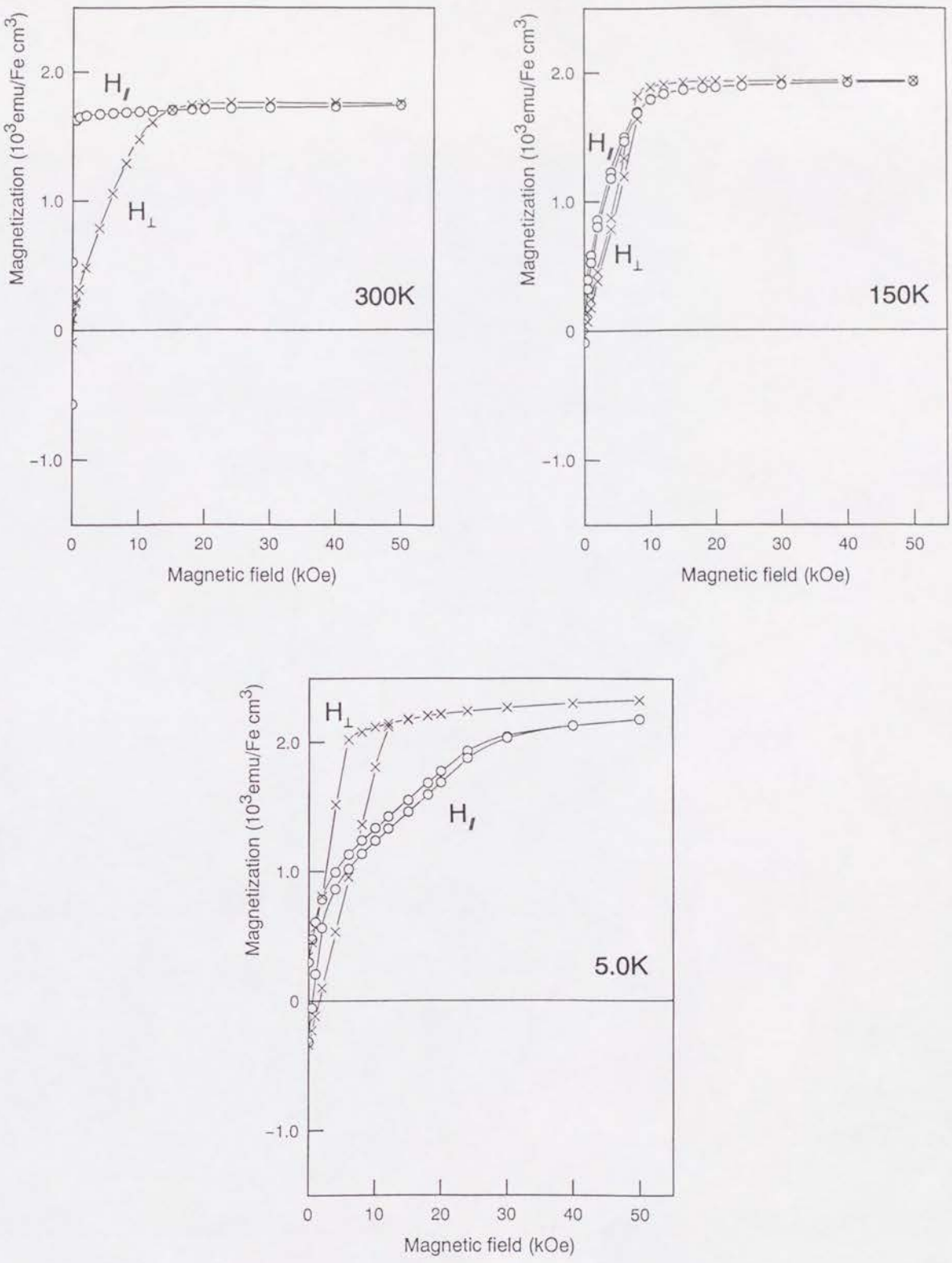

Fig. 67. Magnetization curves for [Fe(26Å)/Nd(28Å)] at 300K, 150K, and 5.0K.

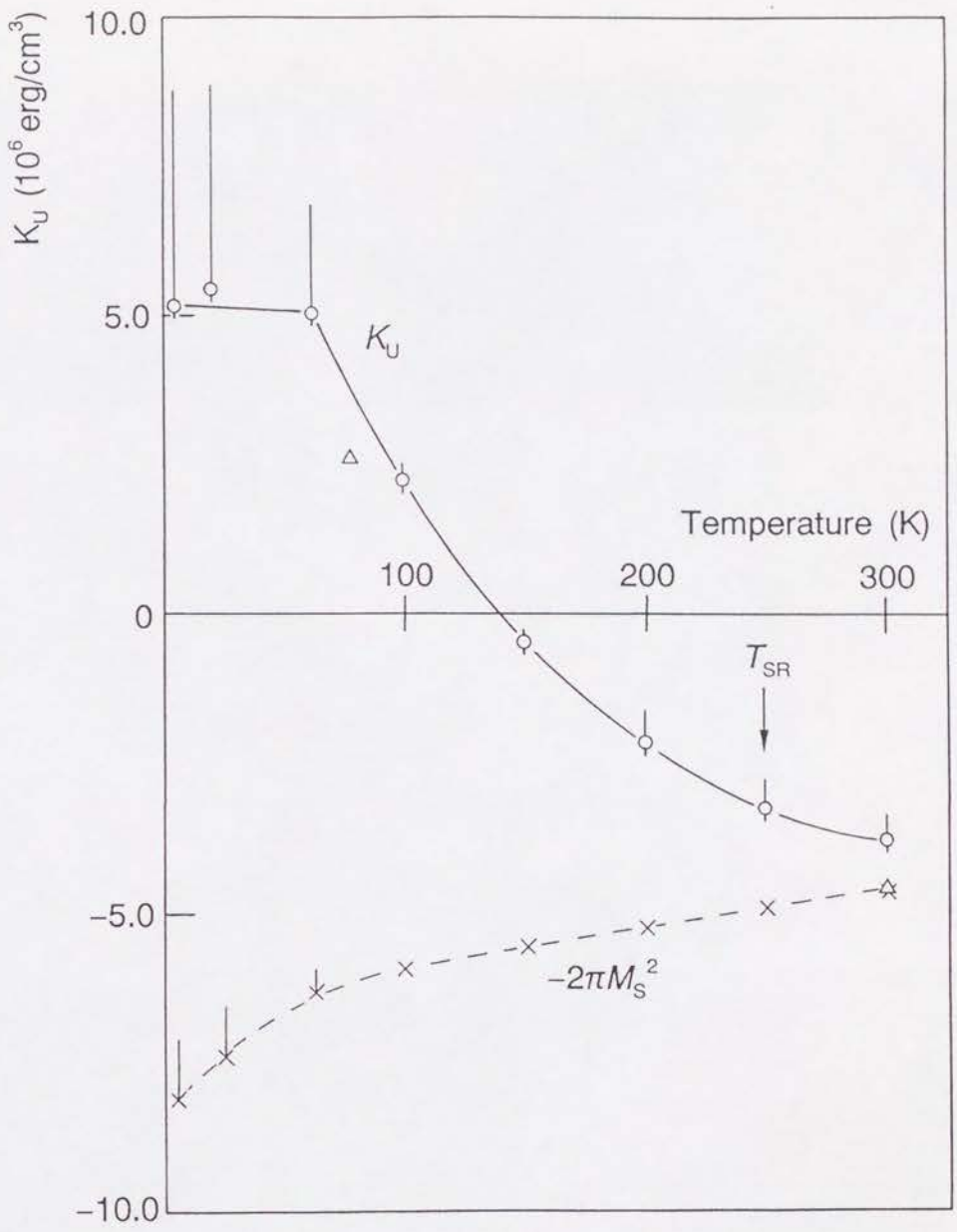

Fig. 68. Temperature dependence of the magnetic anisotropy constant K_U estimated from magnetization measurements (O) and torque measurements (△) for [Fe(26Å)/Nd(28Å)]. The shape anisotropy energy $-2\pi M_s^2$ is also shown for comparison (×). The temperature where the spin reorientation is observed in Mössbauer spectra is expressed as T_{SR}.

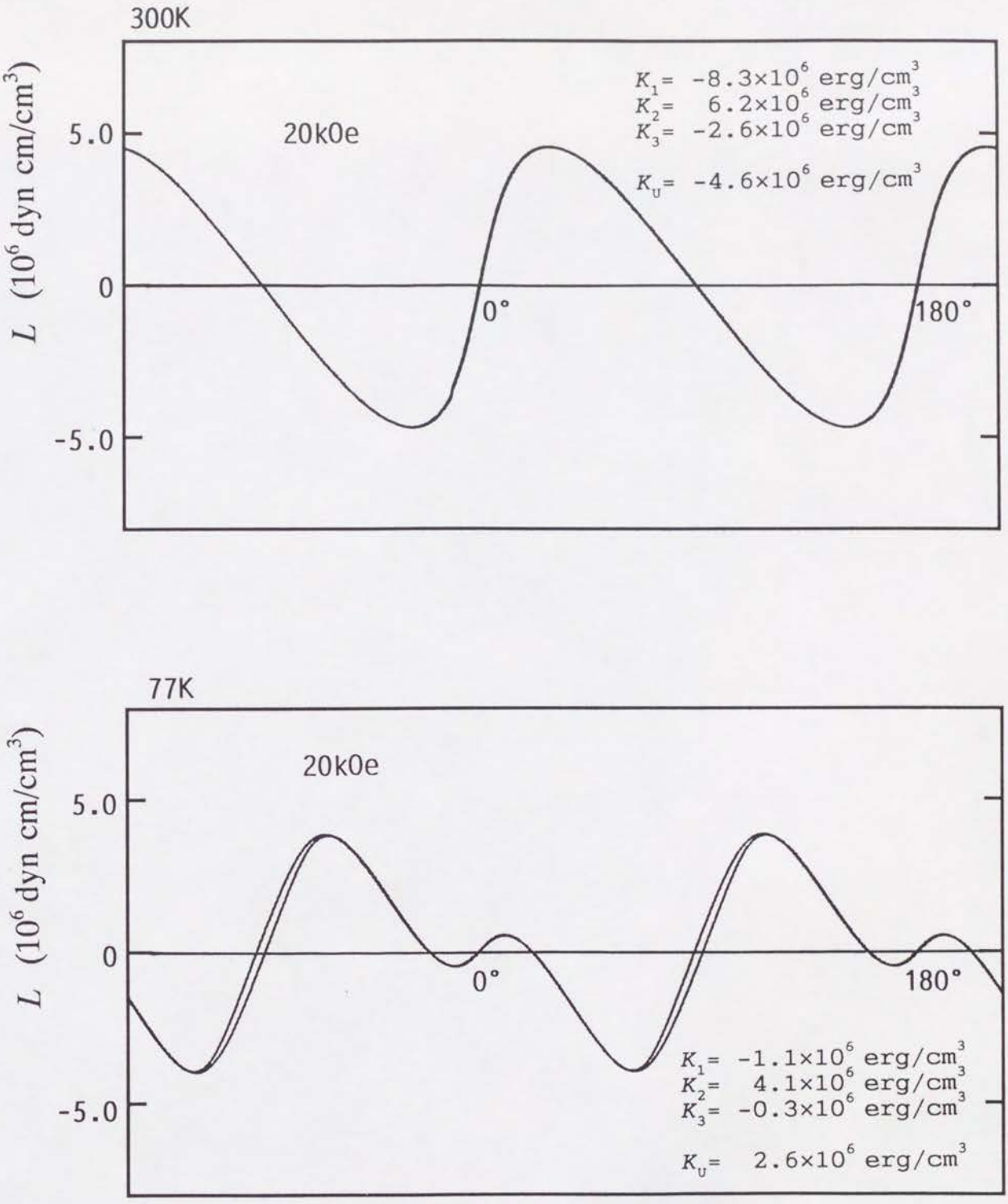

Fig. 69. Torque curves for [Fe(26Å)/Nd(28Å)] at 300K and 77K. For a rough estimation of the anisotropy constants K_1, K_2, K_3, and K_U, the curves were fitted with a single magnetic component with uniaxial anisotropy energy expressed by eq. (6).

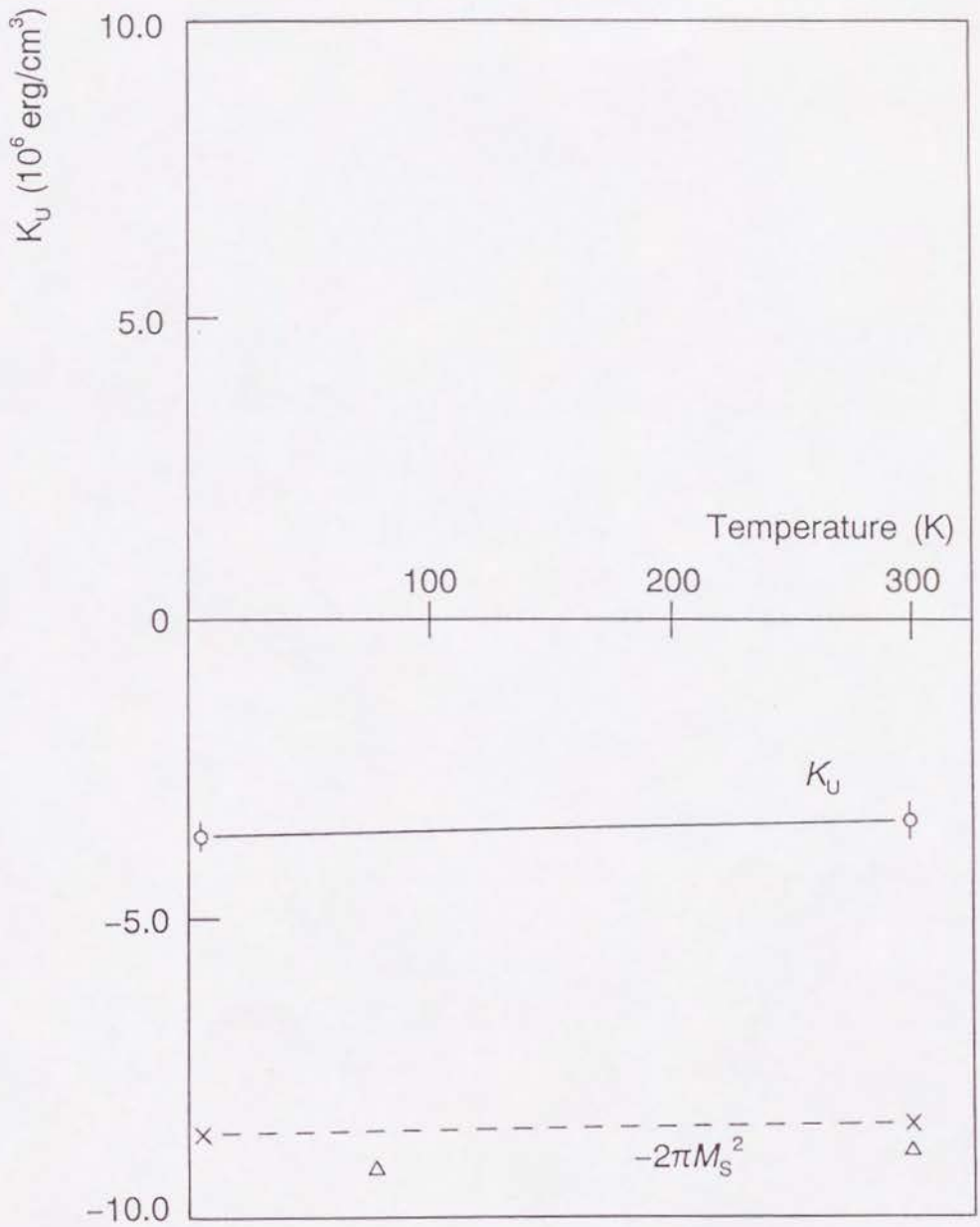

Fig. 70. Temperature dependence of the magnetic anisotropy constant K_u estimated from magnetization measurements (○) and torque measurements (△) for [Fe(50Å)/Tm(10Å)]. The shape anisotropy energy $-2\pi M_s^2$ is also shown for comparison (×).

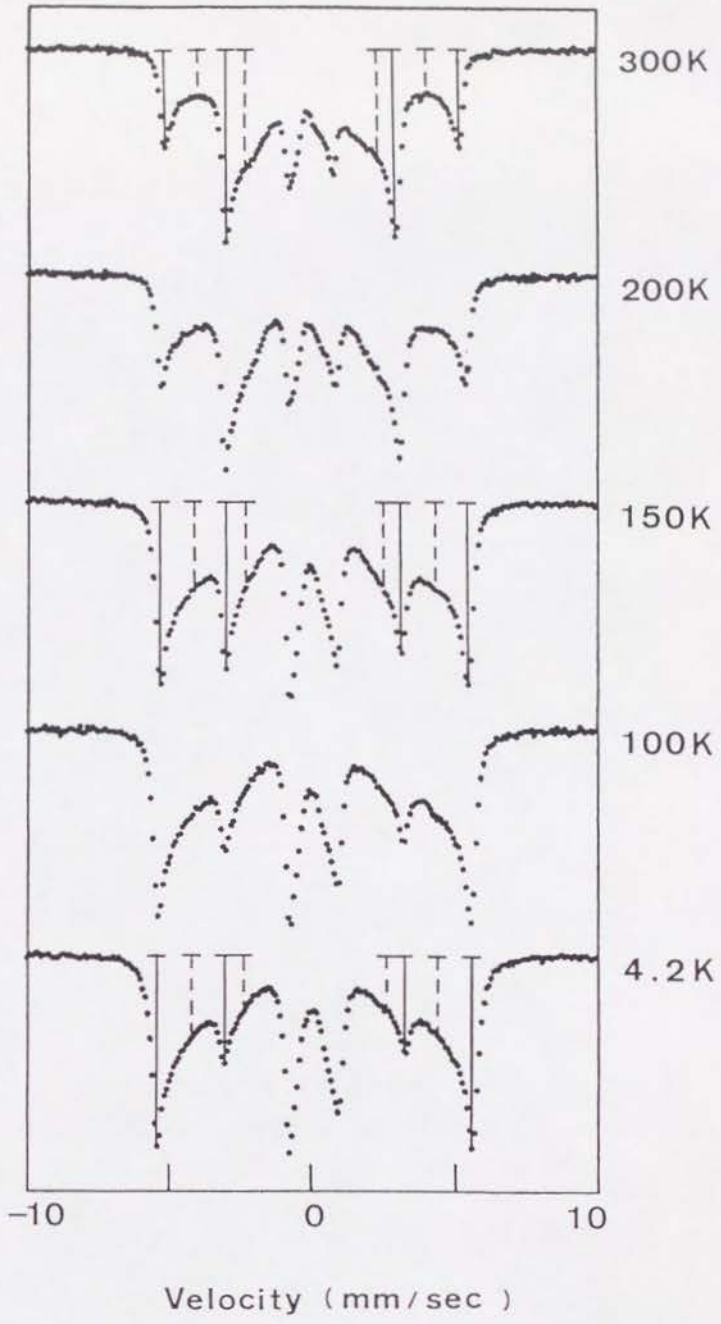

Fig. 71. Temperature dependence of Mössbauer spectra for the ^{57}Fe enriched sample (Sample B). The four outer lines out of magnetically split six-lines are indicated in each spectrum. The solid lines correspond to the hyperfine field at the peak in the distribution, and the broken lines correspond to the hyperfine field 78% of the peak value.

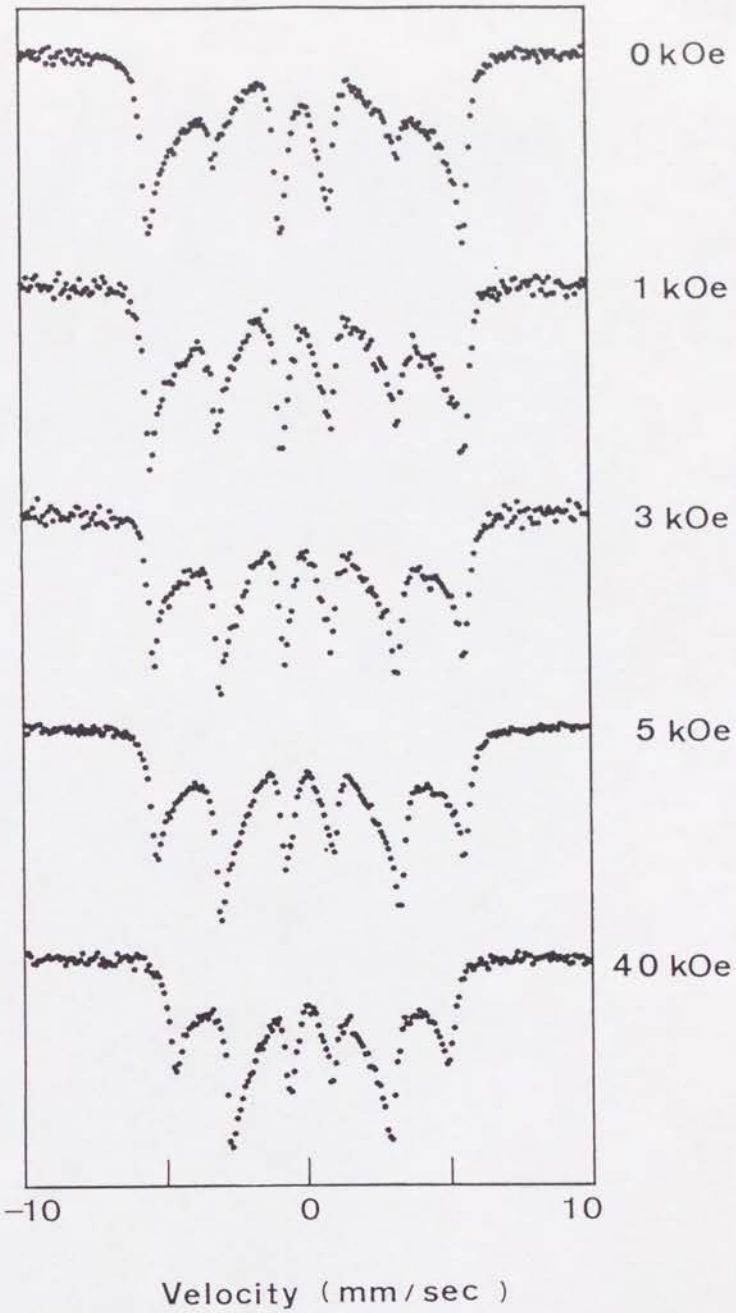

Fig. 72. Mössbauer spectra for the ^{57}Fe enriched sample (Sample B) at 5.0K in magnetic fields parallel to the film plane.

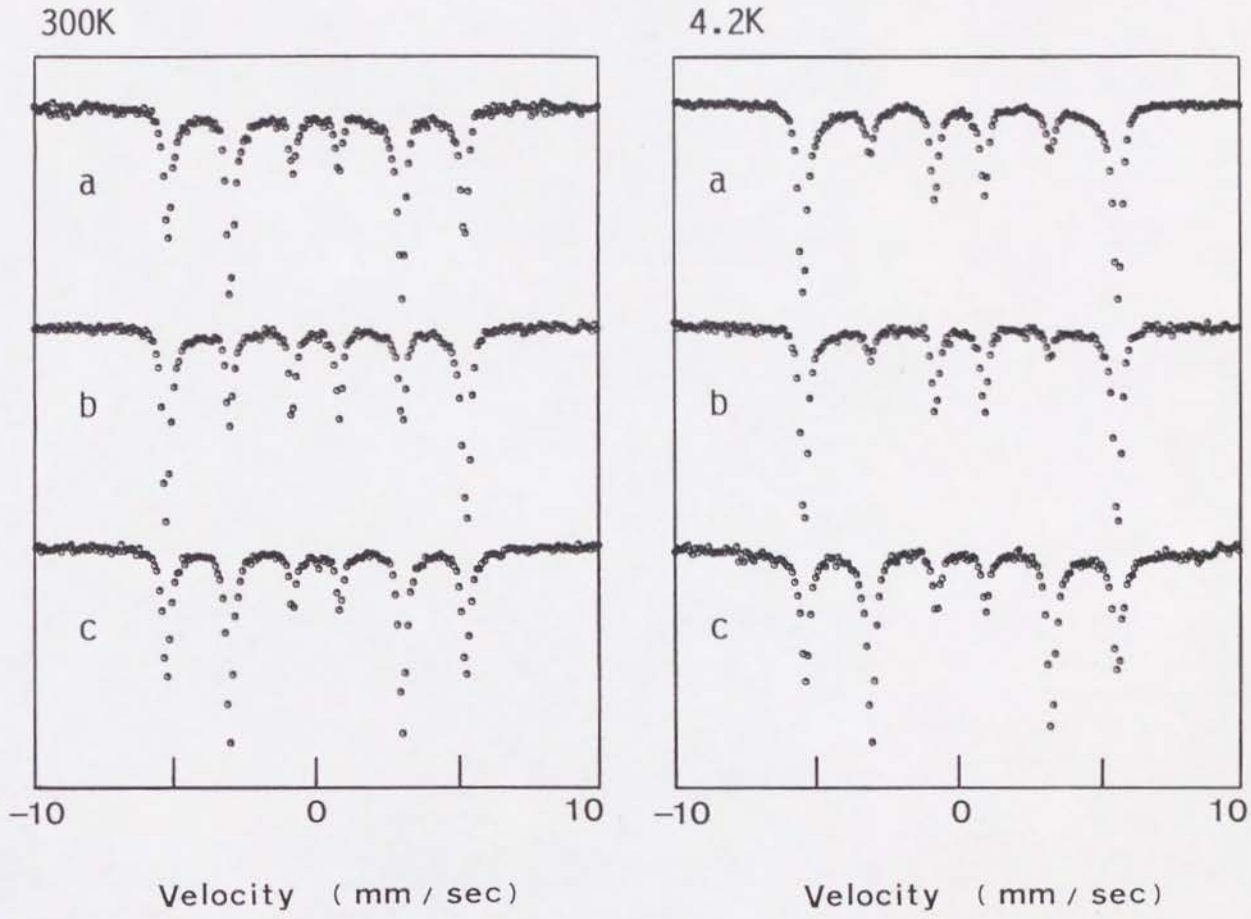

Fig. 73. Mössbauer spectra for [Fe(39Å)/Nd(28Å)] at 300K and 4.2K, (a) before annealing, and after annealing (b) in a vacuum of 10^{-6}Torr at 200°C for 24 hours or (c) in air at 200°C for 24 hours.

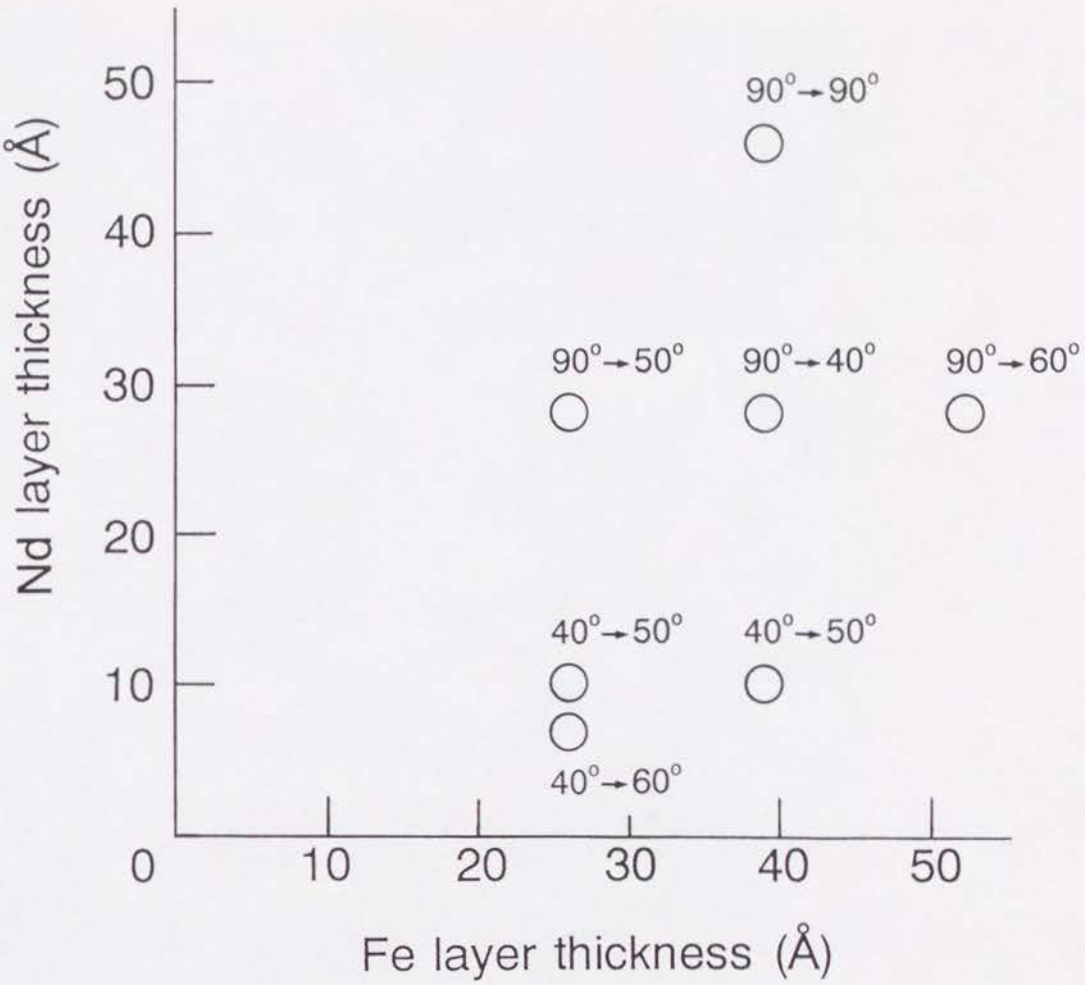

Fig. 74. Change in the direction of the Fe magnetic moment (at 300K) for Fe/Nd multilayers after annealing in 10^{-6}Torr at 200°C for 24 hours.

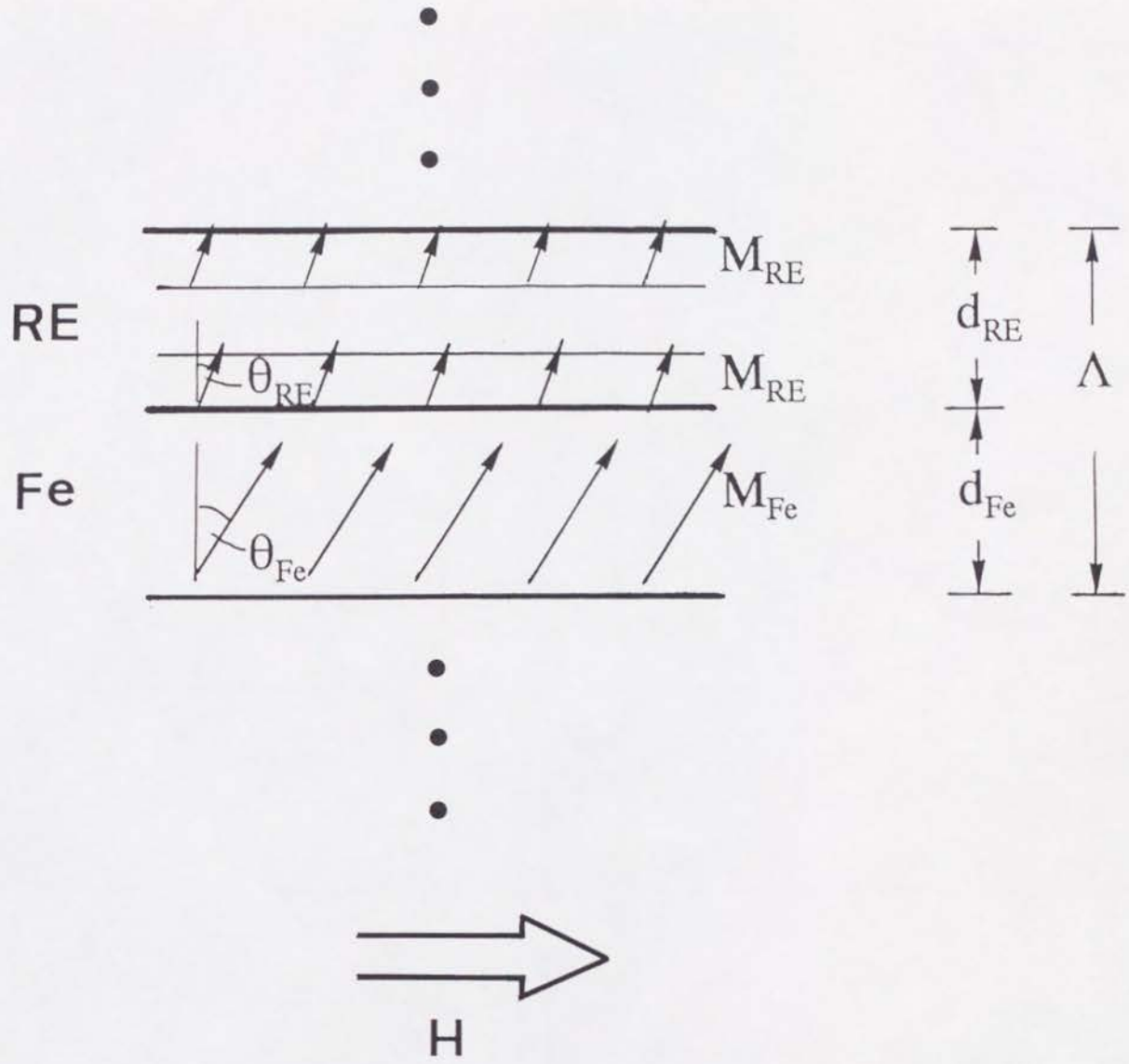

Fig. 75. A simple model of the magnetic structure of an Fe/RE multilayer for calculation of the magnetic energy. It is assumed that the Fe layer is a uniform ferromagnet with the magnetization M_{Fe}, and that the RE layer consists of interface ferromagnetic regions with the magnetization M_{RE} and an inner paramagnetic region.